Technical Support for the Deployment of an L-band radiometer at Concordia Station

FINAL REPORT

European Space Agency

Contract N. 18060/04/NL/CB

Project Manager: Giovanni Macelloni – IFAC CNR

ESTEC Technical Officer: Patrick Wursteisen

ESA Study Scientific Support: Mark Drinkwater

Written by:

Giovanni Macelloni, Paolo Pampaloni

Marco Brogioni, Anselmo Cagnati

DOCUMENT STATUS SHEET

Version	Date	Pages	Changes
1.0	16/12/2005		Draft Version
1.0	20/04/2006		Correction by ESA
2.0	10/05/2006		Final Version

Acronyms and abbreviations

AMSR-E	Advanced Microwave Scanning Radiometer
AWS	Automatic Weather Station
CIP	Campaign Implementation Plan
CVA	Arabba Avalanche Center
Dome-C	Dome Charlie
DOMEX	Dome-C Experiment
EMSL	European Microwave Signature Laboratory
EO	Earth Observation
EPICA	European Project for Ice Coring in Antarctica
ESA	European Space Agency
FOV	Field of view
GPS	Global Positioning System
HPBW	Half-Power Beam Width
HYDROS	Hydrosphere State Mission
IASH	International Association of Hydrological Sciences
IFAC	Istituto di Fisica Applicata "Nello Carrara"
IR	Infrared radiometer
JRC	Joint Research Centre - Ispra
MIRAS	Microwave Imaging Radiometer with Aperture Synthesis
MWR	Envisat Microwave Radiometer
PNRA	Italian Programme of National Research in Antarctica
RF	Radio Frequency
SAR	Synthetic Aperture Radar
SMMR	Scanning Multifrequency Microwave Radiometer
SMOS	Soil Moisture and Ocean Salinity Mission
SSM-I	the Special Sensor Microwave Imaging radiometer
TB	Brightness Temperature
UTC	Universal Time Co-ordinated

TABLE OF CONTENTS

1.0 Introduction

This document, which contains the final report on the ESA contract 18060/04/NL/CB - **Technical Support for the Deployment of an L-band radiometer at Concordia Station** was prepared by the **Institute of Applied Physics "Nello Carrara" (IFAC) – Firenze Italy.** This activity is part of the calibration activities of the SMOS mission, which is a mission of the **Earth Explorers** within ESA's Living Planet Programme.

The main goal of this project was to obtain a time series of microwave radiometric data at Dome-C Antarctica in order to evaluate the potential of the radiometrically uniform and stable areas of the Antarctic Ice sheet in external calibration of satellite data.

An experiment for measuring emission at L- and C- bands from the ice sheet at Dome C was carried out in the 2004/2005 Austral summer. The experiment, which was supported by ESA and by the Italian Programme of National Research in Antarctica (PNRA), included radiometric measurements at different incidence and azimuth angles and snow measurements, using conventional methods.

In the first part of the document (section I) the background and the objectives of the project are described; the instruments and preparation activities are described in section II. The experimental campaign and the results are included in sections III and IV respectively. Lastly the conclusions and idea for future activities are contained in the final sections.

1.1 *Background*

Antarctica is one of the most interesting and challenging natural laboratories on Earth, and plays a fundamental role in hydrological and meteorological cycles. Because of its high albedo, high thermal emissivity, and low thermal conductivity, snow strongly influences the overlying atmosphere and thus, the polar and global climate. The monitoring of glacial environments requires the knowledge of the interaction between snow structure and reflectance properties and this can be achieved by analyzing a large data set of ground measurements, including spectral, snow and climatic data. Satellite sensors are the most suitable tools for observing the temporal and spatial variations in extensive snow-covered areas.

A number of microwave and optical remote sensing satellite missions are currently flying or are about to fly, over the course of the next few years. Microwave data on the Antarctica region at frequencies ranging from 6.8 GHz up to about 90 GHz have been and are still being collected by means of satellite sensors such as the Scanning Multifrequency Microwave Radiometer (SMMR), the Special Sensor Microwave Imaging radiometer (SSM/I) and the Advanced Microwave Scanning Radiometer (AMSR-E), and the results have been reported in several papers (e.g. [1]-[4]). Other missions based on L-band radiometers, such as the ESA Soil Moisture and Ocean Salinity Mission (SMOS) and NASA HYDROS and AQUARIOUS are planned for the near future.

The quality of these radiometric data is a key issue that can be dealt only with the pre-launch calibration of the instruments, together with a comprehensive follow-up of post-launch calibration and validation experiments. External calibration and assessment of long-term performance degradation or drifts in sensor performance can be performed with extremely stable natural targets. For example, methods for calibrating space-borne radiometers by using cold reference targets are indicated in ([5]-[6]).

Compared to other natural scenarios, the ice sheets offer the advantage that they present a cold, dry and uniform, extended target surface. The Antarctic environment, and in

particular the plateau (Dome-C) which hosts the Italian French Concordia station, appears to be appropriate for this issue, thanks to its size and uniform spatial structure accompanied by detailed knowledge of the vertical profile of ice obtained in the European Project for Ice Coring in Antarctica (EPICA) where a cross-section of the ice sheet properties were measured by drilling and recovering an ice core to 3270 m depth [7]. The data provided by this and other experiments were fundamental to express firn and ice physical and chemical properties, including grain size, density, temperature, and dielectric properties of each layer in which the medium could be divided. In turn, these data can be used as input to a multi-layer electromagnetic model able to simulate the Brightness Temperature (Tb).

Penetration of microwaves in the layered Antarctic firn was estimated by using Ku-band data [2], and model simulations [8][9]. At Ku-band, the estimated penetration depth is of the order of several meters, while at P-band it is estimated to be of the order of 4 km. At L-band extinction of ice and snow is low, due to the small imaginary part of the complex permittivity, and is influenced negligibly by the upper 10 m. Below 10m the firn temperature does not exhibit any significant seasonal temperature variation. Thus, though the upper ice sheet layer experiences seasonal temperature variability of the order of 30° C it is almost transparent at L-band. To the expected seasonal brightness temperature variability is therefore extremely small. Measurements from 5 to 37 GHz collected by satellite sensors show that the mean annual variability decreased when the frequency decreased (Figure 1). At C-band the annual variability was of about 5 K while the variability at L-band, extrapolated from the measurements using a polynomial fit, was estimated lower than 0.5 K.

The applicability of the Dome-C plateau as a suitable target for calibrating and monitoring the performance of low frequency microwave radiometers (L- and C- bands) needs a better understanding of its structure as well as of the physical effects governing microwave emission from deep ice sheets. Radiometric time series from SMMR and SMMI and now AMSR show lagged seasonal Tb responses at different wavelengths. This lag implies a frequency dependent depth-weighting of thermal emission. The spectral response and polarisation differences also vary as a function of the seasons.

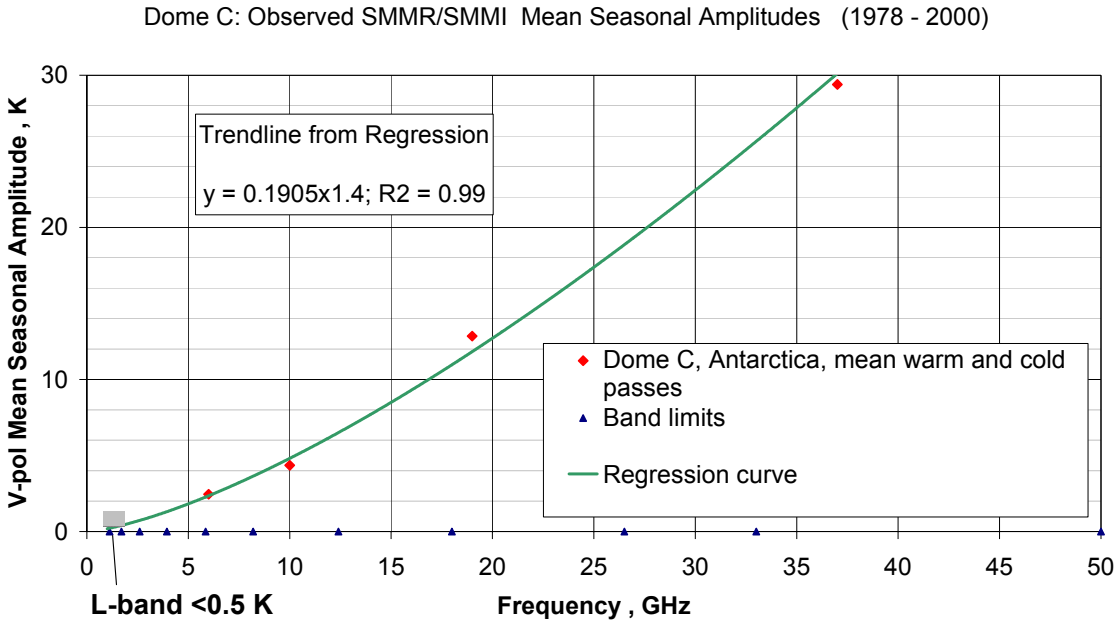

Figure 1 Mean Seasonal Tb Amplitudes as a function of frequency (SMMR-SMMI data 1978-2000)by Drinkwater et al. [10]

None of these rather deterministic characteristics is at present fully reproducible in current state of the art models. An even more significant lack of information exists on the emission at the lower frequencies, which are the most interesting ones for investigating deeper layers of ice. Theoretical models to predict L-band emission from the layered ice sheet are available, but as yet we have no proof or in-situ validation in such ice sheet locations. Furthemore, most model predictions differ, either as a consequence of their assumptions, or our lack of knowledge, for instance, about absorption in inhomogeneous snow/ice mixtures at L-band, and the coupling with the thermodynamics of the system. These kinds of issues are very hard to simulate in the lab or under other field circumstances - since no infinitely deep half-space of snow (with the right absorptive and scattering properties) is available in a convenient location.

The experiment, took place at Dome-C-Antarctica between December 10, 2004, and January 2, 2005. It included radiometric measurements from a tower at different incidence and azimuth angles and snow measurements, using conventional methods. The objective of the study was to improve our knowledge of the temporal variability of the L- and C- band

microwave brightness temperature measured at different incidence and azimuth angles, over timescales from daily to monthly, and to provide the scientific community a first data base of “in situ” measurements to better evaluate and interpret low frequency satellite measurements.

1.2 *The Dome-C test site*

Dome C is a broad topographic Dome roughly centred at 75° 06’06”S, 123° 23’42”E on the polar plateau of East Antarctica (at ~3250 m elevation a.s.l.) (Figure 2). This location is spatially homogeneous and its situation more than 700 km from the coast, offers extremely small surface slopes.

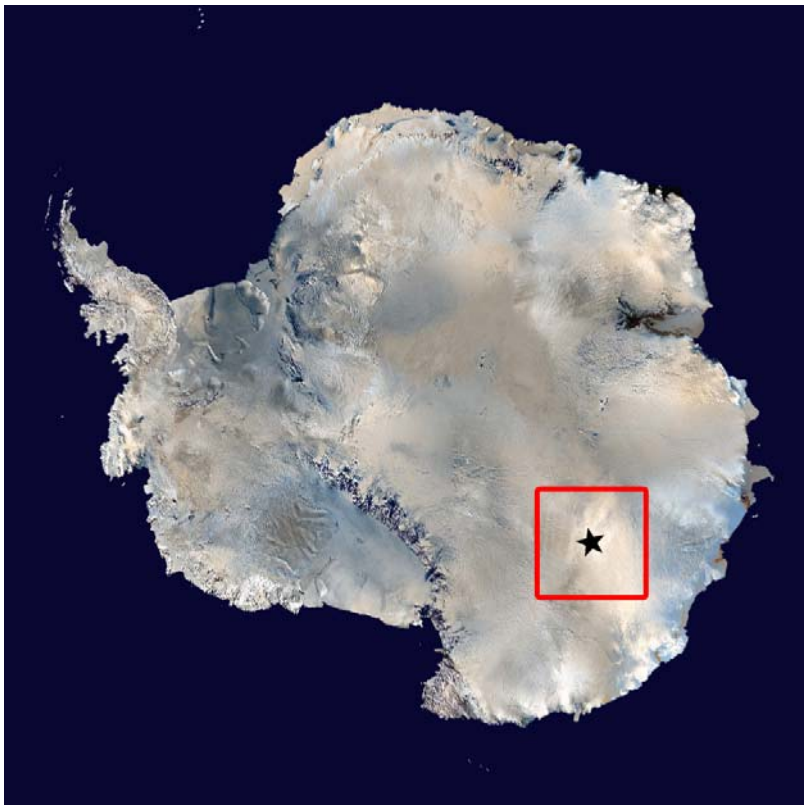

Figure 2 Map of Antarctica showing Dome-C (red square) and location of Concordia Station (star).

This site is well suited for calibration and validation of microwave sensors for the following reasons:

- at a geographic latitude of 75ºS the site is viewed on a frequent (sub-daily) basis by polar-orbiting satellites, at a variety of incidence and azimuth angles.
- the snow surface is relatively homogeneous at the 100 km scale.
- topography is known from satellite altimetry, GPS and SAR interferometry to high precision at km scale.
- surface roughness is minimal relative to other ice sheet locations.
- the sky is clear, and the atmosphere is extremely dry and stable.
- environmental conditions which force microwave brightness temperature variability are well-documented by an Automatic Weather Station (providing barometric pressure, air temperature, and wind speed and direction).

a significant dataset of microwave brightness temperature measured at various frequencies, including C-band from a variety of satellite missions, such as the SMMR on Nimbus-7 and AMSR-E on AQUA, exists.

The average air temperature throughout the year is -50.8° C (-30° C in summer with a maximum close to –15^{o} and -60° C in winter with a minimum close to –80^{o}). The annual (solid) precipitation is of the order of 30-40 mm (snow water equivalent), which, for a typical sublimation of 10/20 % , leads to an annual accumulation of about 25-35 mm (snow water equivalent).

2.0 Instrumentation

In the past 20 years, intensive experimental activity has been carried out the by Microwave Remote Sensing Group at IFAC, using microwave radiometers designed and developed on its laboratory. These instruments have been used in several ground based and airplane international campaigns for studying natural media such as bare and vegetated soils, sea and snow pack ([11]-[14]).

In particular, in recent years several national and international projects have been devoted to the characterization of snow. Within this context, experimental campaigns have been carried out in the Italian Alps in parallel with a theoretical activity which concerns the modelling of emission and scattering from snow. (**Errore. L'origine riferimento non è stata trovata.**-[16])

The IFAC microwave radiometers consist of 5 instruments at different frequencies. The main characteristics are represented in **Table I**.

Table I: IFAC Microwave Radiometers

Band	*Central Frequency (GHz)*	*Bandwidth (MHz)*	*Antenna Type*	*HPBW (degs)*	*Polarization*
L	1.413	20	Pyramidal	35x40	H and V
C	6.8	500	Conical corrugated	16	H and V
X	10	500	Conical corrugated	16	H and V
Ku	18.7	500	Conical corrugated	18	H, V, ± 45^{o}
Ka	36.5	500	Conical corrugated	20	H, V, ± 45^{o}

The instrument package used in DOMEX was composed of two microwave radiometers at C and L band, two polarization (V& H) and an infrared sensor operating in the 8 –14 micron band.

At the beginning of the project the performances and characteristics of existing microwave radiometers were analysed on the basis of project requirements, critical aspects and solutions were identified, and instruments were opportunely modified. In particular the need to provide a reference measurement for future space missions required a significant improvement in the performance of the instruments as regards sensitivity, accuracy and stability. The other necessity was to guarantee the functioning of the instruments in the extreme conditions of the Antarctic environment. As far as this last issue is concerned, since it was very difficult to design equipment that works at very low temperatures (minimum temperature at Dome-C during the summer period is -50°) , the instruments were placed in a thermal controlled box.

The design and calibration of instruments, and consideration on thermal protection are described in the follows sections

2.1 *Microwave Radiometers*

The L and C band radiometers were total power, frequent calibration systems with an internal calibrator based on two loads at different temperatures (cold 250 ± 0.2 K and hot 370 ±0.2 K).
The instruments have been designed in a simple configuration to minimize the risk of failure. A block scheme is represented in Figure 3 .

The antenna system consists of a simple dual-polarized pyramidal horn at L band and a corrugated conical horn followed by orthomode transducer at C- band.

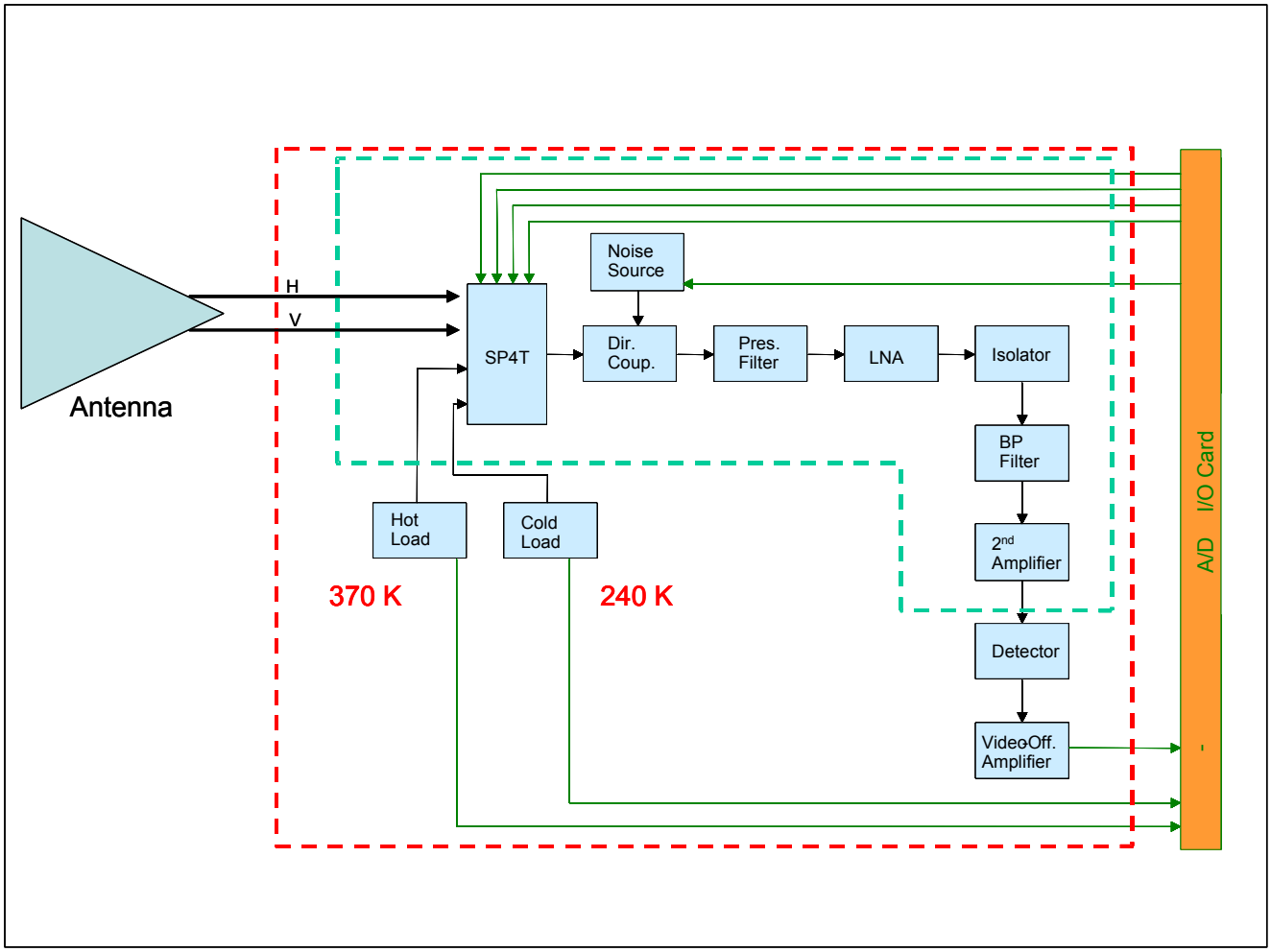

Figure 3 Radiometer block diagram

The 4 inputs of the receiver (the antenna signals at H and V polarization and the hot and cold loads) are connected to the receiver chain by means of a 4-port switch. Direct amplification receivers with a square law detector and an analog/digital converter are employed. Gain and offset variations in the receiver are auto-compensated by alternating the antenna and calibrator measurements. To control the linearity and stability of the receiver, a noise source is inserted at the input of receiver through a directional coupler.

Moreover, several sensors have been placed on the antennas and connecting lines to monitor their temperatures and make possible a further correction for temperature variations in these components that are not compensated by the two-load system. Additional temperature sensors are placed in the critical subsystems of the receivers to monitor their performances.

For the L-band radiometer two identical instruments were realized in order to insure a back-up for the experiment. At C-band the back-up consists of the duplication of the most critical components (amplifier and switch). In addition, the LF section and the A/D are identical, and the compatibility between the two projects makes it possible to interchange the components and spare parts. The electronic and RF components radiometers were selected in accordance with temperature constraints (i.e. storage and operational temperatures of –50 and –10 ^{o}C respectively).

2.1.1 Calibration of the radiometers

Calibration of the radiometers was a key point of the experiment. Although no L-Band measurements had been collected at Dome-C before this experiment, a seasonal variability of less than 0.5 K was expected from model simulations and extrapolation of data taken at higher frequencies (Figure 1). Thus, the instrument accuracy and stability needed to be better than this value.

The methodology used for calibrating the radiometers can be described by using a simplified scheme of the system represented in Figure 4.

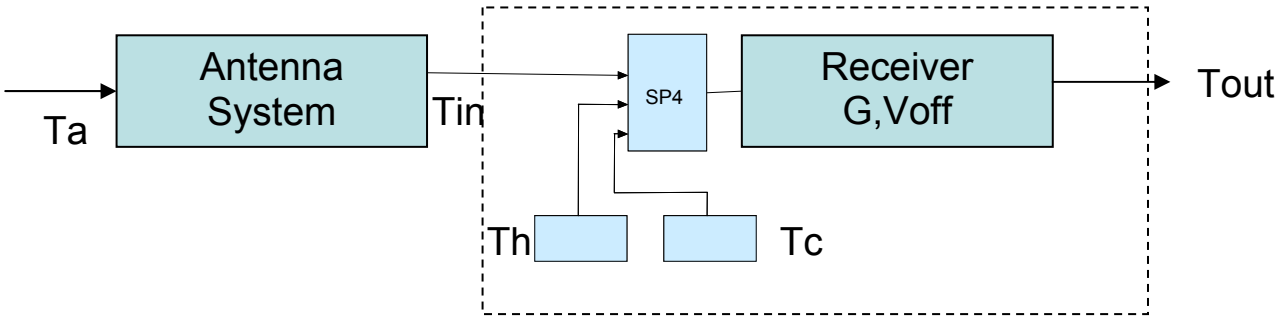

Figure 4 Radiometers calibration scheme

The gain and offset variations in the receiver are compensated by the frequent calibration technique. Nevertheless, uncertainty in the measurement of the load brightness temperature (i.e. the errors in the measurement of the physical temperature of the

matched load connected to the receiver and the differences between the four port of the SP4T) generates an error in the retrieval of the measured brightness temperature which was corrected by using an external target. Indeed the input brightness temperature is related to the output by the following linear equation:

$$Tout = Tin * a + b \qquad (1)$$

Where a and b were computed by using the results of the measurements on the external load.

Lastly, the antenna temperature Ta is related to Tin by the equation

$$Tin = L\,Ta + (1 - L)\,To \qquad (2)$$

Where:
L = losses introduced by the antenna, cables and connectors
To = Thermometric temperature of antenna cables and connectors

In order to compute all the contribution separately the calibration was carried out in two phases:

1) Laboratory calibration of the radiometer excluding the antenna system

2) Calibration of the whole system including the antenna and connecting lines with external reference targets.

Laboratory calibration of the radiometer excluding the antenna system

The laboratory calibration of the two radiometers (L and C bands) was performed by using an external thermo-controlled load connected to the receiver input. The load operates between 1 and 19 GHz and is composed of three basic elements: the heating/cooling system, the microwave termination and the temperature sensor. The latter consists of a platinum resistance (PT100) sealed inside a block of aluminum with a thermal inertia very similar to that of the coaxial termination. Both the termination and the temperature are immersed in a metallic block. They are placed symmetrically with respect to the heating cooling/element, so that the temperature of the thermal sensor is well representative of that of the microwave termination. The heating/cooling system consists of a Peltier cell cooled by means of a fan coil. The load temperature could be decreased or increased by 40 K with respect to the ambient temperature. Measurements were carried out in the 240 – 340 K temperature range. The total accuracy of the load system (i.e. the measurement of the load temperature) was 0.2 K. An example of a measurement cycle is represented in Figure 5.

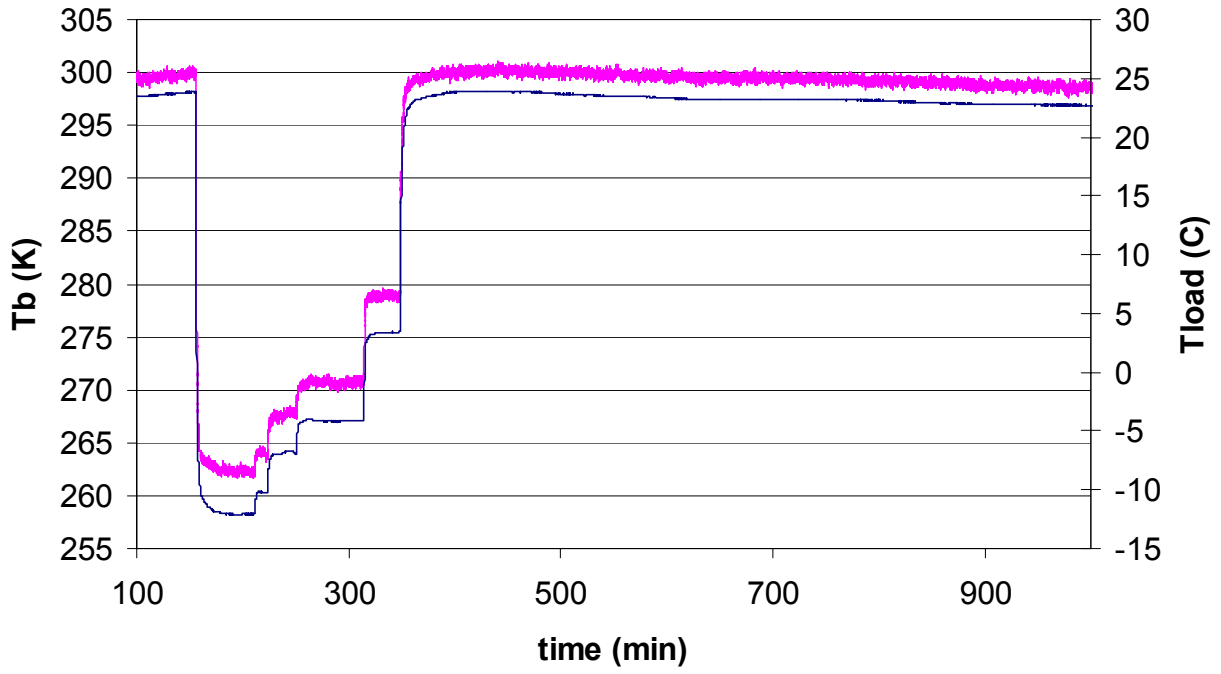

Figure 5 Brightness Temperature and calibration load temperature as a function of time.

Stability of the radiometer was tested by maintaining the load temperature at a stable value (with a standard deviation better than 0.01 K) and measuring the radiometer output for short (1 minute), medium (10 minutes) and long (100 minutes) time intervals, using an integration time τ = 1 sec. An example is provided in Table II.

The mean value of the measured brightness temperature remained constant in time for both short- and long-term variations, with the standard deviation increasing from 0.17 K (short term) to 0.25 K (long term).

Table II
Long-, medium- and short-term receiver (Tb) and load (Tload) stability

	Long (100 min)		Medium (10 min)		Short (1 min)	
	TB (K)	Tload (K)	TB (K)	Tload (K)	TB (K)	Tload (K)
Mean	299.47	296.38	299.45	296.38	299.58	296.38
Max	300.48	296.39	300.03	296.39	299.84	296.39
Min	298.49	296.37	298.65	296.37	299.25	296.37
St. dev.	0.26	0.004	0.24	0.004	0.17	0.004

The sensitivity of the radiometers which was measured for different integration times, τ, with a matched load at 270 K (±0.01 K) connected to the input is represented in Figure 6.
As expected, the sensitivity increased when the integration time increased.
It should be noted that, the obtained values are greater than of those predicted by the well-known equation (represented in the figure):

$$\Delta T_N = \frac{Tsys + Ta}{\sqrt{B\tau}} \qquad \textbf{(3)}$$

where:

Tsys = Temperature of the system

a= antenna temperature

B =bandwidth

τ = integration time

Nevertheless, as described in [17], the rapid gain fluctuations (faster than the integration time) could contribute to a deterioration in radiometer performance and the following term therefore needs to be added to the previous one:

$$\Delta T_G = \frac{\Delta G}{G}(Tsys + Ta) \qquad \textbf{(4)}$$

where $\frac{\Delta G}{G}$ represents the normalized rms fluctuation of the receiver gain G.

Since the terms are statistically independent, the total sensitivity is expressed by:

$$\Delta T_G = \sqrt{(\Delta T_N)^2 + (\Delta T_G)^2} \qquad \textbf{(5)}$$

The computation of this last contribution is not easy but a value of 0.1K appears to be reasonable as shown in [17]-[18].

Since the expected sensitivity of SMOS ranges from 0.8 to 2.2 K, the values obtained were assumed to be adequate for fitting the goal of DOMEX.

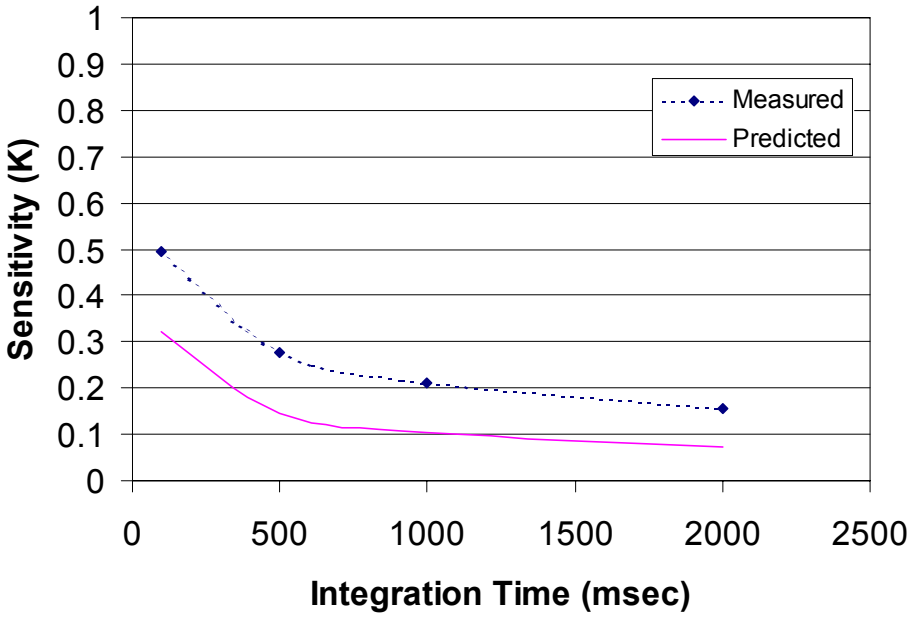

Figure 6 Measured (blue) and predicted (pink) radiometer sensitivity

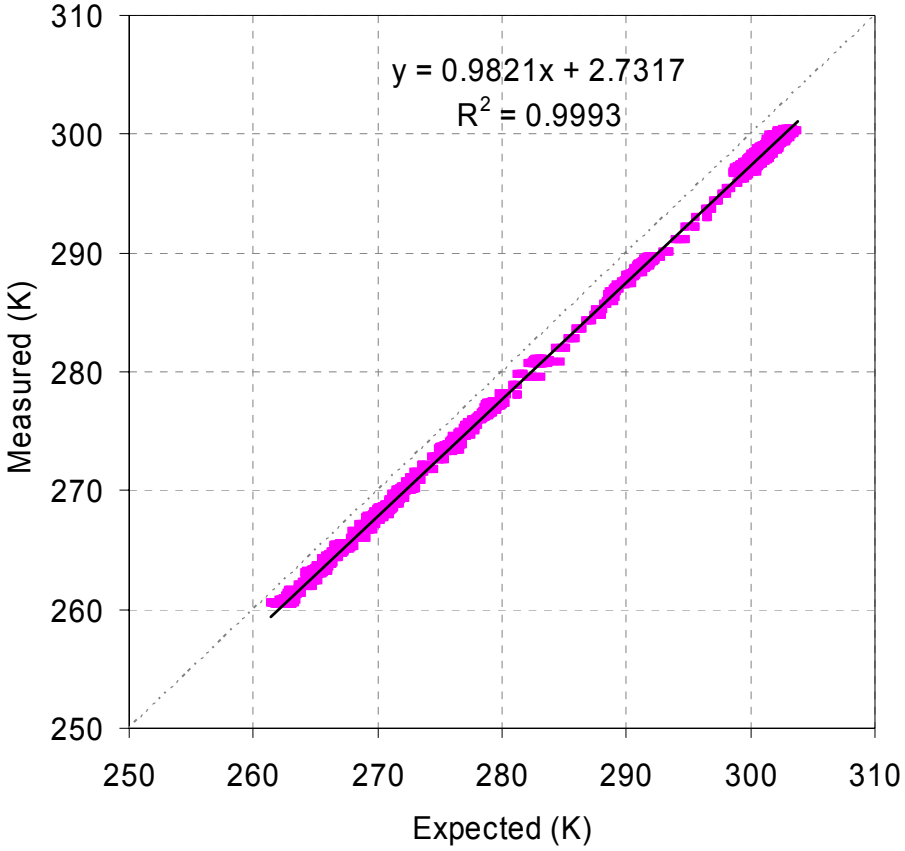

Figure 7 Receiver Calibration curve (L band – H polarization).

At the end of these tests, a calibration curve was computed for both radiometers. The linearity was well confirmed in the temperature range investigated (240 – 340 K) . For example the calibration curve for L band H polarization is represented in **Figure 7**, similar results were obtained at other frequency/polarization.

Calibration of the whole system including the antenna and connecting lines with external reference targets.

Calibration of the radiometers, including the antenna and the connecting circuits, was carried out by observing stable extended targets with known characteristics that were

sufficiently stable in brightness temperature and large enough with respect to the HPBW antenna.

Three types of targets were selected:

1) hot target: the anechoic chamber of the EMSL (European Microwave Signature Laboratory) at the Joint Research Center (Ispra),
2) cold target: clear sky
3) medium temperature target: calm water

The measurements at EMSL were carried from October 5 to 7, 2004. The instruments were installed in the middle of the chamber with the antennas directed towards the absorbing walls (Figure 8). The temperature of the chamber could not be set at a prefixed value, but was carefully monitored during the experiments by means of a calibrated infrared camera that observed the same area of the antenna footprint.

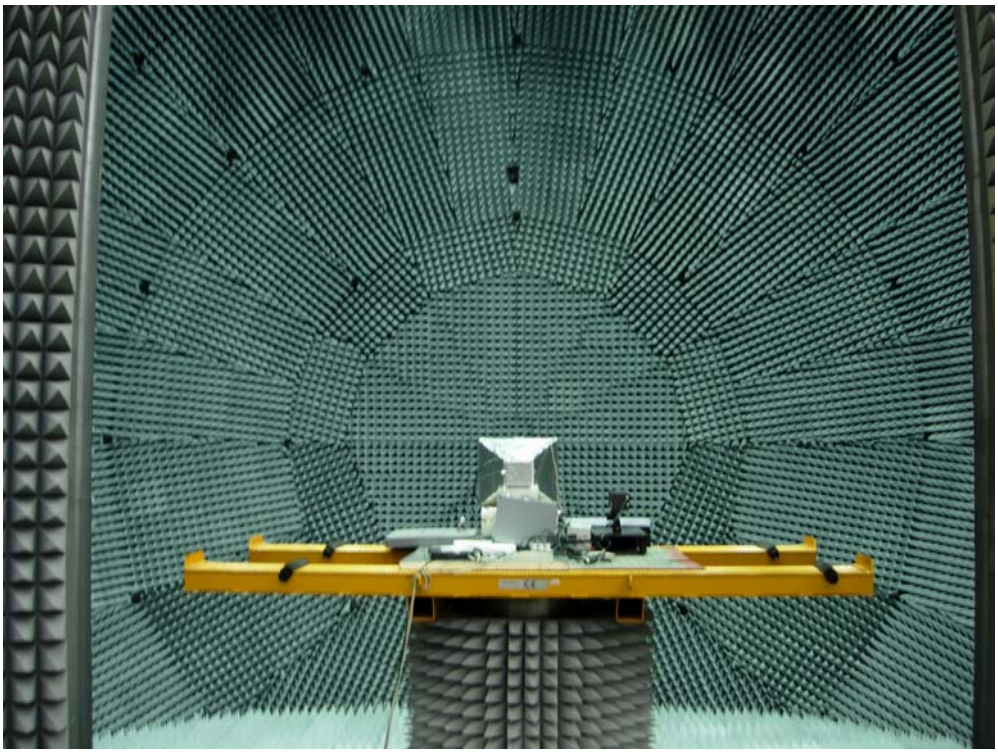

Figure 8. JRC set-up

The absolute accuracy in the temperature measured by a spot infrared radiometer and by a thermal infrared camera was ± 0.1 K. Chamber temperatures measured during the tests for the entire period ranged from 291.5 to 294.5. The temperature of the room walls was homogeneous in space and stable over more than one hour. For example, measurements carried out in thermal equilibrium for 140 minutes exhibited a mean value of the chamber temperature of 291.9 K with a standard deviation of 0.11 K in space and of 0.07 K in time (Figure 9). The eccosorb panels used at JRC were VHP 18 Emerson & Cumming model (pyramidal panels). Depending on the incidence angles the value of the reflectivity ranged from –40dB to – 25 dB at L-band and from –50 dB to –30 dB at C band. The corresponding minimum values of emissivity were, respectively, 0.997 and 0.999. This corresponded to an error of less than 0.1% in the computation of the the brightness temperature.

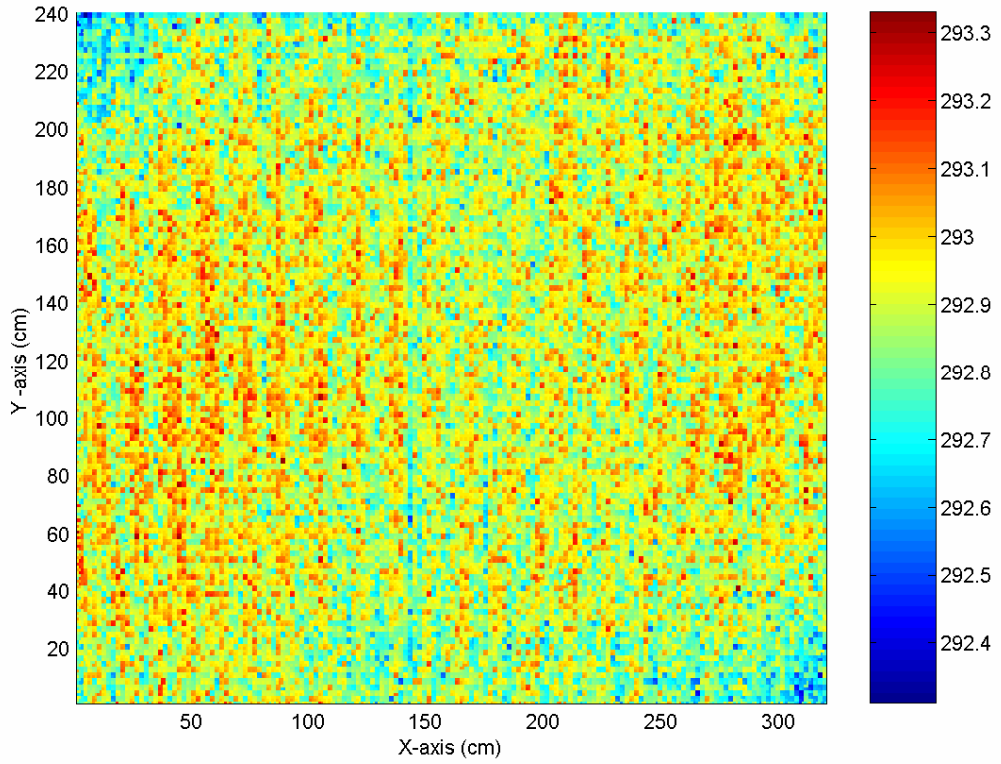

Figure 9 The infrared temperature of the anechoic chamber measured by the AGEMA infrared camera

An example of the measured brightness temperature at both L and C band, IR temperature measured by Everest infrared radiometer and EMSL thermal camera as a function of time is shown in Figure 10. The integration time was 1 second. The corresponding statistical parameters of Tb and Tir, measured in thermal equilibrium condition for a period of 140 min, are reported in Table III.

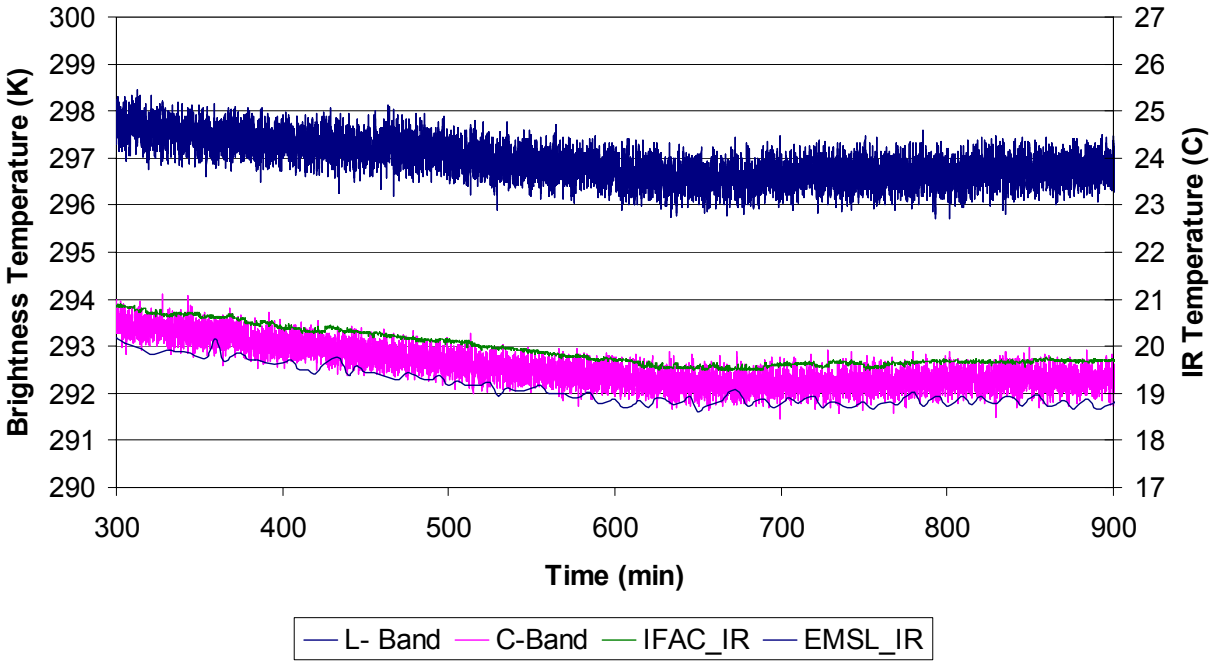

Figure 10 Measured Tb (L –blue , C-pink) and Infrared temperature at normal incidence (Everest = green , Agema =blue) as a function of time

Table III

	L- band	C-Band	Tir - everest	Tir - EMSL
Mean	296.63	291.73	292.61	291.82
Max	297.60	292.40	292.74	292.06
Min	295.71	291.00	292.47	291.62
Dev.st.	0.26	0.19	0.06	0.10

At the end of these tests we found that the measured brightness temperature indicated the need for a correction equal to - 4.7 K at L band and to + 0.2 K at C band with standard deviations (for τ = 1 sec) of respectively 0.26 K and 0.16 K.
It should be noted that the rather high value for the correction factor at L band is due to the higher value of the losses introduced by the antenna and by the cables as described by equation 2.

Clear sky and calm water measurements were performed at a lake close to Firenze, Italy. The instruments were placed on a platform positioned on a cherry picker (Figure 11); the truck was located near to the shore, and the crane was extended 10 m away from the shoreline at an height of 2 meters above the surface . Measurements were carried out at an incidence angle varying from 30^o to 140^o with respect to the nadir in steps of 5°. The dimensions of the lake were wide enough to avoid contamination from the shore, except for observations carried out near the horizon from 80 to 100 degrees of incidence angles

The theoretical sky-brightness temperature value was computed by assuming a plan parallel “standard” atmosphere in isothermal conditions and in accordance with a method described in a recent study [6]. For a radiometer observing clear sky in the celestial northern direction at medium northern latitude, the theoretical brightness value at 1.4 GHz was found to be 3.7 K . At C band the value ranged from 6 K at zenith view to around 30 K when the radiometer facing the horizon (Figure 12). In this case the observation angle is defined as the angle between observation direction and zenith (i.e. for zenith observation this angle is equal to 0 degrees for horizon observation is equal to 90 degrees)

Figure 11 The experimental set-up for sky and water measurements

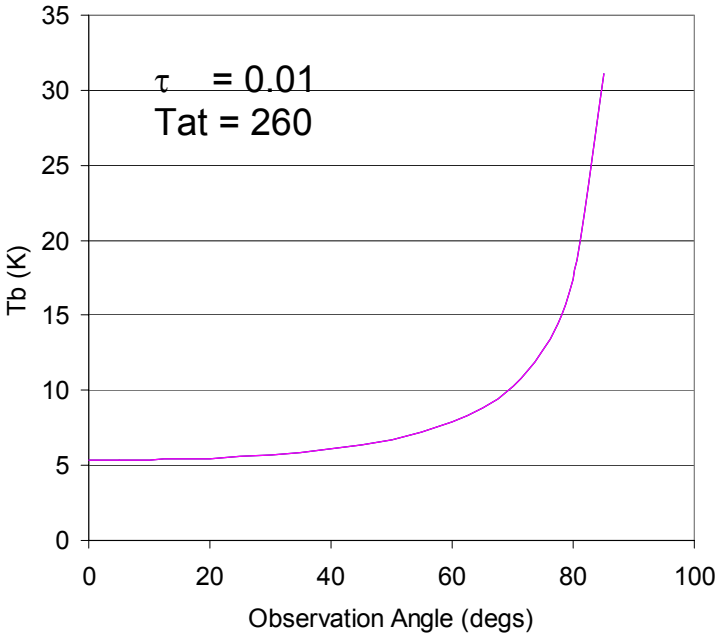

Figure 12 Theoretical Tb value of sky at C band as a function of observation angle

The emissivity of calm water was computed by means of the Fresnel equations [17].

The dielectric constant of water used for the computation was measured using an open coaxial probe and a network analyzer (Dielectric Probe Kit HP 85070A) interfaced with a computer in the frequency range 1-3 GHz. The results of these measurements are shown in **Figure 13**. Good agreement between the data and the classical Debye model was observed. The model value was used for the 6.8 GHz computations.

In order to compare theoretical and measured brightness temperature of calm water the data were pre-calibrated using a linear curve obtained from the measurement of clear sky and eccosorb.

At C-band (Figure 14) the measured Tb was in good agreement with the model except for measurements collected at a 35° incidence angle, since the signal was influenced by the contribution of the metallic wall of the truck on which the instruments were installed, and higher than a 75° incidence angle where the contribution of the background of the lake was not negligible.

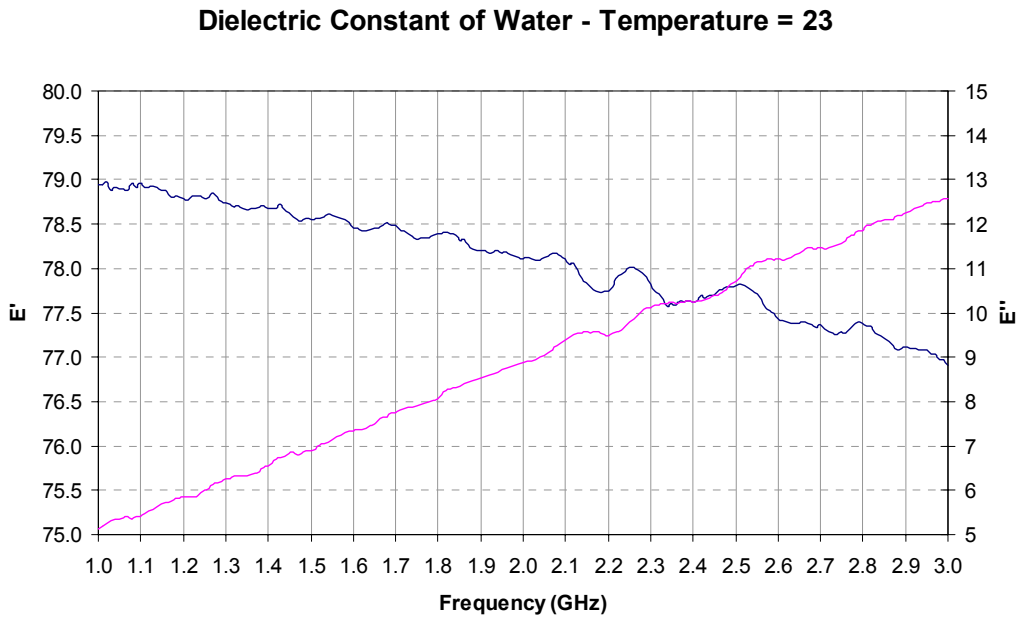

Figure 13 Measured dielectric constant of water

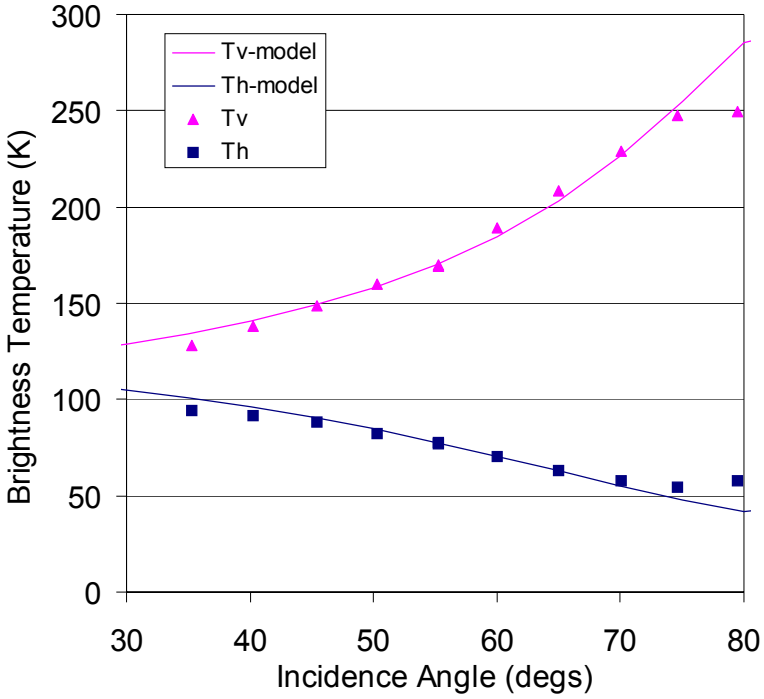

Figure 14 Measured and theoretical Tb value of calm water at C-band, H (blue) and V (pink) polarization

A comparison between measured and estimated Tb values at L-band in the whole incidence angle range is represented in Figure 15 (measurement in the 20° – 90° range were collected on calm water, while measurement in the 90°-120° range were collected on clear sky). In the figure we can note a great discrepancy between data and model which is due to the relatively large pattern of the L-band antenna .

Indeed, the Tb measured at a given incidence angle (θ,φ) is influenced by the emission at all others angles as expressed by the equation:

$$T_B(\theta,\varphi) = \frac{1}{\Omega_A} \int_{-\pi/2}^{\pi/2} \int_{-\pi/2}^{\pi/2} T_{AP}(\theta',\varphi') \cdot F_n(\theta-\theta',\varphi-\varphi') \ \sin\theta' \, d\theta' \ d\varphi' \quad \textbf{(6)}$$

Where:

$$\Omega_A = \int_0^{2\pi} \int_0^{\pi/2} F_n(\theta',\varphi') \sin\theta' \, d\theta' \, d\varphi' \qquad \textbf{(7)}$$

$F_n(\theta,\varphi)$ = Antenna Pattern

The Antenna pattern of the L-band pyramidal antenna is represented in **Figure 16**.

The estimated Tb was convolved, using equation (6), and compared to the measured one (Figure 17). In the figure we can observe that after these correction the measured and theoretical Tb were in closer agreement (the improvement is more evident at V polarization) even though some differences were noticed for incidence angles in the 70°-110° range.

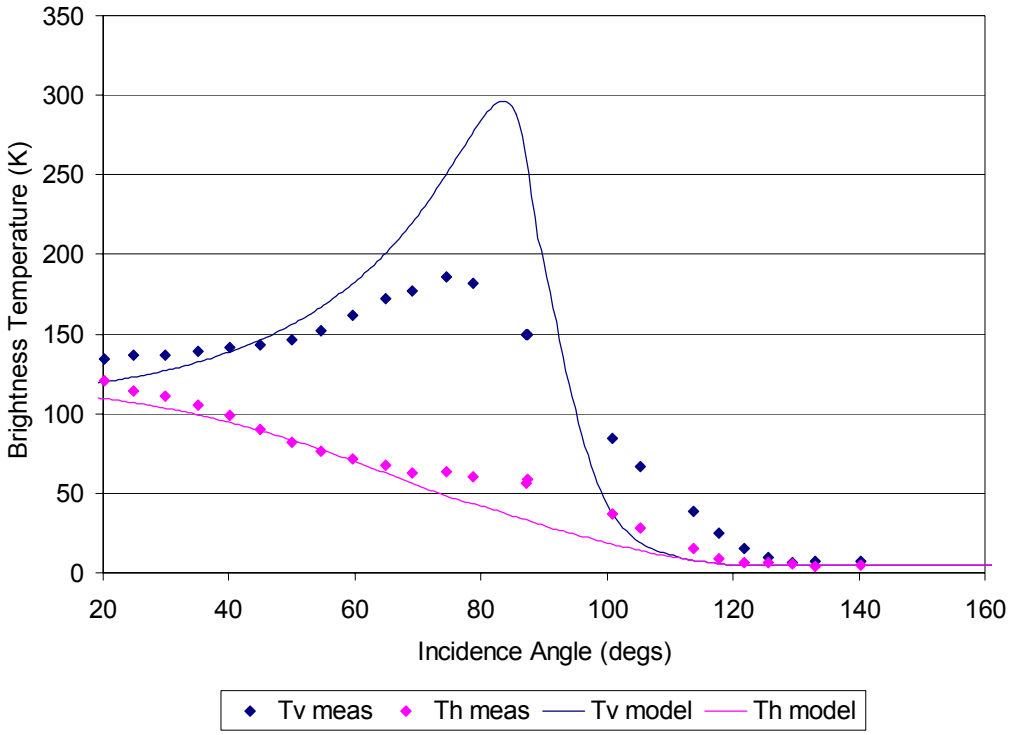

Figure 15 Measured and theoretical Tb value of calm water and clear sky at L-band, V (blue) and H (pink) polarization

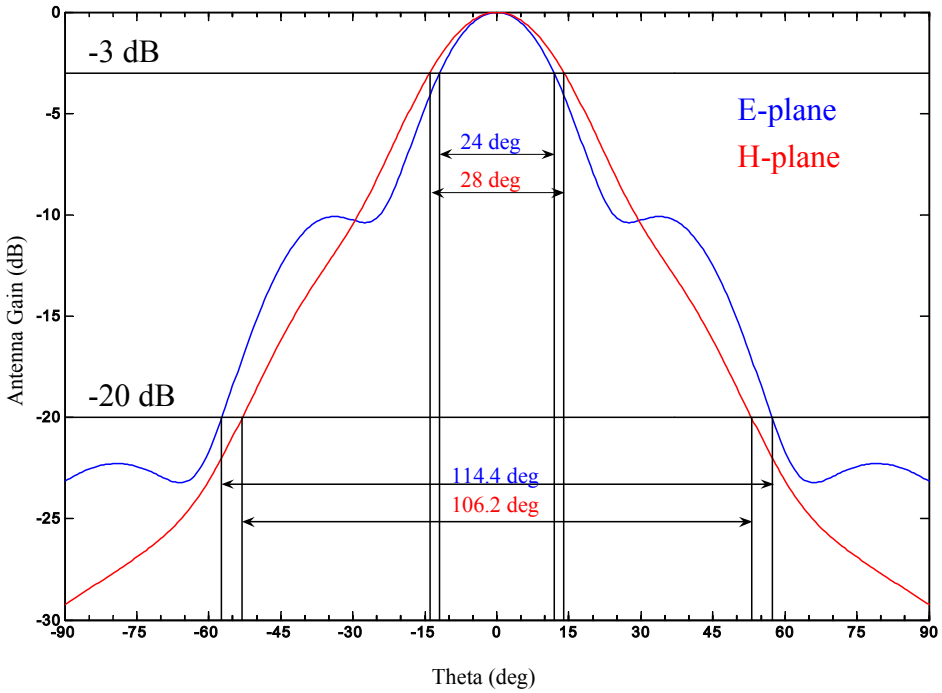

Figure 16 L-band Antenna pattern at E (blue) and H (red) plane

The residual discrepancies were due to the fact that the contribution of the background of the lake was not taken into account in the previous computation (i.e. we assumed a brusque transition between sky and water). In fact, if we add this contribution the difference between measured and theoretical Tb decreases (Figure 18).

At the end of the measurements collected on the three extended targets the calibration curves were computed. They are represented in Figure 19 at L and C band H polarization (these curves were computed for T_0=20°C). The results for V polarization were similar. The plots confirmed the linearity of both receivers over the entire range of Tb (10-300K). As expected, while the discrepancies between measured and expected values for the C-band were small (i.e. the receiver is almost self-calibrated), the losses introduced by the antenna and by the cables at L-band involved a rather high value for the correction factor. The latter was a function of temperature, and needed to be compensated in order to compute the “true” brightness temperature in accordance with equation (2).

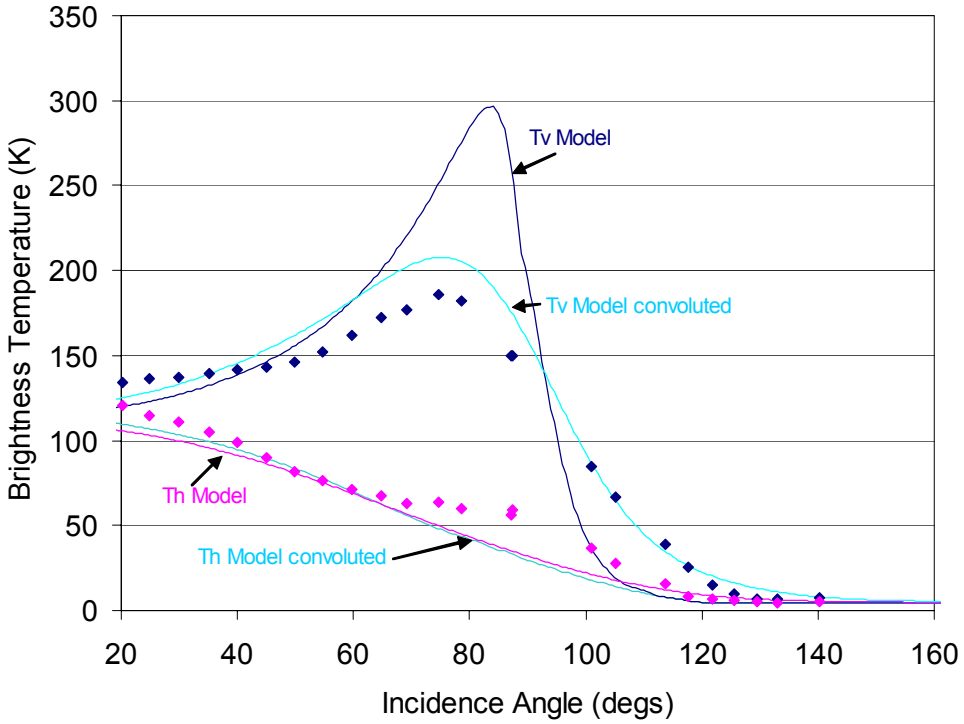

Figure 17 Tb measured, modelled, and modelled convolved at L band

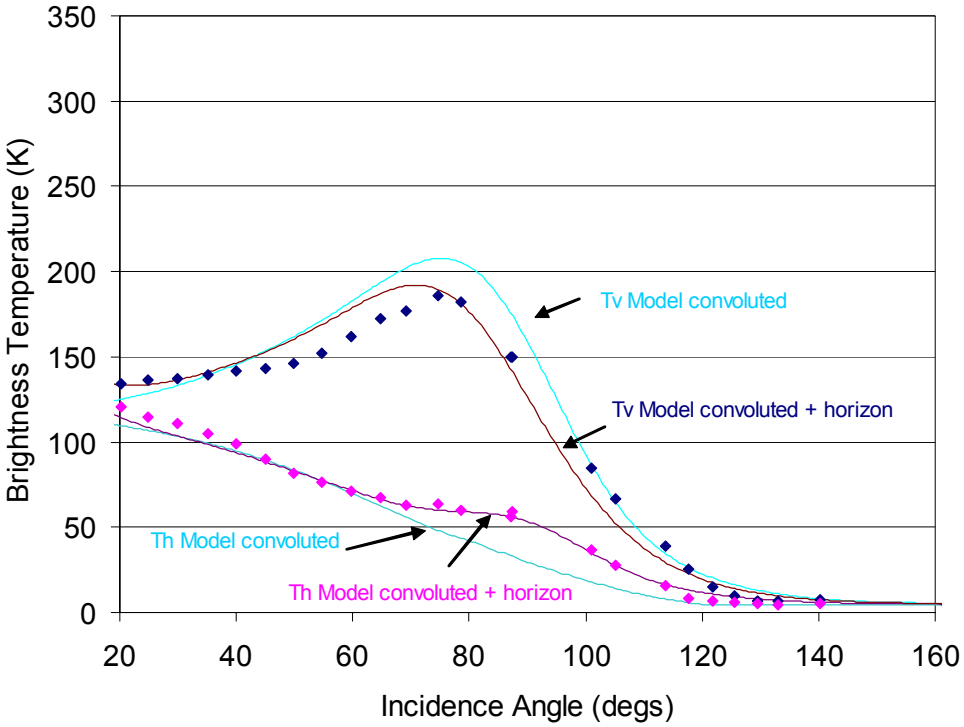

Figure 18 Tb measured, modelled convolved and modelled convolved including the effect of background at L band

At the end of the calibration phase, we concluded that the linearity of the receiver in the 10 – 300 K range was fully acceptable. The minimum detectable temperature variation of the radiometer (sensitivity) was 0.3 K with τ = 1 sec, and the accuracy (repeatability) was better than 0.5 K over a period of 30 days.

During DOMEX, clear sky measurements were periodically performed in order to control the calibration process. At the end of the DOMEX campaign, other receiver and absolute calibration tests were carried out. The measurements confirmed the results obtained prior to the experiment. Indeed, the measured brightness temperature of free water and clear sky was found to have the same value, with an uncertainty of < $\pm$ 0.3 K. For example the measurement collected using the external target connected to the receiver input before and after DOMEX are represented in Figure 20.

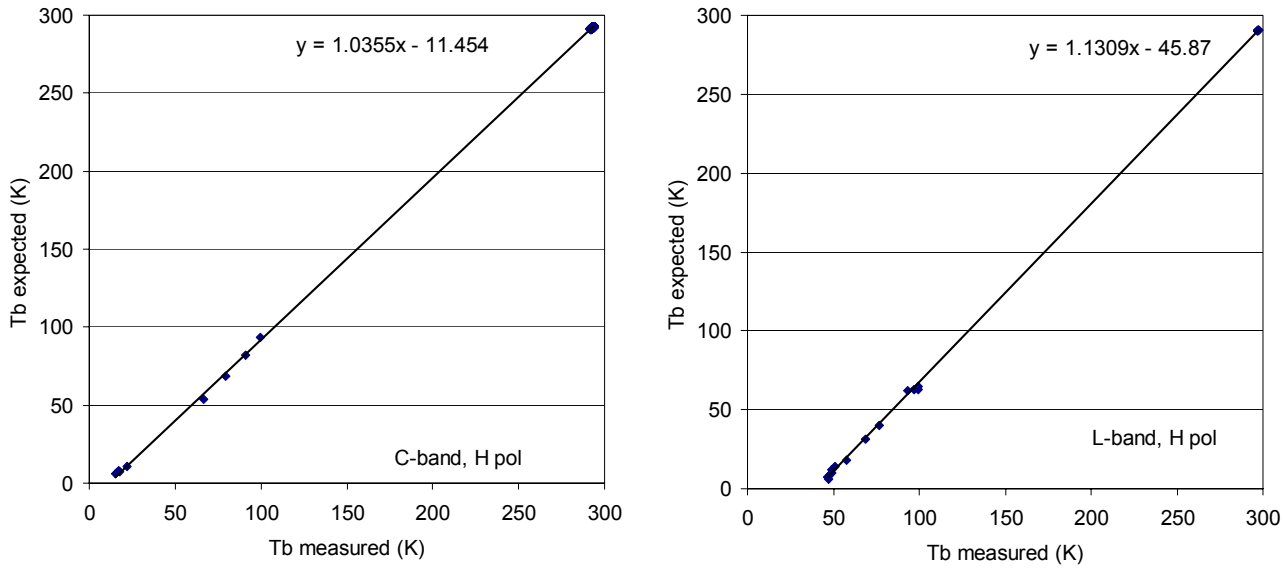

Figure 19 Calibration curves for the C (left) and L (right) band radiometer, H polarization

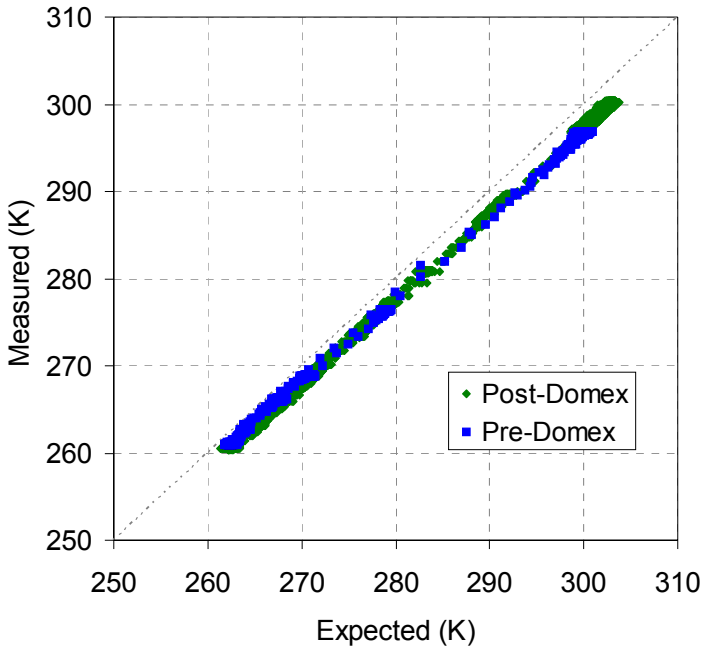

Figure 20 Measured and Expected Tb of the external load before (blue) and after (green) DOMEX

2.2 *Infrared Radiometer*

The radiometer used for DOMEX was a commercial infrared radiometer developed by Everest Interscience (Figure 21). Its main Characteristics are summarized in Table IV .

Table IV Infrared radiometer characteristics

Spectral Pass Band	8-14 Microns
Scale Range	-40°C to 100°C
Resolution	0.1°C
Accuracy	±0.5°C
Repeatability	±0.1°C
Field of View	15°

Calibration of the radiometer was performed by means of a calibration source produced by Everest. The source (Figure 22) consists of a target (a blackbody) and of a NIST thermometer for checking the temperature of the thermistor that is implanted in the middle of it. It should be noted that, since the thermometer provided by Everest can calibrate the sensor only in the 0/60°C range, the source was modified by IFAC by installing a new thermometer (PT 100 class A). Low temperature values (from -35°C to 0°C) were measured during the thermal tests, while values in the 18/22 °C range were measured at the IFAC laboratory.

Figure 21 The Everest Interscience infrared radiometer

Figure 22 The infrared calibration source

In addition, the data collected during the tests that were carried out at JRC were compared with data acquired by a calibrated infrared camera available at JRC (AGEMA 8-12 microns). The results are represented in Figure 23. The leakage of data in the interval around –20° C was due to a malfunction in the acquisition system.

As the diagram shows the linearity of the system was well confirmed in the –35° + 25° C range.

The calibration curve is expressed by the equation:

Tirc= 1.0472 Tirm - 1.462

In Tirc and Tirm are, respectively, the measured and the calibrated infrared temperatures. Calibration checks, performed after and during DOMEX using the calibration source, confirmed these results.

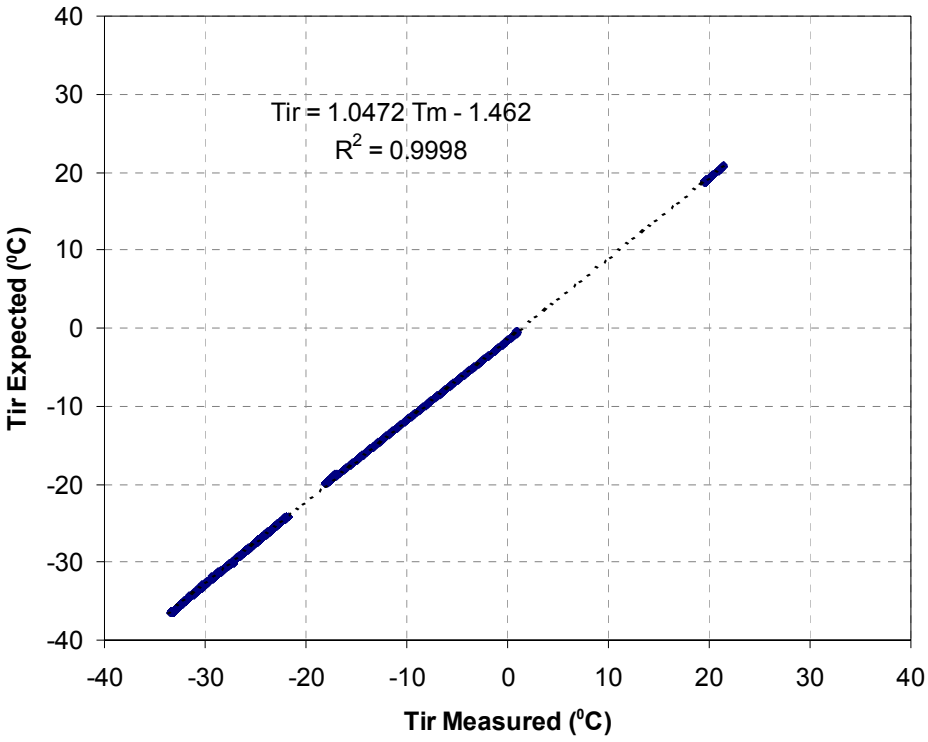

Figure 23 Expected versus measured Infrared Temperature

2.3 *Platform and Thermal Tests*

2.3.1 The platform

An important technical activity that was carried out within the framework of the DOMEX project was the development of a mechanical platform on which the instruments were installed. The layout of the platform is shown in Figure 24.

The platform provides for two fundamental aspects:

1. Thermal protection of the equipment
2. Incidence and azimuth angular scanning

As far as the first point is concerned the platform was designed by taking into account the Dome-C climatic conditions.

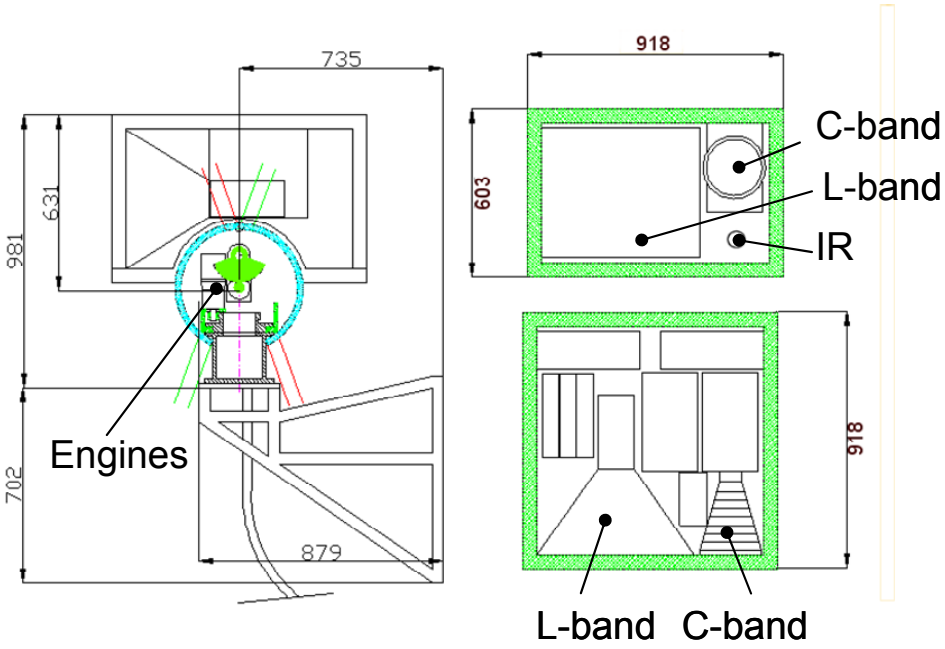

Figure 24 layout of the platform

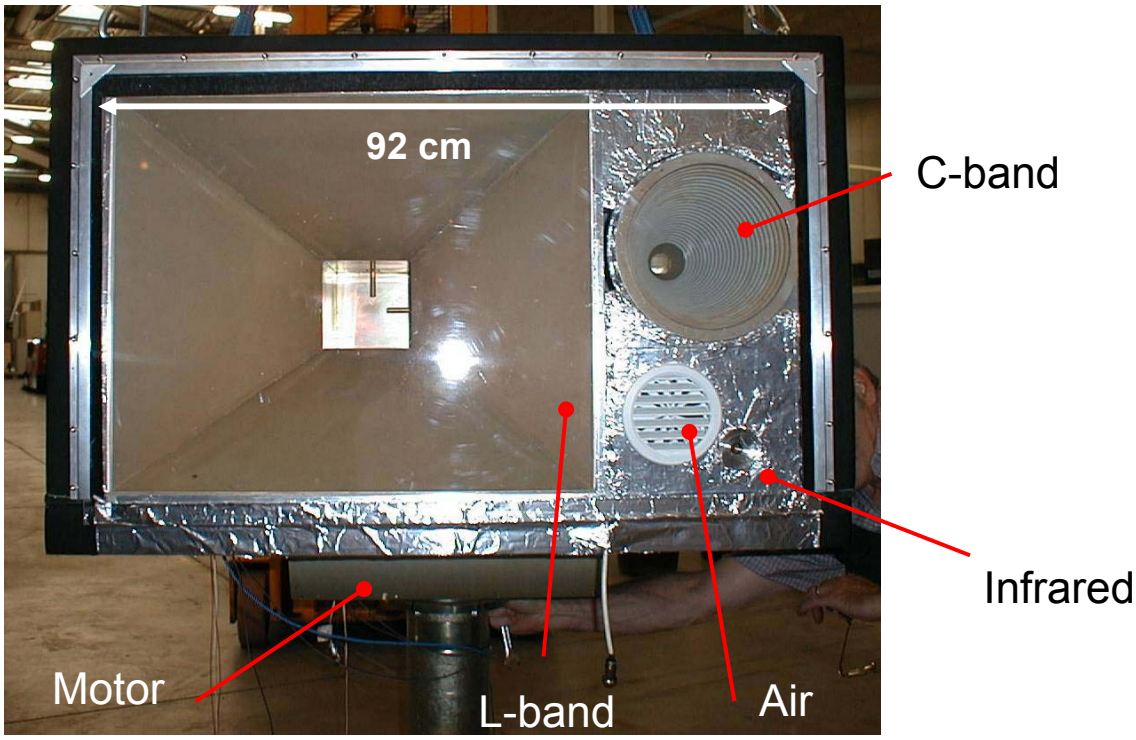

Figure 25 The platform

The microwave and infrared radiometers and the electronics (including the motors and the acquisition system) were placed in a special box installed on the mechanical platform. The walls of the box consisted of insulated material (**insulated panels** in reinforced resin with fiberglass (temperature range -80°C to +130°C, relative humidity around the 100%), for more information please refers to http://www.coldbox.it/inglese/pannelli/home.htm).
. Observations were carried out through a window sealed with a low-loss sheet of polystyrene, the attenuating properties of which were known [16]. The box was thermo-controlled in order to obtain an internal working temperature of about 0 ^{o}C.

The platform was designed in order to have an elevation angle of from –70 to 70 degrees from the horizon and an azimuth variation of about 200 degrees. The movements were regulated by two step-motors controlled, by means of a digital interface and using the same software that provides for the acquisition of the radiometers.
The front part of the platform is represented in Figure 25.

2.3.2 Thermal Tests

Thermal tests on the platform were, carried out prior to DOMEX, were conducted in two different phases:

1. in phase 1 microwave and infrared radiometers as well as the electronics were tested at an operational temperature of 0°C
2. in phase 2 the entire set-up was tested under simulated Dome-C thermal operational conditions.

Phase1:

Microwave Radiometers:

The objective of these measurements was to verify the performance of the radiometers at an operational temperature of 0 °C. In particular, long term receiver stability was controlled and receiver total gain (which varies with changes in the temperature) was adjusted in order to obtain a correct level value at the A/D input. Internal and external receiver temperatures were measured in several points during the experiment.

Platform:

The aim of these measurements was to test and calibrate the thermal control system and to verify the correct operation of the acquisition system and platform motors. In particular, the control concerned, the power necessary for the heater system to obtain an internal box temperature of 0 °C, and to maintain this temperature once that the instruments and motors have been turned on.

Phase2:

The tests were carried out from 19 to 23 July 2004 in a thermal chamber made available by Galileo Avionica – Firenze. The chamber measured 250x290x300h cm^3 , and could operate down to a minimum temperature of –70°C with an accuracy of 1° C. A temperature speed varying from 2 °C to 0.1 °C /min could be selected. The equipment was installed as illustrated in Figure 26, which also shows the position of the temperature probes installed to control the temperatures of the chamber, panel, upper part of the box , and motors.

Several phases were individuated during the tests: cooling, heating and equilibrium phase, During the cooling phase the chamber temperature was set at -45 °C and after a period of about 24 h the temperature inside the box reached thermal equilibrium (on 20/07 at 15:00 h). The chamber temperature was maintained at -45 °C and the heating system was switched on until the internal temperature of 0° was reached. At that point the radiometer were turned on and the chamber temperature was varied in order to simulate the daily temperature variation of Dome-C (i.e. a variation of about 12° around a mean value of -25°).

At the end of the tests, we concluded that the equipment (radiometers, PC, motors) did not exhibit functional problems after a storage period at –45 °C and that the system was ready to operate in the Antarctic environment.

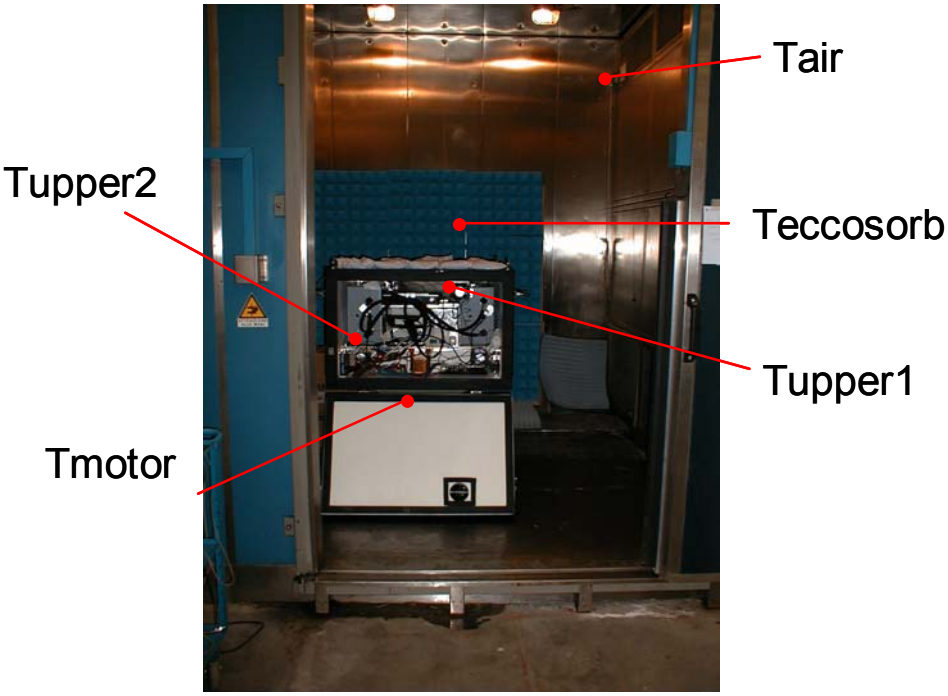

Figure 26 Setup used during the thermal tests at Galileo Avionica

3.0 The Experimental Campaign

The DOMEX campaign was carried out at Dome-C Antarctica from 4 December 2004 to 2 January 2005. The campaign was conducted by :
Dr. Giovanni Macelloni - IFAC – CNR (Firenze-IT) , person in charge of the project and Dr. Anselmo Caganti – CVA –Arabba (Belluno-IT) who was responsible for the snow measurements.

3.1 *The Dome-C station*

The base was located on the top of the Dome-C in the middle of the East Antarctic plateau, 1,100 km inland from the French coastal base of Dumont D'Urville and 1,200 km inland from the Italian coastal base of Terra Nova Bay. An overview of the area is shown in Figure 27. Two main spots are distinguished in the photo: the summer station which consisted of several building (the total covered area is almost 1,500 m^2) and has been fully operational since 1995 and the winter station which has been opened in February 2005. The latter station significantly increases the potential of this site since experiments can now be performed all year round. Other buildings and constructions are located at a maximum distance of about 1 Km from the bases and are used for scientific experiments in several fields (e.g. glaciology, astrophysics, seismology and atmospheric science). The tower where the platform was installed is recognizable at the upper left corner of the photo. The red line indicates the protected area where the snow was pristine and undisturbed by human activity.

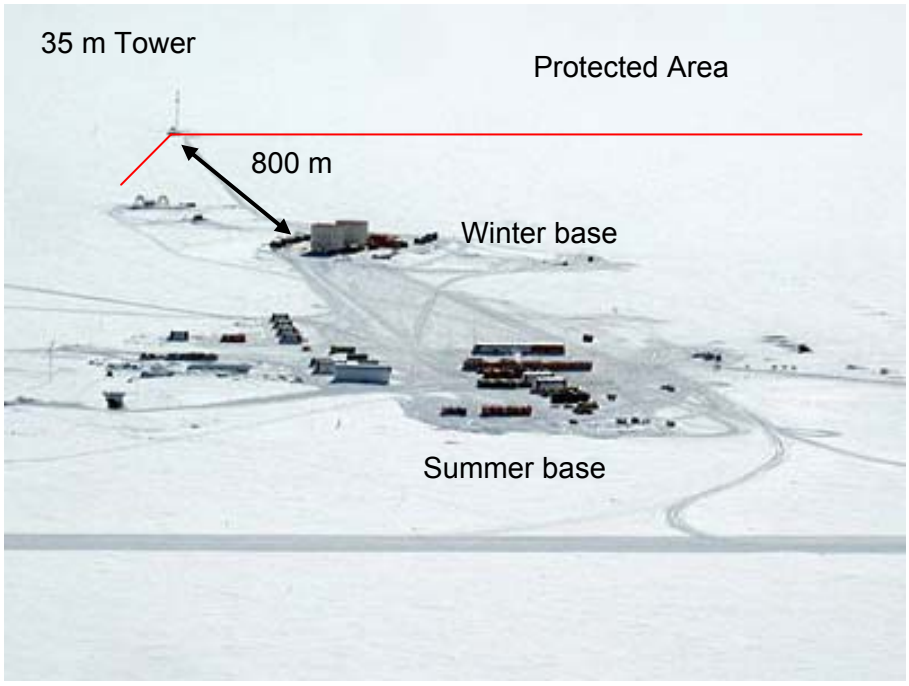

Figure 27 Aerial view of the Dome-C area.

3.2 *Tower measurements*

The box containing the microwave and infrared instruments was placed on the observation tower, that was originally installed for the calibration of optical space-borne sensors [19][20].

The 4 corners of the tower point north, south, east, and west and the box was installed on the north-west side looking out over at pristine snow as facing in the opposite direction with respect to the station where possible sources of RFI were located

Indeed, no RFI were registered during the experiment.

The system was positioned at a height of 13 m from the snow surface. This height was computed on the basis of the area observed by the antenna, the duration of the observation cycle, and in order to reduce the tower effect on the field of view of the radiometers. More details are contained in the Campaign Implementation Plan (CIP), a document of the project. An overview of the installation on the tower and a zoom where the box and the hocking system were highlighted are represented in Figure 28.

The system was prilimary tested for 2 days; data were then collected for 20 consecutive days 24 hours/day, at different incidence angles, θ, within the SMOS range (30° - 70°) and over a span of 120° in azimuth. Periodic observations of the sky were performed during the observations in order to check the calibration of the instruments. The foot-print (HPBW) ranged from 10x20 m^2 at θ = 20° to 10 x 700 m^2 at θ = 70° at L- band, and from 5x5 m^2 at θ = 20° to 5x50 m^2 at θ = 70° at C-band . The data acquisition and platform movements were automatic controlled by means of a PC placed in the box; the experiment was monitored remotely using a LAN connection.

Figure 28 Tower installation

3.3 *Snow Measurements*

In order to characterize on a monthly scale the spatial variability and the time stability of the surface layers of the test site, conventional snow measurements were carried out from the very beginning of the experiment. Some snow pits were dug manually in the area, as shown in **Figure 29** . The main pit (4 m deep) was excavated 150 m away from the tower just outside the unperturbed area, and three more pits 1 m deep were excavated on the site to test the homogeneity of the area on a scale of 1 square km. The strategy for describing the snow characteristics was based on the fact that the snow was very stable and no changes in the characteristics of the snow layers were expected during the experiment, except for the upper snow layer (the first 2-3 cm) which was monitored daily.

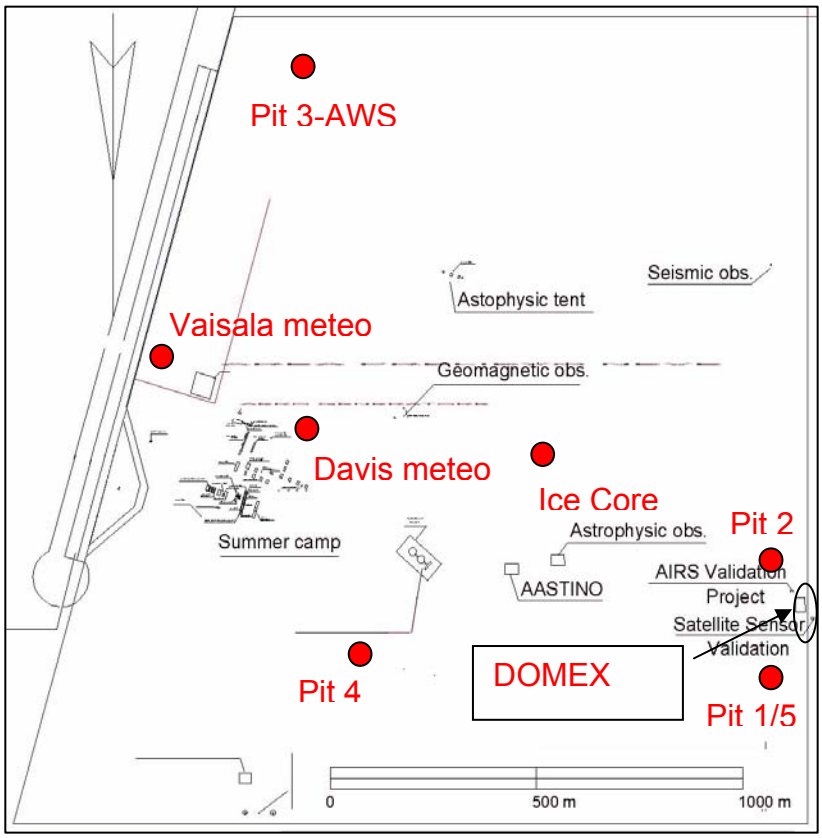

Figure 29 Location of the snow pits and meteo stations

The snow measurements were aimed to obtaining an accurate description of snow layering, by identifying the following parameters for each layer: temperature, height, density, hardness, grains shape and size (were measured using conventional “standard” methods [21]) and dielectric constant (measured using the Toikka snow fork). In addition, the main characteristics of an ice core 10 meters deep (diameter 10 cm) drilled during DOMEX, and were measured. Table V shows a summary of the measurements.

Day by day, systematic observations made of on surface roughness and of the meteorological conditions with special attention to snow depositions.

Snow temperature was also monitored by means of a thermal infrared sensor, and by a string of thermistors embedded into the snowpack at different depths down to 10m. It should be noted that the probes in the first 100-cm layer were embedded in the snow, whereas the other probes were placed in an existing hole. The hole was sealed and thermal equilibrium with the snow pack was reached a few hours after the closure of the hole.

Thanks to a researcher who was present in Concordia in the winter too, the snow temperature measurements continued during the austral autumn and winter, and likewise the systematic observations of the entity (thickness and snow water equivalent) and quality (Crystal typologies) of the snow depositions.

Table V Summary of the measurements and observations effected on snowpack at Dome C in the period 5-30 December 2004

SITE	DATE	DEPTH	MEASUREMENTS TAKEN
American tower 1 (AT1)	16-17-18-19/12/2004	400 cm	Stratigraphy Temperature every 10 cm Density in layers, density every 10 cm, density with Snow Fork Hardness indices (up to 89 cm)
American tower 2 (AT2)	23/12/2004	100 cm	Stratigraphy Temperature every 10 cm Density every 10 cm
Meteorological station (AT3)	24/12/2004	105 cm	Stratigraphy Temperature every 10 cm Density every 10 cm
Thermometric probes hole (AT4)	28/12/2004	108 cm	Stratigraphy Temperature every 10 cm Density every 10 cm Hardness indices

4.0 The Results

4.1 *Meteorological Data*

Meteorological data were automatically acquired by three meteorological stations installed in the area of Dome-C and represented in **Figure 29**: AWS, Davis weather station and Vaisala weather station. The main station was the official AWS station, which is part of Antarctic Automatic Weather Stations Project [22], located 2 Km distant from the base camp. These data were not available at Dome-C but they are freely distributed by internet and were downloaded at the end of the campaign. Moreover, during DOMEX other meteorological data were available from two stations managed by the PNRA. The data collected by the two PNRA stations were very similar, a maximum difference of 2 °C for air temperature, 1 mbar for pressure and 1 m/s for wind speed were registered. Indeed the data measured by the AWS exhibits big differences with respect to the others two: up to 10°C for temperature, 5 mbar for pressure and 4 m/s for wind speed. From the measurements collected during the campaign we conclude that the AWS data were not well calibrated (actually the precision of this station has not been checked for many years) and we refers to the average values measured by the other two stations.

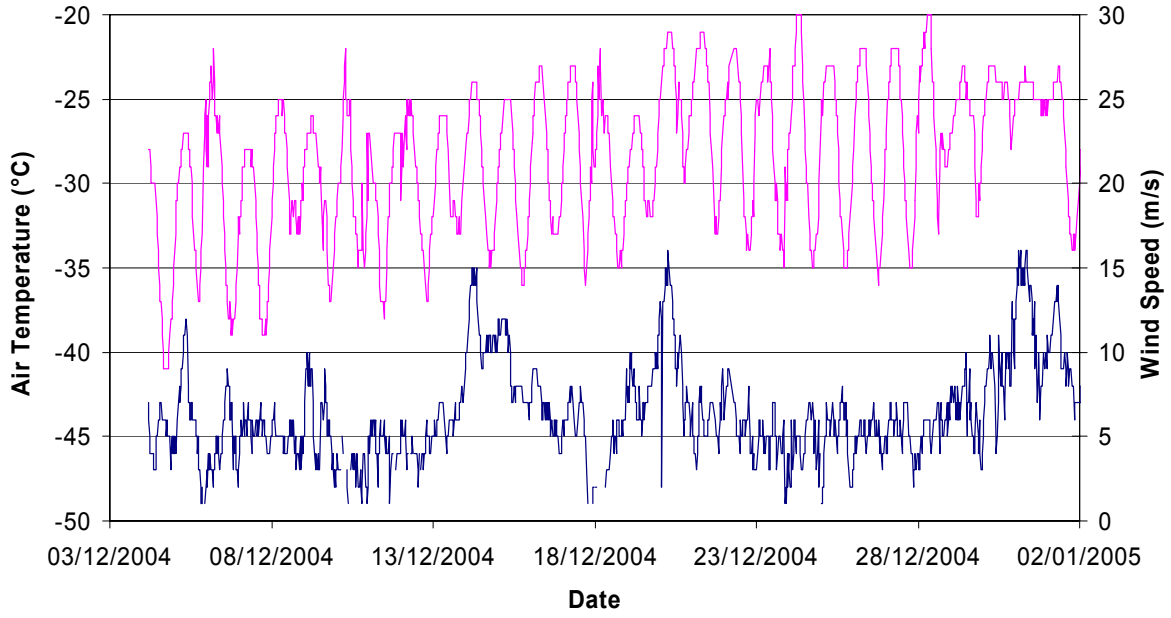

Figure 30 Air temperature (pink) and wind speed (blue) as a function of time

Figure 30 represents the air temperature and wind speed measured during the observation period. The mean daily value increased from -35°C to -25°C with a typical daily variation of around ± 7°C. Wind speed was in general lower than 7 m/s except for short period when values up to 10 m/s were recorded. Air pressure shows a mean value of 655 mbar with a fluctuation of around ± 7 mbar. The sky was in general clear (as typical in this period), light clouds occasionally occurred and only one snow event, with larger snow grain falling from clouds (0,5-1,0 mm), was registered on December 20th. It should be noted that at this latitude the majority of snow event is characterized by a sublimation of ice crystals (the dimension of the ice particle is of about 0,2-0,5 mm) in air. Deposition of snow on ground was limited to a few millimeters.

4.2 *Snow*

4.2.1 Snow depositions

The observations of snow depositions at Dome C (which were carried out from December 2004 to October 2005) indicated that the quantities were continuous but small. Snow depositions were observed on 85% of the days, but most of them had a thickness of less than 2 mm. Only in one case, in June, the deposition exceded 5 mm (Table VI). With regard to the quality of the depositions, these can be separated down into the following categories: precipitation crystals (crystals formed in the clouds), diamond dust (crystals formed in the atmosphere at very low temperatures), rounded grains (due to snow being transported by the wind), air hoar (crystals produced by sublimation of the aqueous vapour present in the air) and surface hoar (crystals sublimated on the snow surface).

Table VI Distribution of snow depositions at Dome C (values expressed in mm of snow)

	April	May	June	July	August	September
Tot Dep. mm	24,5	22,0	41.8	40.8	24.6	20.0
Dep. > 5 mm	0	0	1	0	0	0
Dep. 2-5 mm	4	0	9	8	4	3
Dep. <2 mm	25	29	14	22	25	25
Average density kg/m^3				90,95	112,79	72,88

The main characteristics of these crystals and their classification, according to the system proposed by Magono and Lee, are shown in Table VII. As regards the density of the snow depositions, the average values are about 90 kg/m^3, while the extreme values are in the range between 20 kg/m^3 (precipitation crystals) and 160 kg/m^3 (blowing snow).

Table VII Snow deposition typologies (shapes classified according to Magono and Lee) and maximum dimensions of crystals expressed in mm

Crystal typologies	Prevailing shapes	Maximum dimensions (mm)
Precipitation crystals	C2a + C1f	0,5-0,7
Diamond dust	C1e + C1g + N1e	0,2-0,5
Blowing snow	N/A (rounded grains)	0,1-0,2
Air hoar	N1a + C1f	0,5-2,0
Surface hoar	C1b + C1d + P1a	0,5-2,0

4.2.2 Snowpack

Snowpack structure

In summer, during DOMEX, the snowpack at Dome C has a succession of soft layers, that consist of kinetic growth grains alternating with harder layers of rounded grains. In the upper part of the profiles (generally down to a depth of 50 cm) the hard layers often have the typical appearance of wind crusts (very hard, with thickness values ranging from 0.5 to 1 cm) (Figure 31). At greater depths, the crusts tend to disappear and the hard layers are thicker and made of larger grains. In general, an activity of kinetic reconstruction of the grains is evident along all the profiles. This is due to the thermal gradient which, even if not particularly great, acts continuously through time. The water vapour flux is partially blocked by the presence of hard layers in which larger grains are generally found. The reconstruction which leads to the formation of large faceted crystals is active during the whole year, except in periods when the thermal gradient is reversed (end of February and end of September) and when the snowpack is in quasi-isothermal conditions.

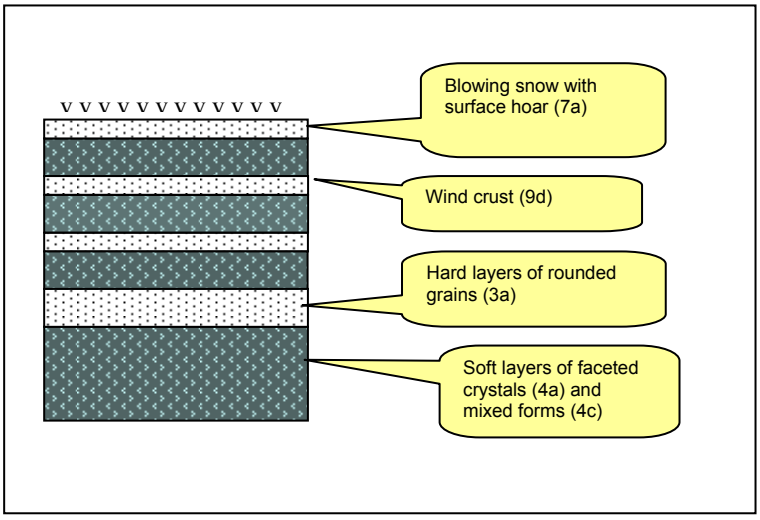

Figure 31 Scheme of the snow structure

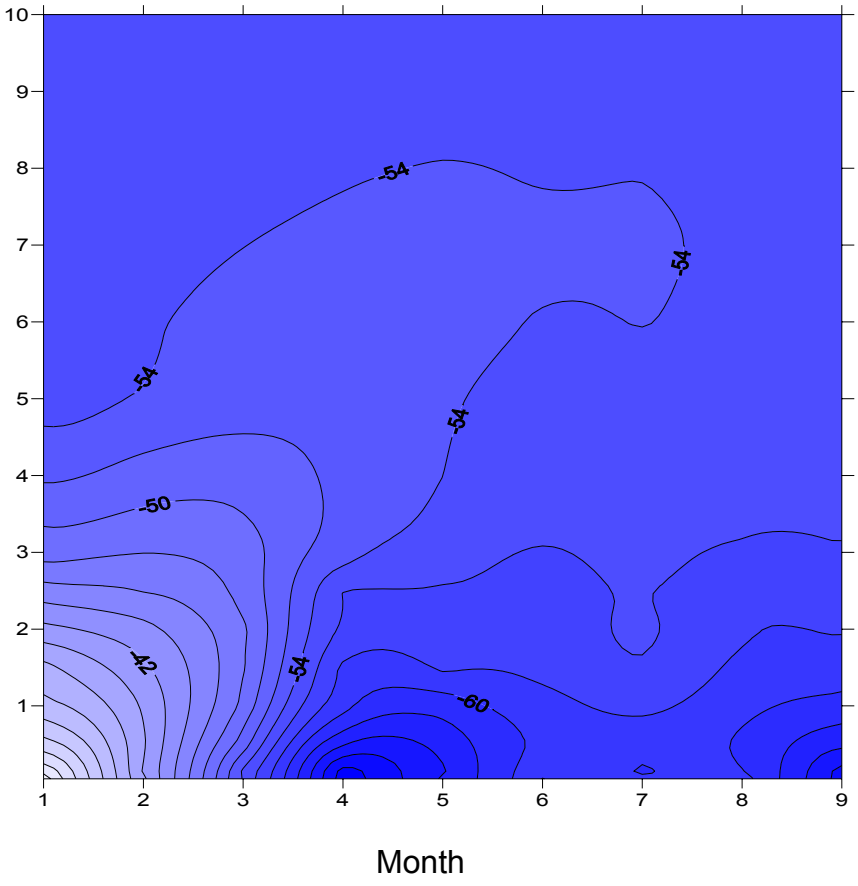

Figure 32 snow temperature as a function of depth and month (1 =jan, 2 feb., etc.)

During 2005, the new drop in temperature that occurred after the first half of August caused a secondary maximum of the positive thermal gradient (after the one in April) at the beginning of September (Figure 32).

Shapes and dimensions

According to the IASH classification [21], the kinetic reconstruction grains can be ascribed to mixed shapes (sub-class 4c) with dimensions from 0.7 to 1.5 mm, or to faceted crystals (sub-class 4a), with dimensions which can reach as much as 2.5 - 3 mm. These typologies of grains clearly predominate along all the profiles that we examined, and lend the snowpack an incoherent appearance. The presence of depth hoar (sub-class 5a) with crystal dimensions of 2-3mm in the rounding phase was noted in only one case (at the AWS site),nd can perhaps be attributed to the lesser accumulation which determines a higher thermal gradient. Surface hoar (sub-class 7a), almost always present on the snowpack surface has dimensions of about 0.5 mm. Wind crusts (sub-class 9d) were, instead, generally made up of small rounded grains with dimensions of about 0.2 - 0.3, whereas in the layers formed by rounded grains (sub-classes 3a and 3b), grain dimensions tend to increase up to a maximum of 0.7 mm. Table VIII provides a summary of the grain typologies identified, together with their measured dimensions (maximum dimension), as well as the estimated sphericalness and dendricity. Although cases of discontinuity exist, due to the succession of layers with different characteristics, in general it can be noted that grain dimensions increase at greater depths (Figure 33).

Table VIII Characteristics of the snow grain typologies observed (classification according to [21])

Shape	Class	Max dimensions (mm)	Sphericalness	Dendricity
V	7a	0,5	0,5	1,0
•	9d, 3a, 3b	0,2-0,7	0,9	0,1
⌂	4c	0,7-1,5	0,3	0,3
□ Λ	4a, 5a	2-3	0,1	0,1

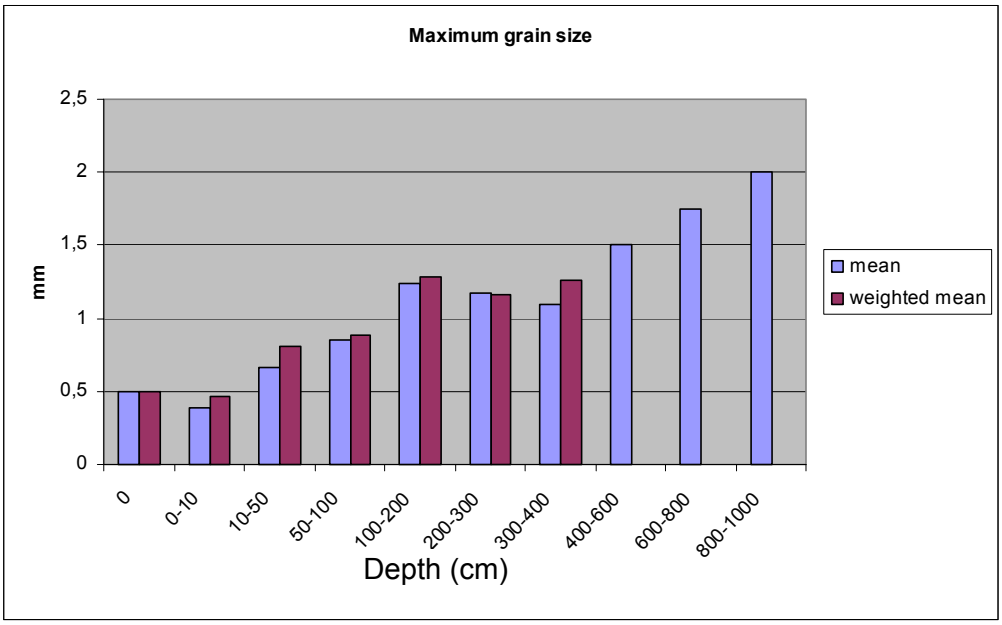

Figure 33 Mean grain size as a function of depth

Snow density

The snow density changed according to the characteristics of the layers and, in particular, depended on the typology of the grains which made up the layers. For this reason, especially in the first meter, the trend was rather discontinuous. Data gathered down to a depth of 10 m (data of snow profiles down to 4 m and core data from 4 to 10 m), showed layers composed of faceted crystals or mixed shapes with a density varying from 300 to 410 kg/m^3 as a function of depth (with minimum values of 260 kg/m^3), whereas the layers composed of rounded grains had higher density values, ranging from 370 to 510 kg/m^3 according to the depth (with maximum values of 520 kg/m^3). On average, snow density increased with depth, although in the first 4 metres, the densifying process was rather low and changed from 360 kg/m^3 in the first meter to 390 kg/m^3 in the fourth meter reaching 480 kg/m^3 at 8-10 m (Figure 34). Clearly, the process of kinetic reconstruction leading to the formation of large highly porous grains prevailed with respect to the evolution toward equilibrium forms and to the compacting action of wind. This lends a rather low cohesion to the snowpack also in the relatively deep layers.

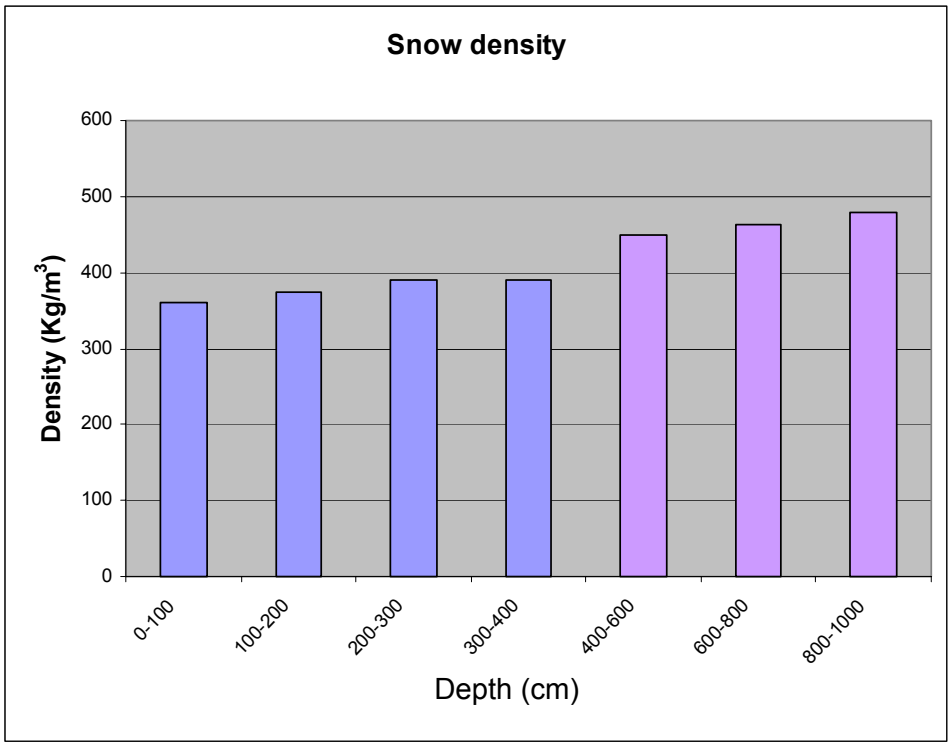

Figure 34 Average snow density as a function of depth

Snow temperature

Measurements collected from December 04 to October 05 shows that at a depth of 10 m, snow temperatures are stable at about -54.5/-55.0°C and are not influenced by seasonal variations. Nevertheless, conditions are already quasi-isothermal at a depth of 5 m, with maximum variations of 2-4°C. Seasonal variations are particularly evident in the first 4 m, where the differences between surface and 4m-deep temperatures can exceed 25°C. The thermal gradient is negative during the spring and part of summer, while it is positive during the rest of the year (Figure 35). The surface temperatures vary from maximum values of -20/22°C in November and December, to minimum values of -68/70°C which are reached in April. Daily variations occur only at 20-30 cm of depth during the spring and summer coinciding with significant variations in air temperature. Maximum daily variations occur in January and February, with values of 6-8°C at a depth of 5 cm and of 4-6°C at a depth of 10 cm . The temperature measurements, taken every 10 cm along the snow profiles, indicated – during DOMEX - a negative thermal gradient, decreasing according to depth from 0.193°C/cm in the first meter to 0.016°C/cm in the fourth meter. (Figure 36).

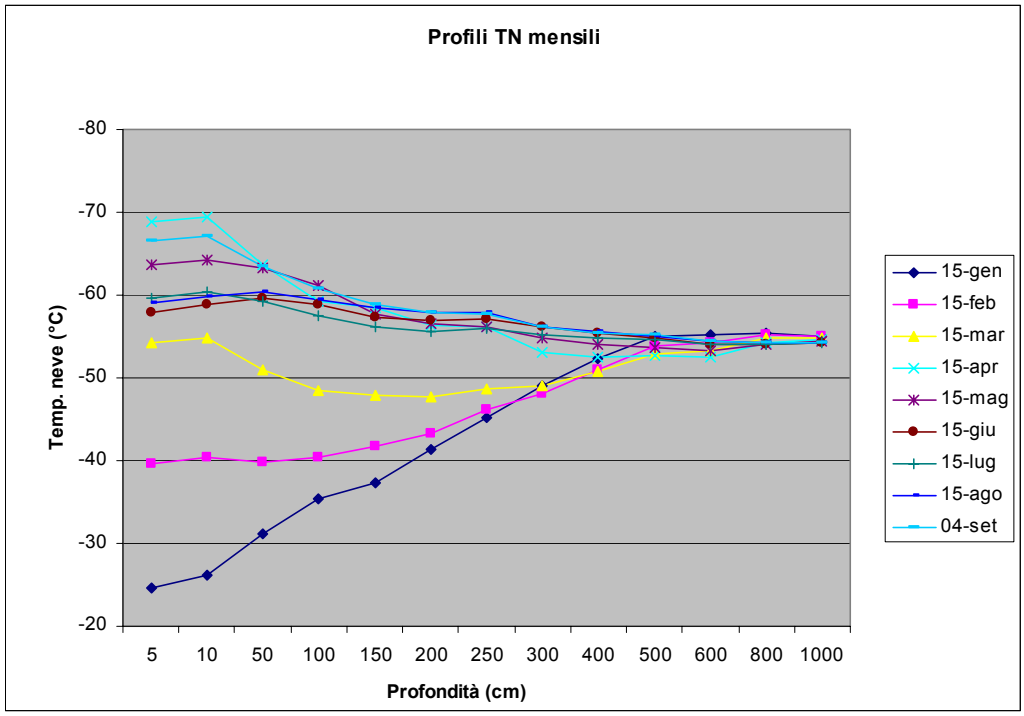

Figure 35 Snow temperature as a function of depth measured at different DOY

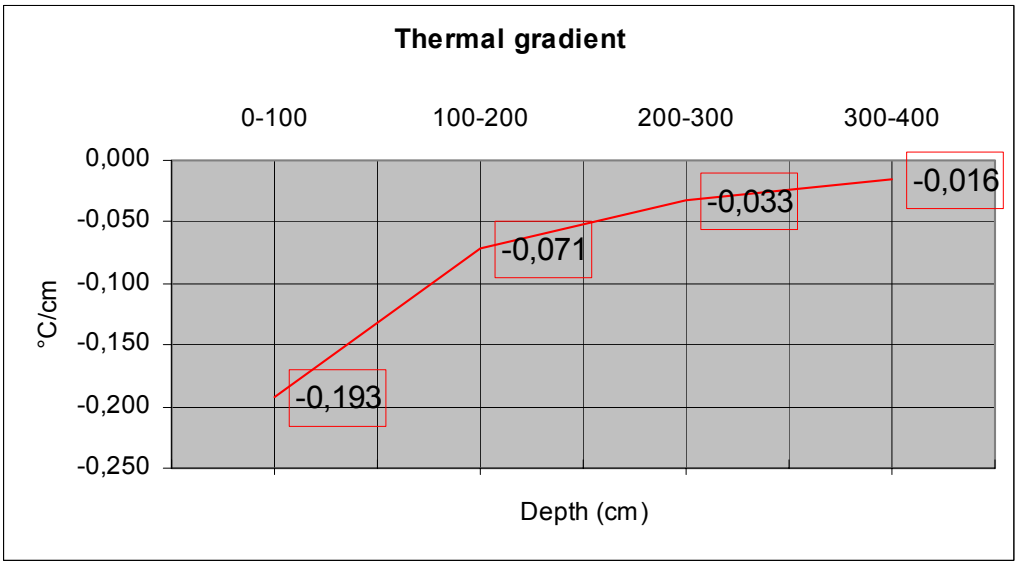

Figure 36 Thermal gradient as a function of depth measured during DOMEX

Spatial variability

The snowpack had a very similar general structure in all four of the sites surveyed. The main parameters (shape and dimensions of gains, density, thermal gradient, hardness,

etc.), at equal depth, exhibited slight variations which were part of the normal variability in nivological parameters over uniform areas. Thus we can say that, at Dome C, the snowpack has low spatial variability.

4.2.3 Dielectric Constant

The dielectric constant was measured using a commercial electromagnetic probe (a Toikka Snow Fork) designed to operate in extreme conditions. The sensor was a steel fork used as a microwave resonator in the 500 to 900 MHz frequency range and measures the following electrical parameters: resonant frequency, attenuation and 3-dB bandwidth. The results of the measurements were used to calculate accurately the complex dielectric constant of snow. Furthermore, the liquid water content and density of snow were calculated using semi-empirical equations.

The real part of the dielectric constant, measured at the main pit, and the corresponding calculated snow density are presented in Figure 37. The density is in good agreement with that measured using conventional method.

The measured imaginary part of the dielectric constant is not represented since the results obtained were an order of magnitude greater than those expected from model simulations (references). It should be noted that similar results were obtained from other research projects carried out in recent years in Antarctica [23]-[24].

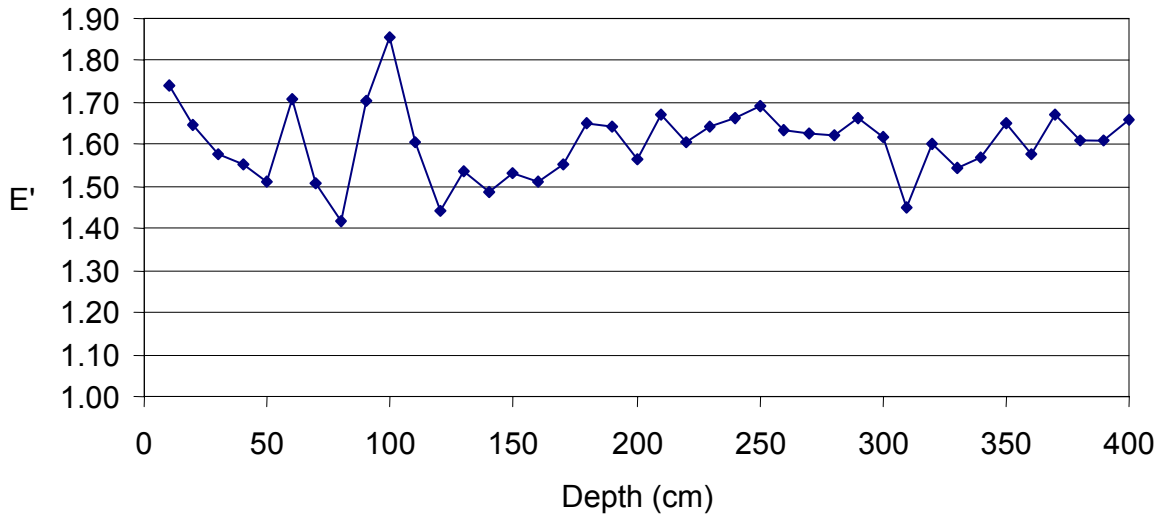

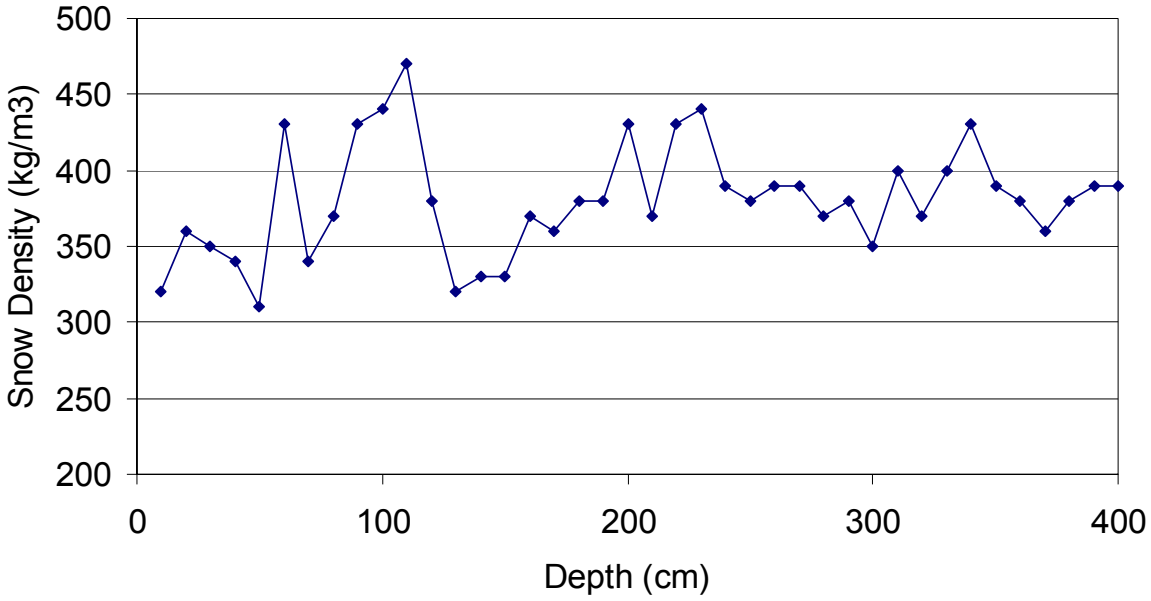

Figure 37 Real Part of dielectric constant of Snow (top) and snow density (bottom) measured as a function of depth for the main pit.

4.3 *Microwave and Infrared radiometers*

The Tb acquired during DOMEX at L and C band are represented as a function of the incidence angle in Figure 38. From the figure we can note that, for each incidence angle, the signal exhibits a spread around an average value. In addition, it should be noted that the data are almost homogeneously distributed over the angular range. This last fact is due to a malfunctioning of the position system that generates an absolute difference of ± 3-4 degrees (unstable) in incidence angles compared to the nominal position set in the system. These discrepancies were measured using an external independent inclinometer, that was added in the platform. In the results we refer to this measurement.

In order to estimate the stability of the average value, the Tb measured at a time difference of two weeks was represented as a function of incidence angle in Figure 39 .
From this figure we could observe that the average trend of Tb at L-band versus the incidence angle remained constant as well as the dispersion of data. Instead at C-band the

data dispersion and Tb trend versus the incidence angle were similar but the average value increased from December 14 to December 28. This rise was related to the increase in the air and snow temperatures during the period in which the Tb daily average values increased, respectively, from -28 °C to -24 °C and from -29.9 °C to -26.7 °C.

With the aim of evaluating the homogeneity of the observed area, data were collected at different azimuth angles. For example, data collected at 45° incidence angle are represented as a function of azimuth angles in Figure 40. While Tb remained almost constant in the -30 , 30 azimuth range, some discrepancies were observed at -60 and 60 degrees. In effect, we discovered that, during construction of the tower, the snow characteristics were modified in some parts of the area observed by the radiometers. In particular, to install the connecting rods of the tower (placed at the four corners) the builders put in wooden beams at approximately 2 meters below the surface. In these parts the snow density was double of the normal snow density (i.e. 800 kg/m^3 , instead of 400 kg/m^3).

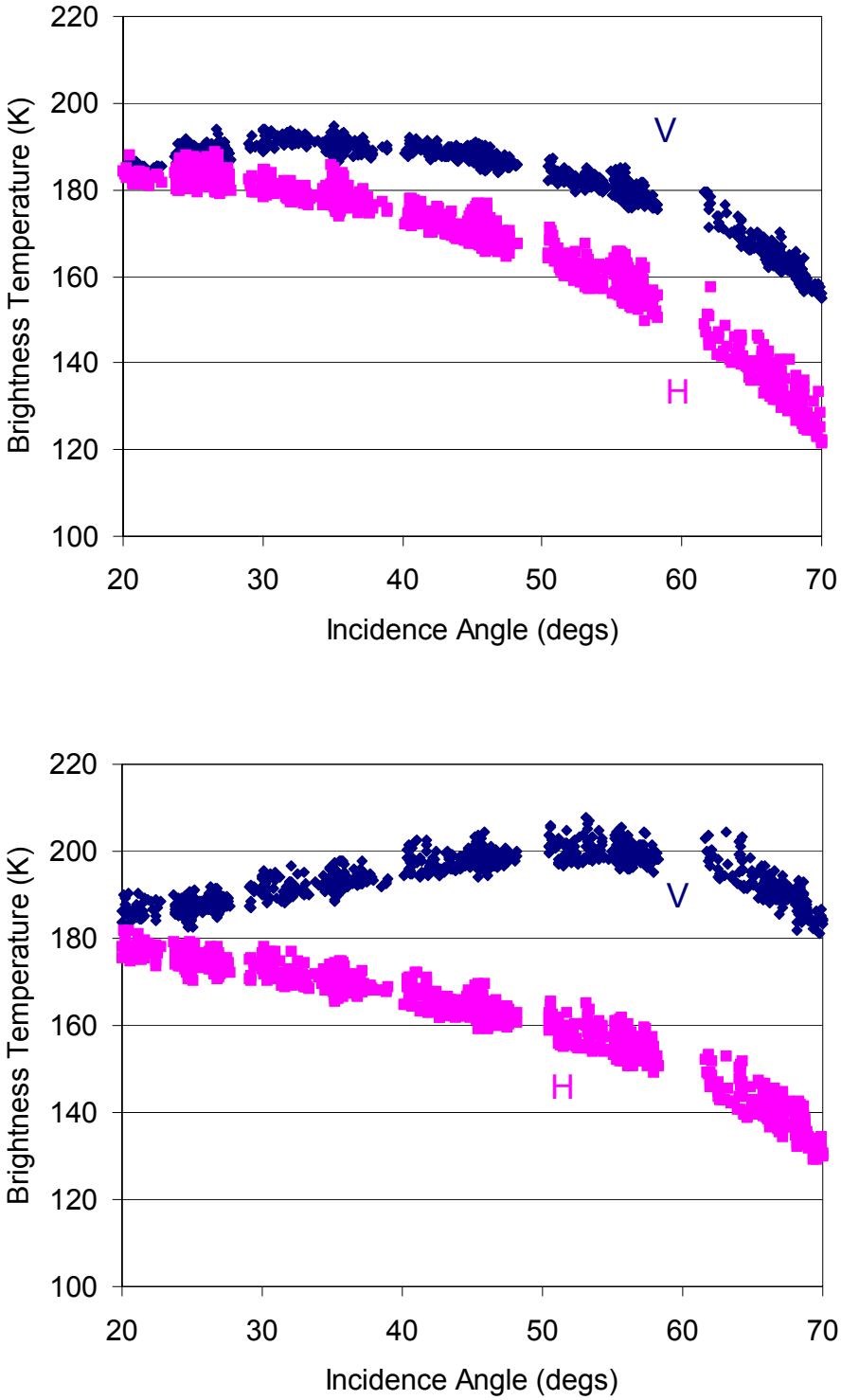

Figure 38 Tb at L (top) and C (bottom) band (V and H polarization) measured during DOMEX as a function of time

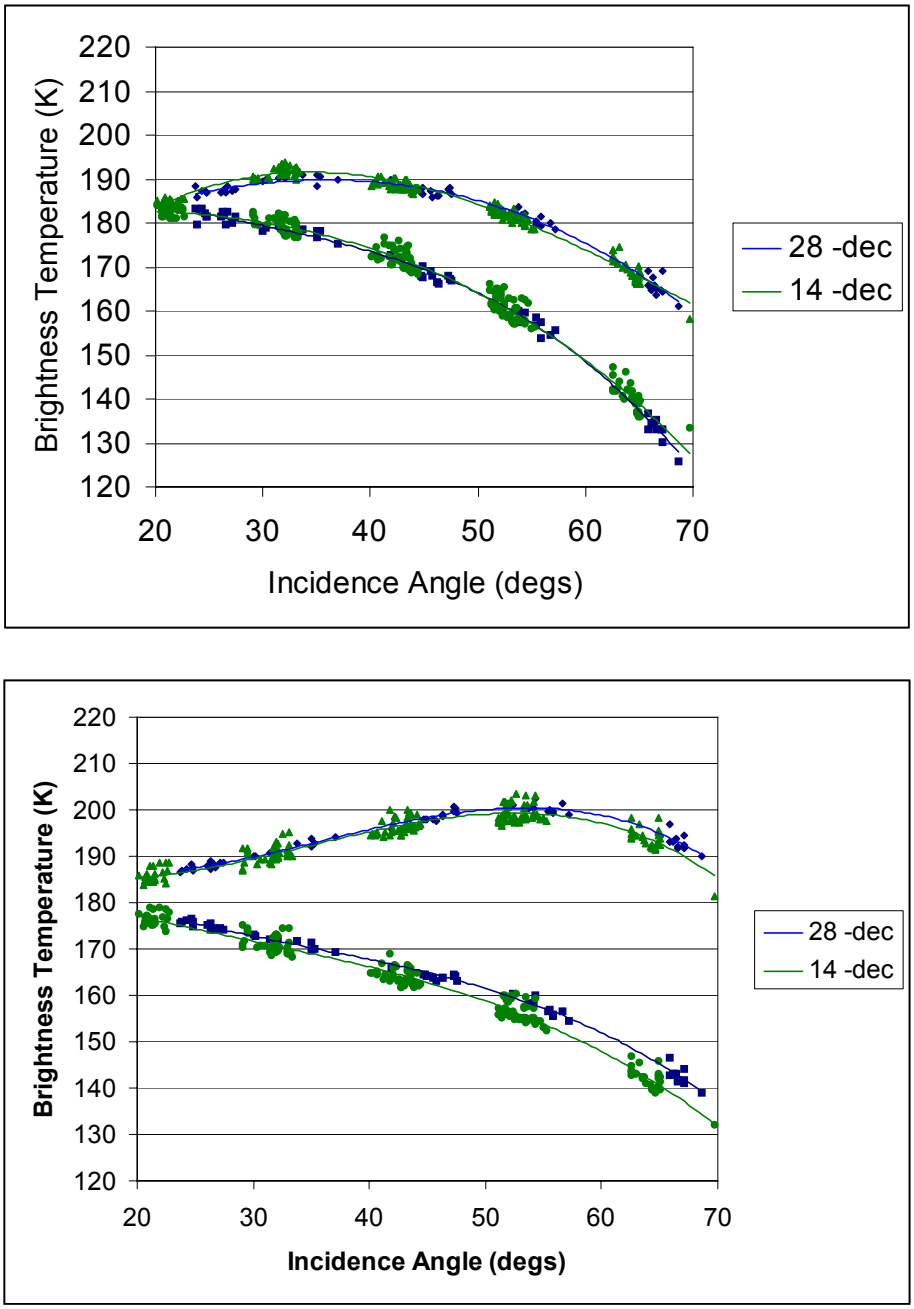

Figure 39 Tb versus incidence angle at L (top) and C (down) band measured at December 14 and 28.

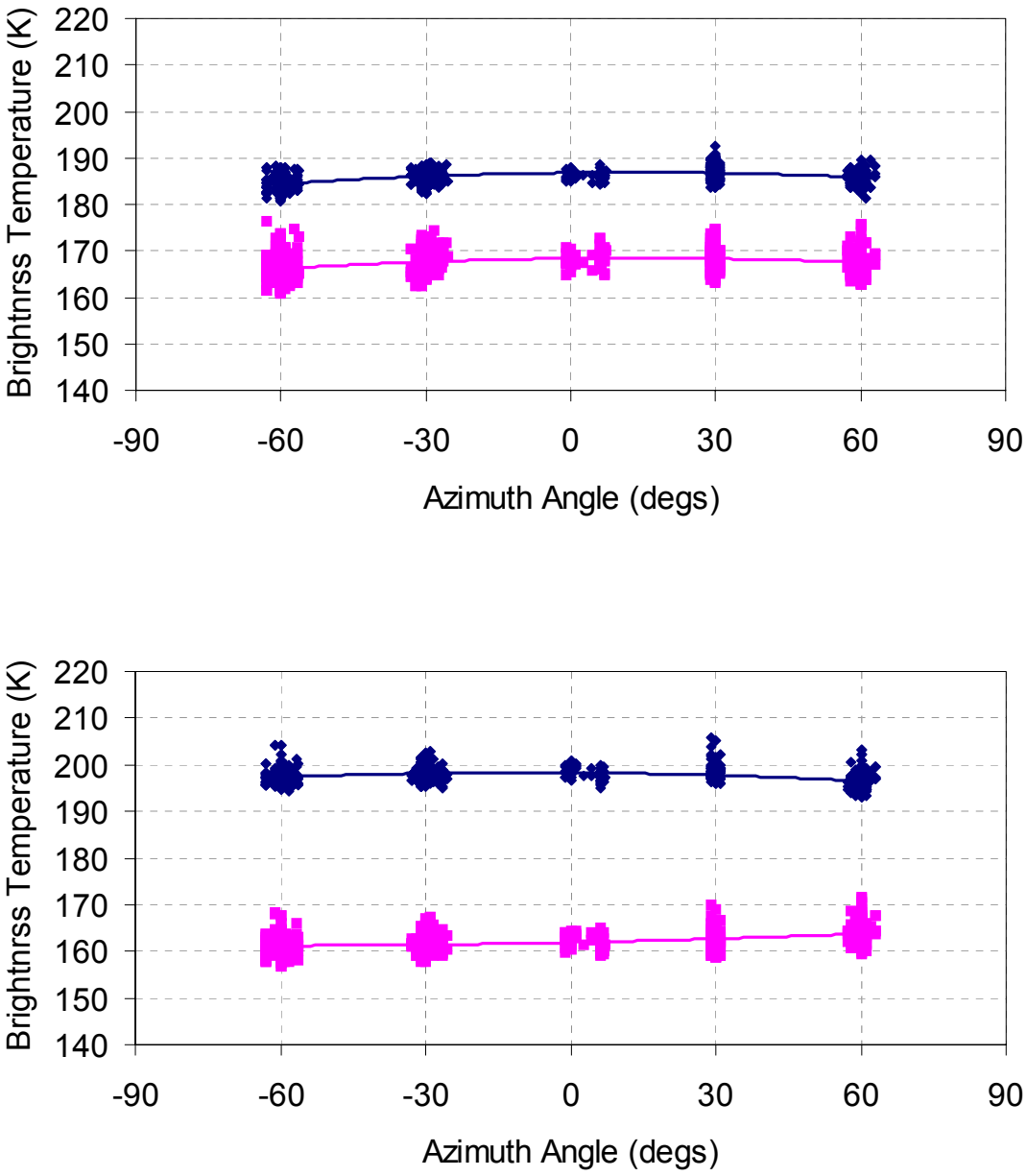

Figure 40 Tb measured at 45 degrees of incidence angle as a function of azimuth angles at L (top) and C (bottom) band

Also in this case the stability of the mean Tb value was estimated from a comparison of data measured at a distance of two weeks (Figure 41). At L-band the average value remained constant while, at C-band it increased due to an increase in the air and snow temperatures.

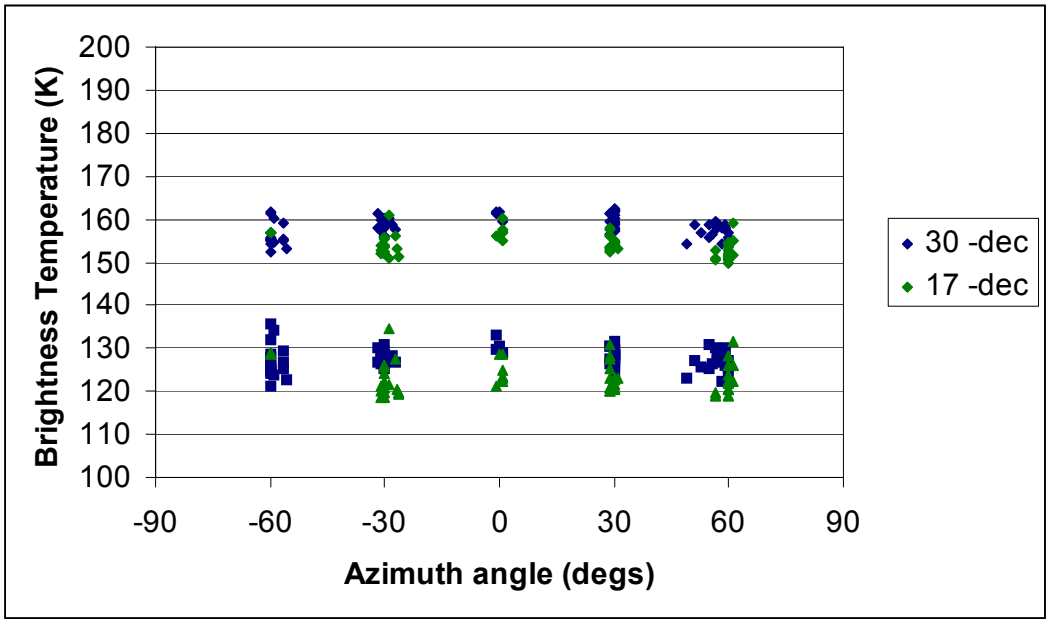

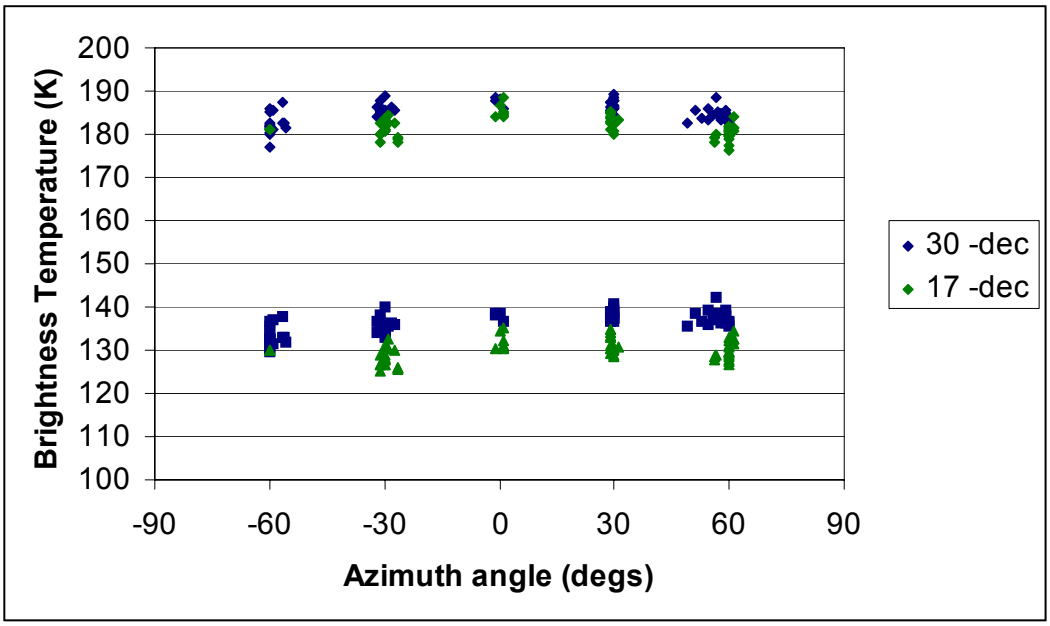

Figure 41 Tb measured at 45 degrees of incidence angle as a function of azimuth angles at L(top) and C (bottom) band measured at December 17 and 30

From these analyses we can conclude that the spread of the data around the average value observed at any incidence and azimuth angle did not depend on fluctuations in snow emissivity (since this is time- and value-independent) but, as will be explained in section 5.2 , was generated by a thermal fluctuation of the radiometer and was partially corrected.

The temperature measured by the infrared radiometer is presented in Figure 42, together with the air temperature. As expected, the data were highly correlated, the daily excursion was similar (about 15 K) and the average infrared temperature was higher than the air temperature. The infrared temperature is a measurement very close of the surface temperature and provides information about the diffusion of the thermal flux from air to snow. In fact if we represent infrared and snow temperatures, collected up to a depth of 50 cm, (Figure 43) we can observe that the daily variation was strongly attenuated in the first 10 cm (from 15 K to 6 K) and disappeared at 50 cm. In addition, the penetration time of the thermal flux from surface to 5 cm was about 6 hours, while the time from 5 cm to 10 cm was about 2 hours.

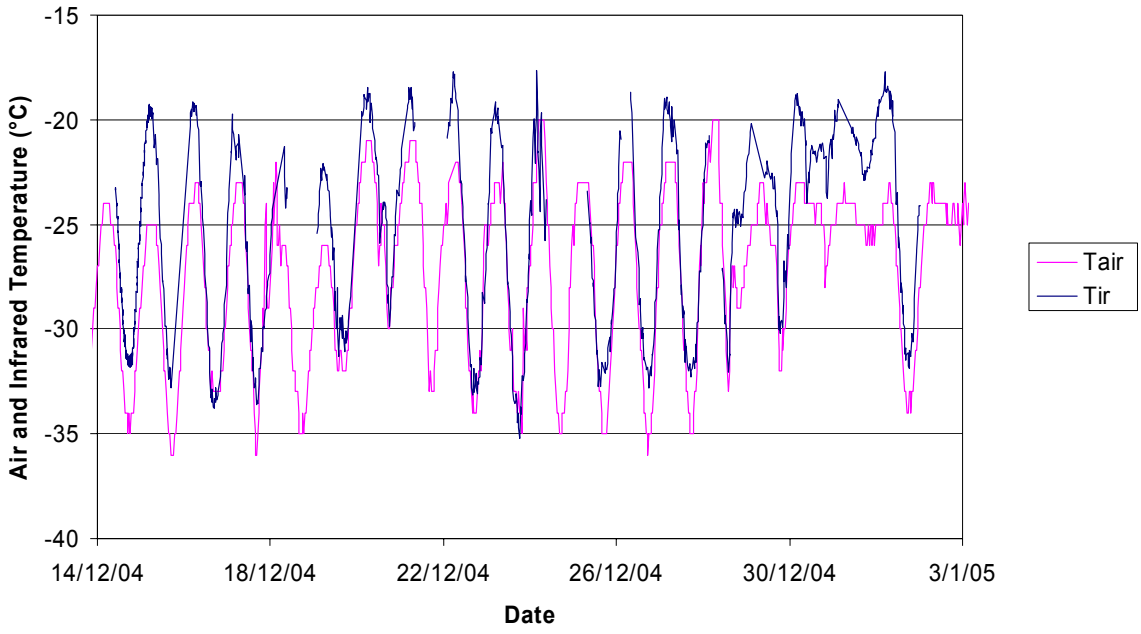

Figure 42 Infrared and air temperature as a function of time

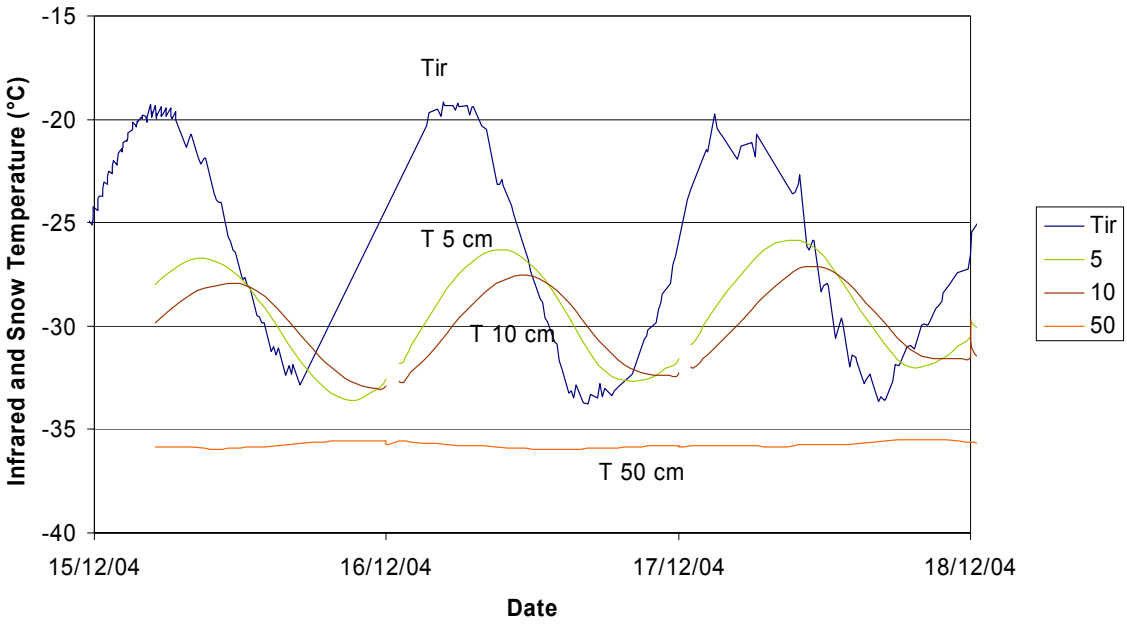

Figure 43 Infrared and snow temperature at different depth as a function of time

5.0 Data Processing

Raw data collected during the experiments were found to be affected by several errors due to a residual sensitivity of the system to temperature variation inside the box and to the wide beam of L- band antenna. These aspects are dealt with in this section, a summary of the obtained results are express at the end of the section. The possible contribution of Sun and Galactic to snow emission were also evaluated.

5.1 *L-band Antenna Deconvolution*

As noted in the calibration phase over the lake (section 2.1.1),because of the wide beam of the L-band antenna the brightness temperature measured at a certain nominal incidence angle was influenced by the radiation coming from the snow at other angles and, at high incidence angles, from the sky. The “true” value of Tb at the various incidence angles was then retrieved after deconvolution of the antenna lobe. The deconvolution was computed for the mean values and the angular correction was then applied to all the data. The algorithm implemented was based on a semi-empirical iterative approach which made used of the Matlab Image processing toolbox for convolution and deconvolution routines.

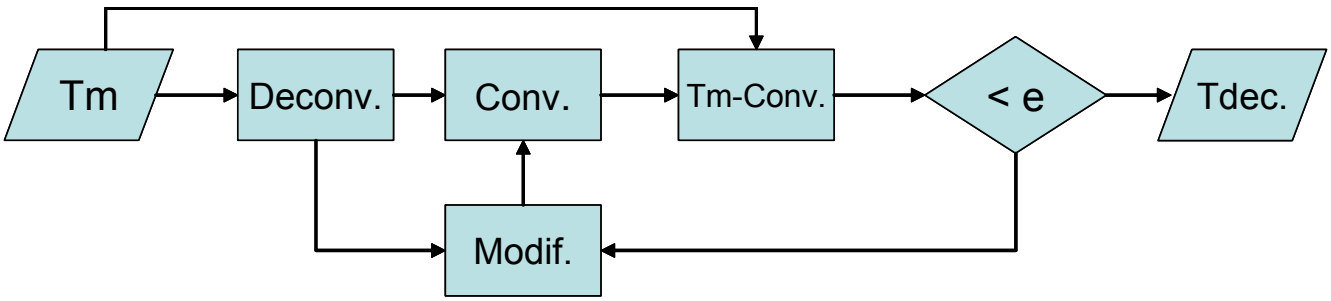

Figure 44 Flow-chart of the deconvolution process

The flow chart of the process is represented in Figure 44: the measured Tb was deconvolved in order to retrieve a first guess of the "true profile". This profile was then modified and convolved again with the antenna lobe until the difference between the measured and convolved profiles was minimized.

The first step of the procedure consisted in the retrieval of a best function that represent the data. In our case, we used a sigmoidal functions (Figure 45). As final results, the deconvolved Tb at H and V polarizations are represented in Figure 46, together with the measured Tb, and the deconvolved-convolved Tb. The difference between measured and decovolved-convolved Tb, which represents an estimate of the error of the process , is represented in Figure 47. As can be observed from the diagram the error was minimized in the first angle range (0-60°), which corresponded to the range of interest for snow observations, whilst higher values were obtained at the angles near to the horizon.

A zoom of the 0-60° range (Figure 48) shows that the maximum absolute error was 0.25 K.

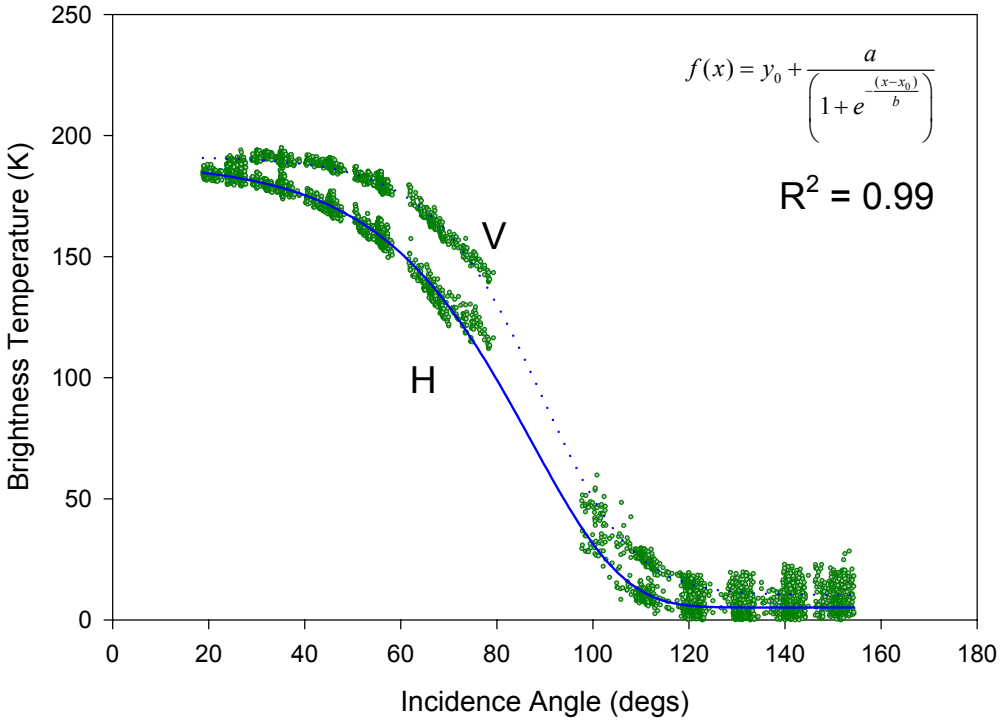

Figure 45 Tb value (L-band) vs incidence angle

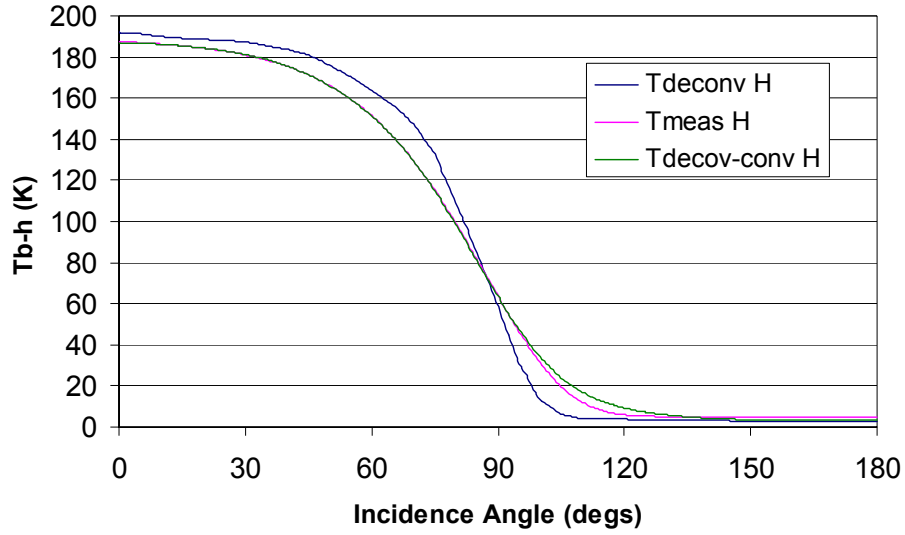

(a)

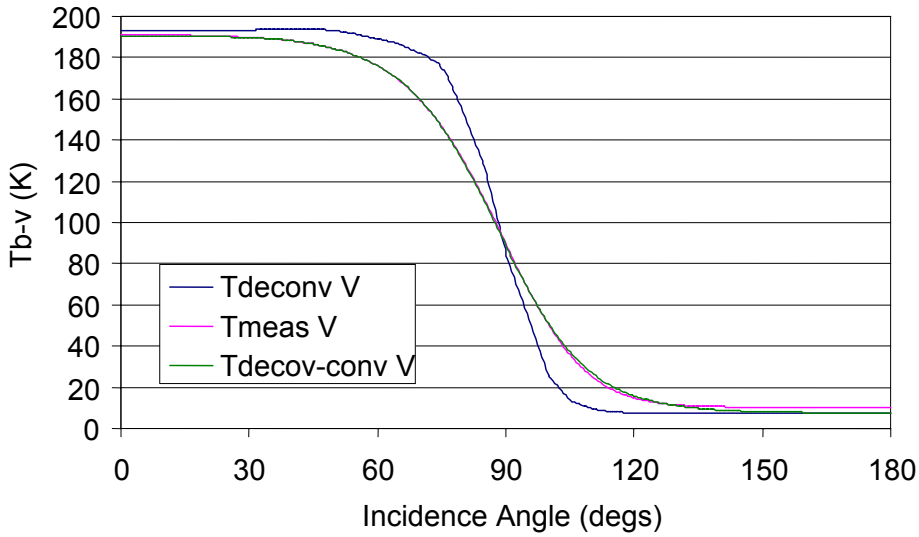

(b)

Figure 46 Tb measured (pink), deconvolved (blue) and deconvolved-convolved at H (a) and V (b) polarization as a function of incidence angle.

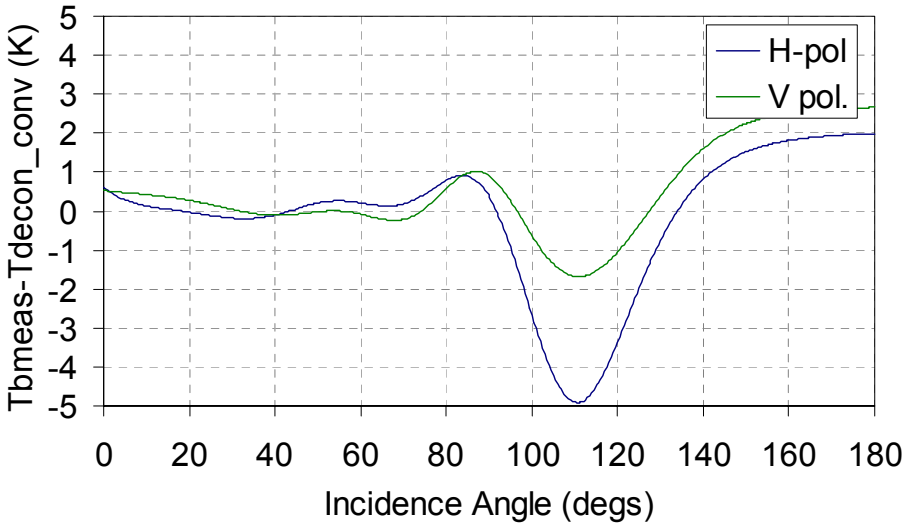

Figure 47 Tbmeasured - Tdeconvolved/convolved as a function of incidence angle in the 0°-180° range

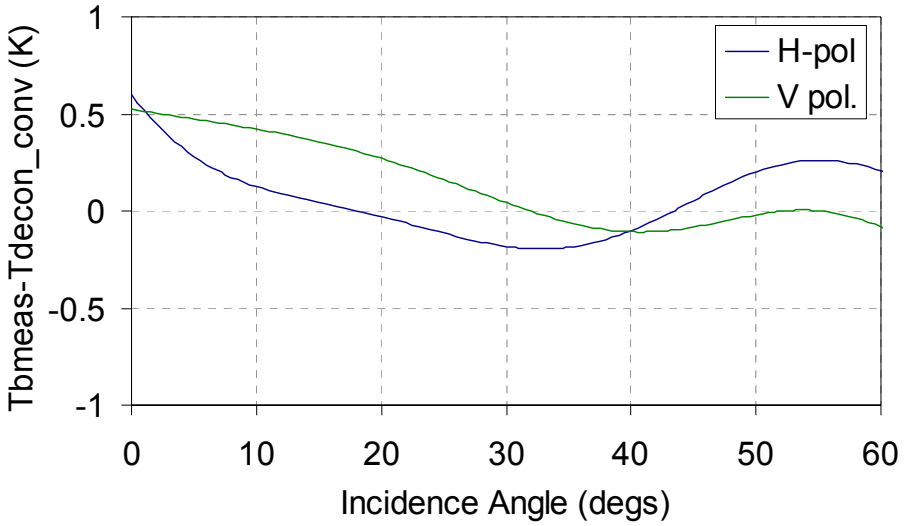

Figure 48 Tbmeasured - Tdeconvolved/convolved as a function of incidence angle in the 0°-60° range

Lastly, from a comparison between measured Tb and deconvolved Tb (Figure 49) we can note that the effect of deconvolution led to an increase in the Tb values. Due to the different projection on snow of the antenna pattern in the two planes (E and V) the increase was much higher at V than at H polarization (i.e. when the radiometer observed the snow at a given incidence angle, the fraction of the antenna pattern influenced by the sky emission was higher at V polarization).

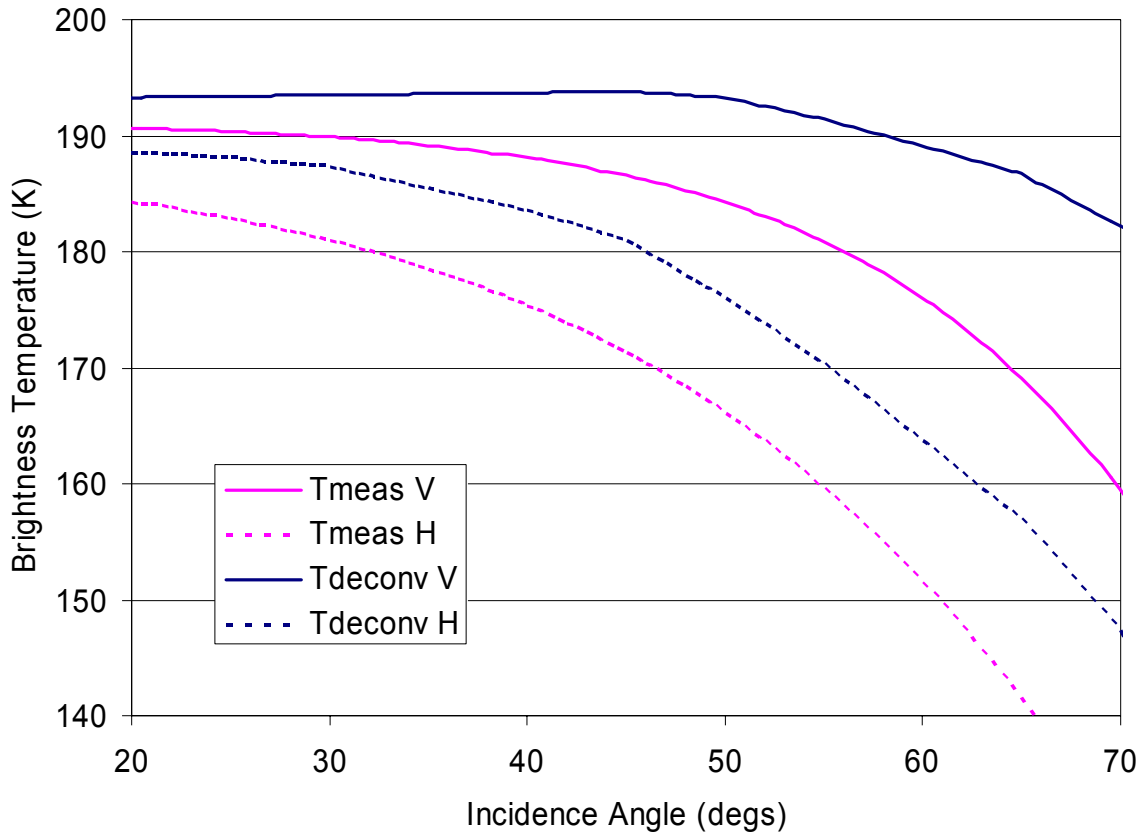

Figure 49 Tb measured and Tb deconvolved at L-band H (dotted line) and V (continuous line) polarization as a function of incidence angle

From the above computations the Tb was deconvolved as mean value fitted as a function of incidence angle. In order to retrieve the corrected Tb value for each single measurement a polynomial relationship between the measured and deconvolved Tb was applied for the specific incidence angle reported by the inclinometer. The deconvolved Tb at H and V polarization as well as the error introduced by the polynomial approssimation are represented, respectively, in Figure 50 and Figure 51.

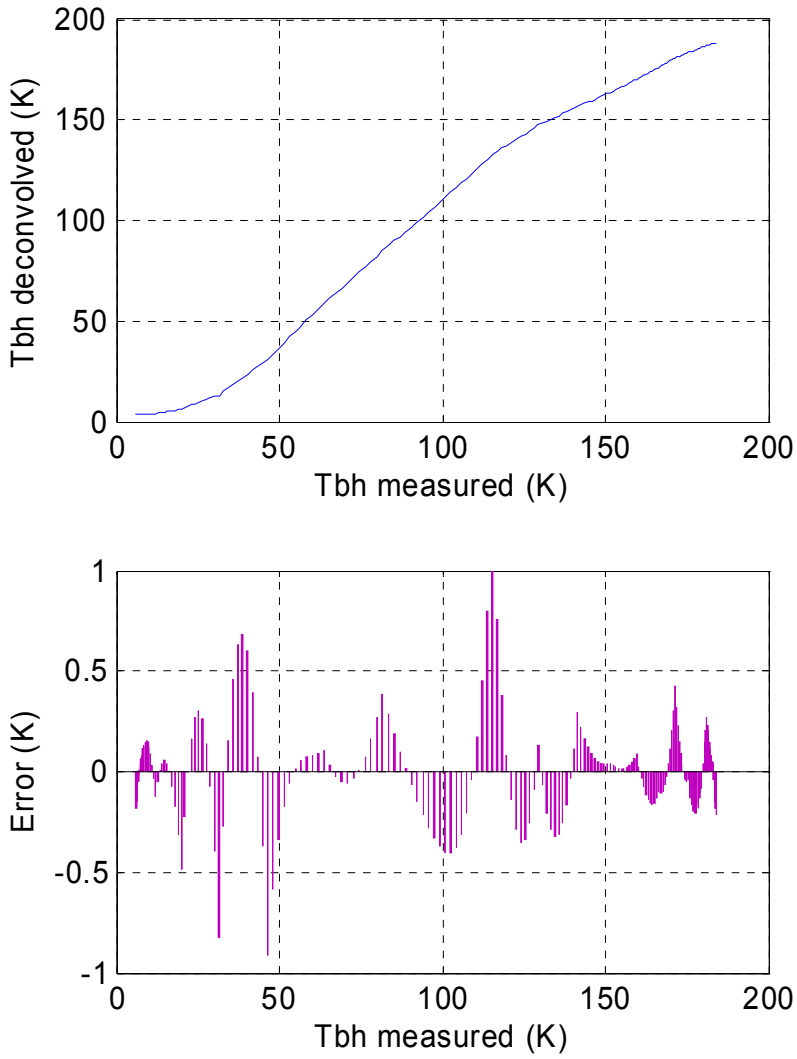

Figure 50 Tb deconvolved versus Tb measured (top) and the error introduced by the polynomial fitting (bottom) at H polarization

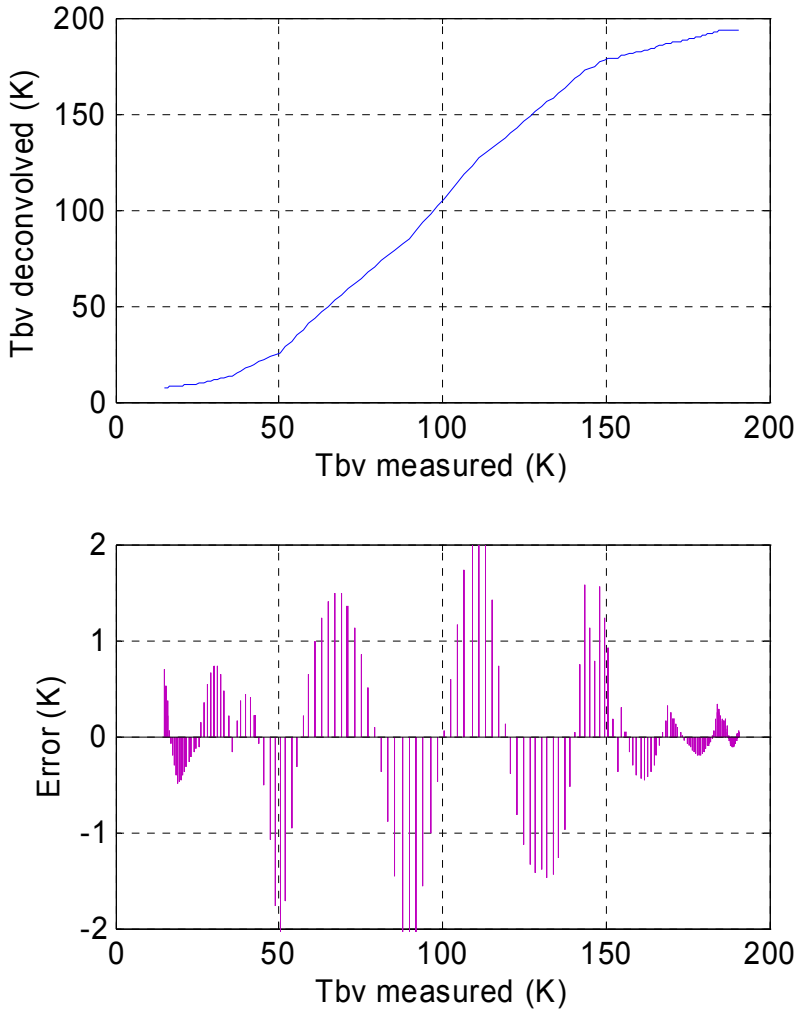

Figure 51 52 Tb deconvolved versus Tb measured (top) and the error introduced by the polynomial fitting (bottom) at V polarization

The residual error (expressed in Kelvin) is the difference between the polynomial interpolation and the deconvolved value and is a measure of the error introduced in the devolution process for each single measurements. It should be noted that in the brightness temperature range 150 – 200 K (the range measured for snow observations) the residual error is lower than 0.4 K.

5.2 *Thermal Compensation*

As noted in the results, the Tb was not stable as expected. For example if we represent the Tb of sky at a fixed incidence angle as a function of time we can observe that the value does not remain constant in time, as expected, but exhibits a daily fluctuation of around 10K (**Figure 53**) at both L and C band. It can be noted, in the same figure, that it is strictly related to the fluctuation of the physical antenna temperature measured by a thermistor located at a position in the back part of the antenna at both L and C band (represented in figure).

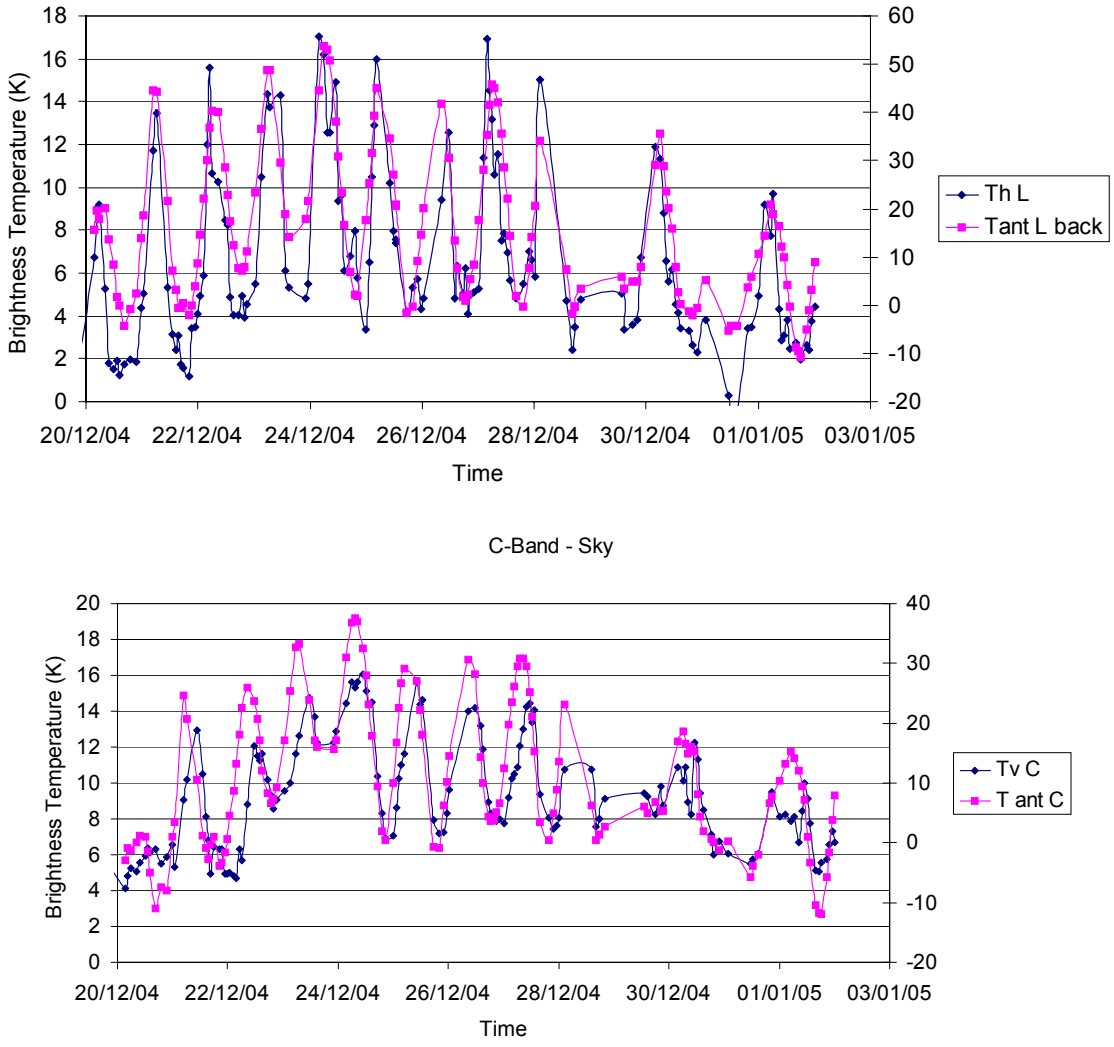

Figure 53 Brightness Temperature (blue) at V polarization, 135°incidence angle, L (top) and C (bottom) bands of clear sky and antenna temperature (pink) as a function of time

In fact, as described in section 2.1.1 , the measured Tb was related to the input of the antenna Ta by the equation:

$$Tb = L\,Ta + (1 - L)\,To \quad (8)$$

Where:

L = losses introduced by the antenna, cables and connectors

To = Thermometric temperature of antenna cables and connectors

During the calibration phase, this effect was considered, L was estimated and Tb was corrected by using temperatures measured by probes placed in the box containing the instruments.

In the preparation phase we assumed that the maximum daily variation of the internal box temperature corresponded to the daily temperature variation (around 12° C) and that the box temperature was homogeneously distributed.

Unfortunately, during DOMEX, we found that these conditions were not verified. The temperature inside the box was not uniformly distributed and the daily fluctuation was much higher than expected. For example for the 26/12 to 01/01 period (Figure 54) the daily fluctuation was around 60°C, and the difference between the temperatures measured in different points of the instruments was higher than 20°C.

We believe that these fluctuations were due to the effect of sun irradiation on the external walls of the box and, in particular, on the window side, which was not protected by thermal insulation.

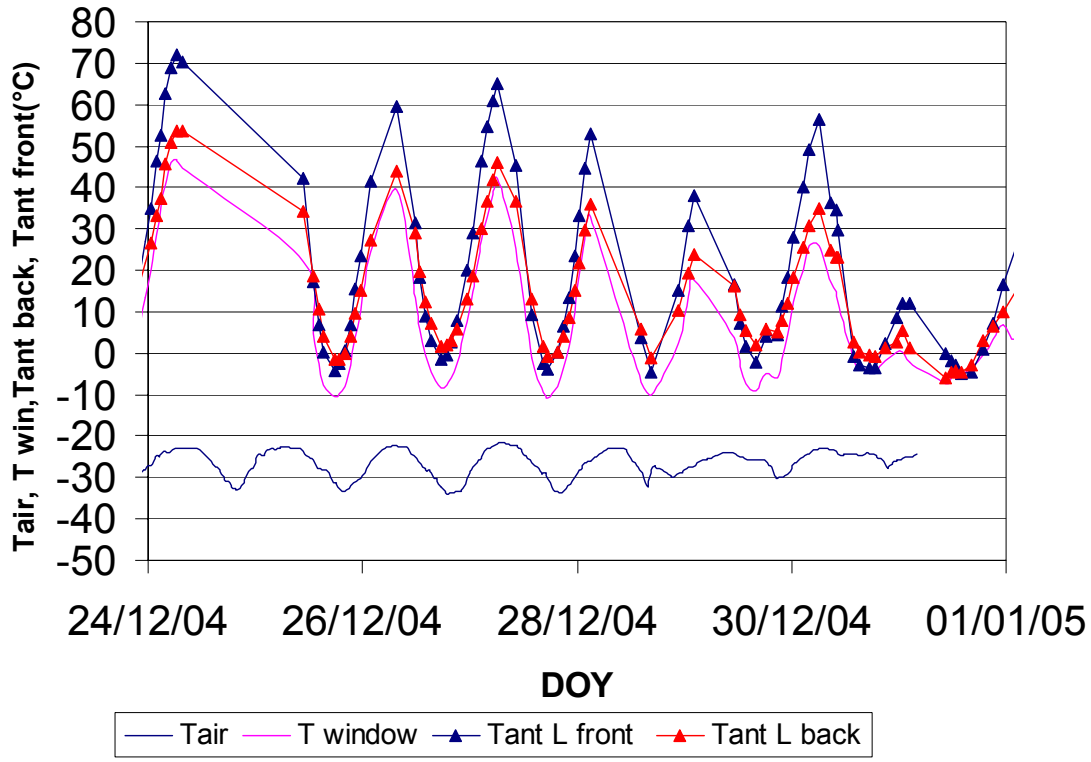

Figure 54 Tair and temperatures measured in different point inside to the thermal box (window, back and front part of L band antenna) as a function of time

Due to the thermal dispersion inside the box the equation (8) needed to be rewritten in a more complex form:

$$Tb = L_1 ..L_n Ta + L_2 ..L_n (1 - L_1) To_1 + L_3 ..L_n (1 - L_2) To_2 + ... (1 - L_n) To_n \quad (9)$$

Where

$L_1..L_n$ = losses introduced by the antenna, cables and connectors

$To_1..To_n$ = Thermometric temperature of antenna cables and connectors

From a theoretical point of view if all terms of equation were known, it would be possible to estimate Tb exactly. Nevertheless, due to some leakage of information, this was not possible with the Domex data. Data were thus corrected by using the L value computed in the calibration phase and an average To value. For example, a comparison of the Tb before and after the deconvolution and thermal correction are presented in Figure 55 for sky, and Figure 56, Figure 57 for snow observations at 56 degrees incidence angles. It

should be noted that while, in both cases, the mean Tb value remained stable in time (increased for snow and decreased for sky) the standard deviation decreased (from 1.76 K to 0.83 K at V polarization and from 3.15 K to 1.8 K at H polarization for snow and from 3.8K to 0.33 K for sky) . Another example (Tb at L-band vertical polarization 45 degrees incidence angle) is represented in Figure 58. Even in this case the standard deviation was considerably decreased (0.35 K instead of 1.46 K).

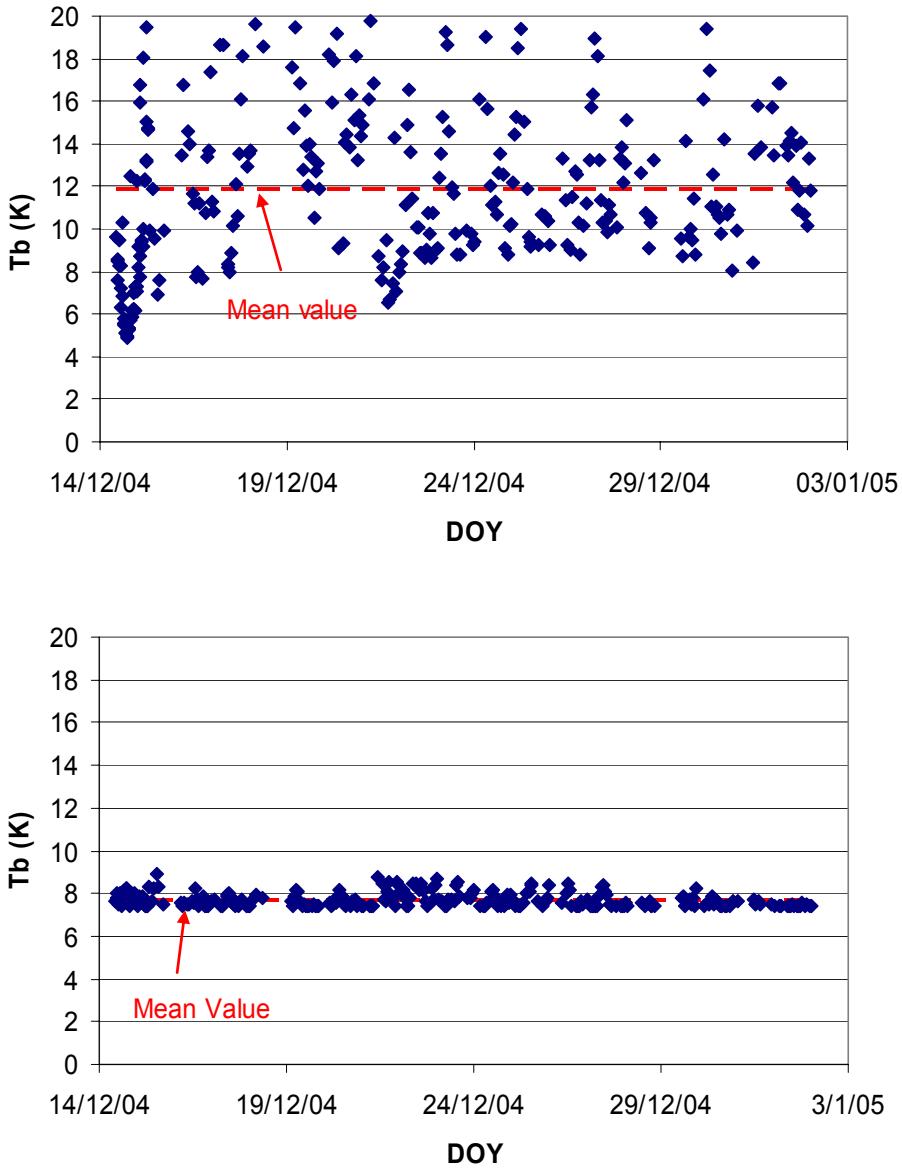

Figure 55 Tb of sky at L-band vertical polarization as a function of time before (top) and after (bottom) the thermal correction.

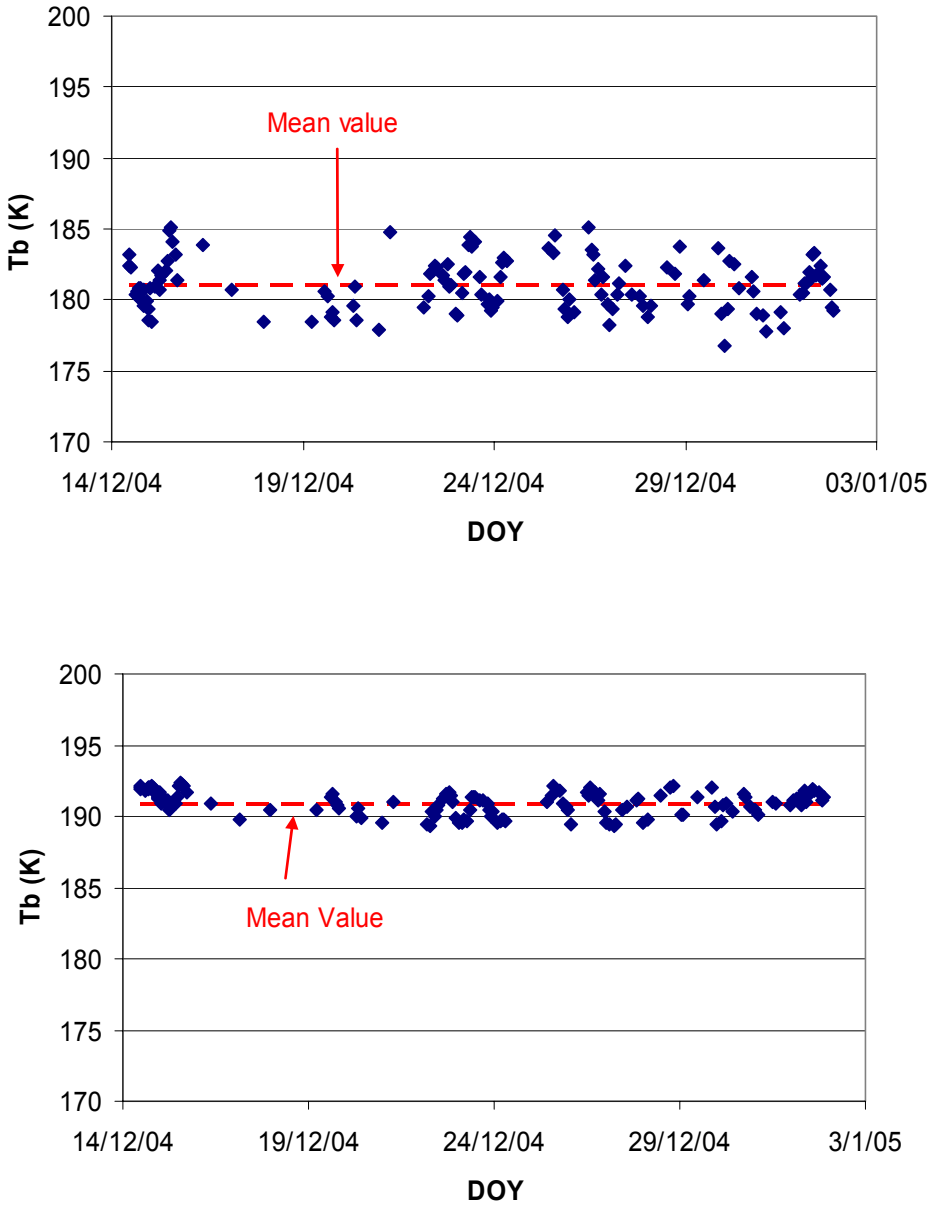

Figure 56 Tb of snow at theta 56 degrees, L-band vertical polarization as a function of time before (top) and after (bottom) the thermal correction.

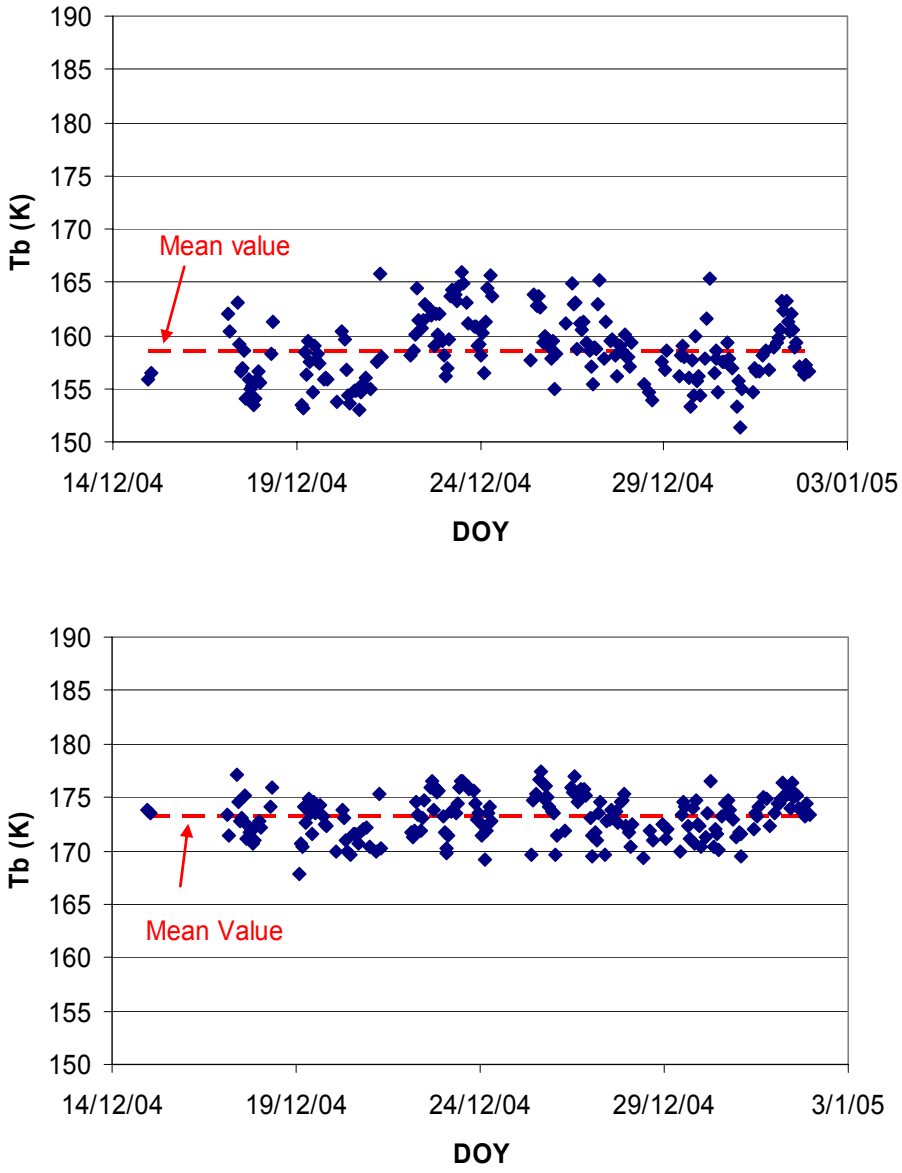

Figure 57 Tb of snow at theta 56 degrees, L-band horizontal polarization as a function of time before (top) and after (bottom) the thermal correction.

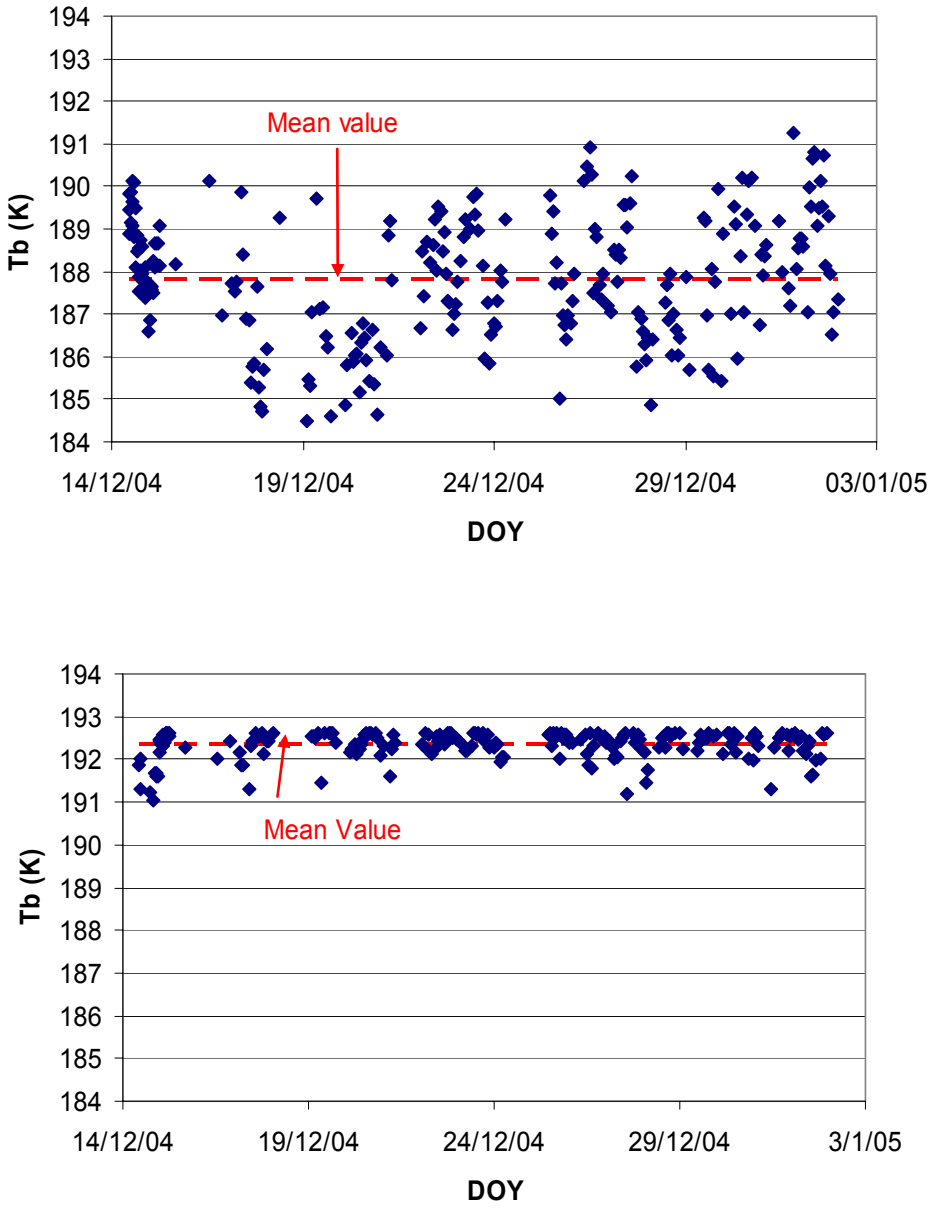

Figure 58 Tb of snow at theta 45 degrees, L-band vertical polarization as a function of time before (top) and after (bottom) the thermal correction.

5.3 *Sun and Galactic Contribution*

An important issue in the analysis of Domex data was the evaluation of possible external sources that contribute to firn measured brightness temperature.

Within the framework of SMOS and other L-band missions (e.g. Hydros) recent papers [6],[24]-[26] dealing with the calculation of the sky and sun contribution at L-band have been published. This contribution is important for the retrieval of surface sea salinity from remote sensing data because the sea surface is a good reflector and its sensitivity to sea salinity is relatively small. From these papers we can expect a brightness temperature contribution from the sky of 3 - 9 K depending on antenna type, latitude and atmospheric effects. It should be noted that at Dome-C, it was possible to disregard the effect of atmospheric attenuation due to the high altitude, the low-pressure value and, in general, good weather conditions.Nevertheless, at L band, radiation from the galaxy is not negligible. This contribution needs to be computed in order to obtain an appropriate value of clear sky when this is directly observed by the radiometer (observed for calibration purposes). On the other hand, due to the low reflectivity of snow, we suspect that this contribution is not important for snow observations.

Sun and Galactic contributions were then evaluated in detail.

5.3.1 Sun Contribution

At L-band the sun can be considered to be as a blackbody at a temperature of about 100000K. By considering the sun as a point source (the angular subtended by the sun is much smaller than the antenna beamwidth), the antenna temperature when the antenna is oriented in the direction of the sun is expressed by:

$$T_a = \frac{\Omega_i}{\Omega_a} Ts \qquad \textbf{(10)}$$

where:

Ω_i = solid angle subtended by the sun (about 0.00007 srad)

Ω_a = antenna pattern solid angle (= $\beta_{xz}\,\beta_{yz}$; where β_{xz} and β_{zy} are the half power beamwidths (in radians) respectively in the xz and yz regions).

When the antenna is oriented towards the ground, the apparent antenna temperature can be expressed by [25]:

$$T_a = Ts\frac{\Omega_i}{(4\pi)^2}\sum_{\alpha}\int\frac{\cos\theta_i}{\cos\theta_s}\;\sigma_{\alpha\beta}(\theta_s,\phi_s,\theta_i,\phi_i)\,d\Omega_s \qquad \textbf{(11)}$$

where:

$\sigma_{\alpha\beta}$ is the bistatic scattering coefficient of the surfaces at $\alpha\beta$ polarization; θ_i, and θ_s are the incidence and scattering angles on the surface ; ϕ_i and ϕ_s are the incident and scattering azimuth angles, and $d\Omega_s$ is the solid angle of the surfaces viewed from the antenna.

In the case of a smooth surface (as for Dome-C Antarctic snow), we can simplify the formula and assume that the surface reflectivity can be computed by using the Fresnel reflection coefficient. This implies that reflection occurs only when the incidence and scattering angles are equal. The apparent temperatures are now expressed by:

$$T_a = \frac{\Omega_i}{\Omega_a}|R|^2 Ts \qquad \textbf{(12)}$$

where R is the Fresnel reflection coefficient of the surface.

The L band antenna half-beamwidth in the xz and yz planes are respectively, β_{xz} = 24° and β_{zy} = 28° (See Figure 16) ; then Ω_a = 0.204 srad.

When the antenna directly observes the Sun, then apparent antenna temperature is about 23K (from equation (8)). This value is much higher than the cosmic background (3 K); it is

therefore important, in defining calibration procedure, to avoid this condition when the sky is directly observed by the radiometer.

When the antenna was directed towards the surface, the surface reflectivity was simulated by using the electromagnetic model available at IFAC [27], [28]; the apparent antenna temperature was computed using equation (12) and is represented in Figure 59.

From 20 to 60 degrees (the DOMEX incidence angle range) the antenna temperature shows a maximum value of 0.7 K at V, polarization and changes from 1.2 K (for theta = 20 degs) to 5 K (for theta = 60 degs) at H polarization.

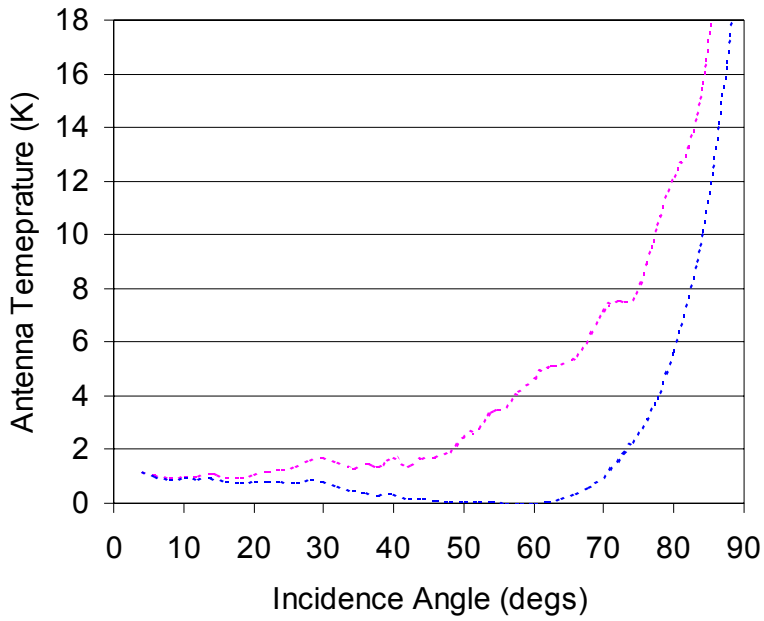

Figure 59 Apparent Antenna Temperature due to the sun reflected by the surface as a function of incidence angle at L-band , V (blue line) and H (in pink) polarization.

While the contribution at V polarization was negligible, at H polarization the maximum value was significant with respect to the variations in the brightness temperature that were expected during the experiment. Consequently, the sun position during DOMEX was computed as a function of daytime and the sun contribution was evaluated. In any case, it should be noted that, as described by equation (12), this contribution was important only

when the radiometer observation and azimuth angles were equal to the sun elevation and azimuth angles.

5.3.2 The cosmic background and the Galactic contribution

The *cosmic background* radiation is assumed to be constant in frequency, space and time and to have a value of 2.7 K.

The galactic emission is composed by two different sources of radiation:

- discrete line emission;
- continuum emission (by thermal sources);

The discrete line emission is due to the of neutral atomic hydrogen transition at 1420.406 MHz. The radiation is concentrated around the plane of the galaxy. A maximum value of 2.6 K was observed in this direction while values of 0.5 K (or less) were encountered for angular distances greater than 10 degrees away from the galactic equator.
The continuum emission is composed of a superimposition of discrete and diffuse galactic and extra-galactic radiosources. Examples of these sources are Cassiopea A, Cygnus A and Crab Nebula.
For observations in Antarctica it is not important to distinguish between the different contributions but it is important to have a single map that took all effects into account.
Once this map is available, the brightness temperature Tb of the background radiation received by the antenna is expressed by:

$$Tb(\Omega_0) = \frac{1}{\Omega_a}\int T(\Omega) Pn(\Omega_0 - \Omega)\, d\Omega \qquad \textbf{(13)}$$

where:

$Pn(\Omega)$ = the power pattern of the antenna
$T(\Omega)$ = the sky map
Ω_a = the beam solid angle

Ω_0 = a point in the celestial sky (declination and right ascension)

The antenna pattern of the L-band antenna is represented in **Figure 16**, while the sky map was provided by ESA (Figure 60) on the basis of investigations by Reich& Reich [29]-[31] The sky map as seen in the L-band antenna FOV using equation (13) is represented in Figure 61. We can observe that the large antenna pattern produced a smoothing effect on the map and the peak values were strongly reduced. For example the brightness temperature of the sky and the corresponding values observed by the L-band antenna as a function of right ascension at declination -29.25 degrees are represented in Figure 62. The maximum value (higher than 80 K) was reduced to 6 K.

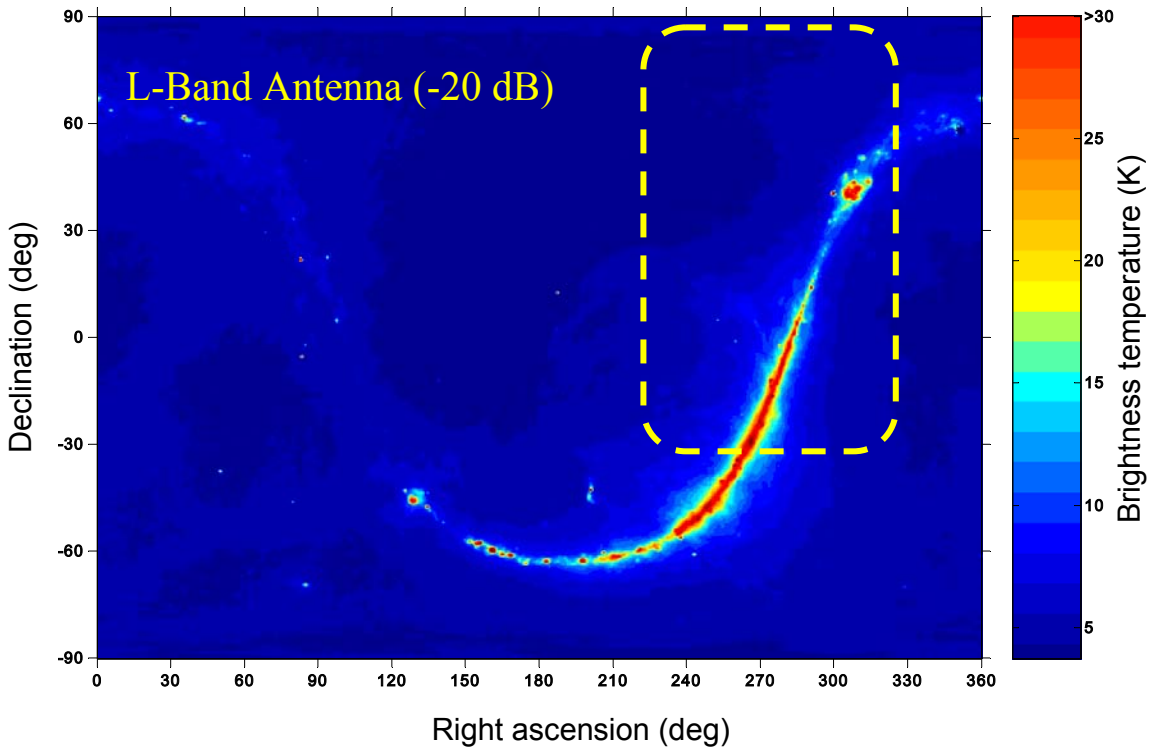

Figure 60 The sky map by Reich & Reich.
The L-band -20 dB antenna pattern is represented in yellow.

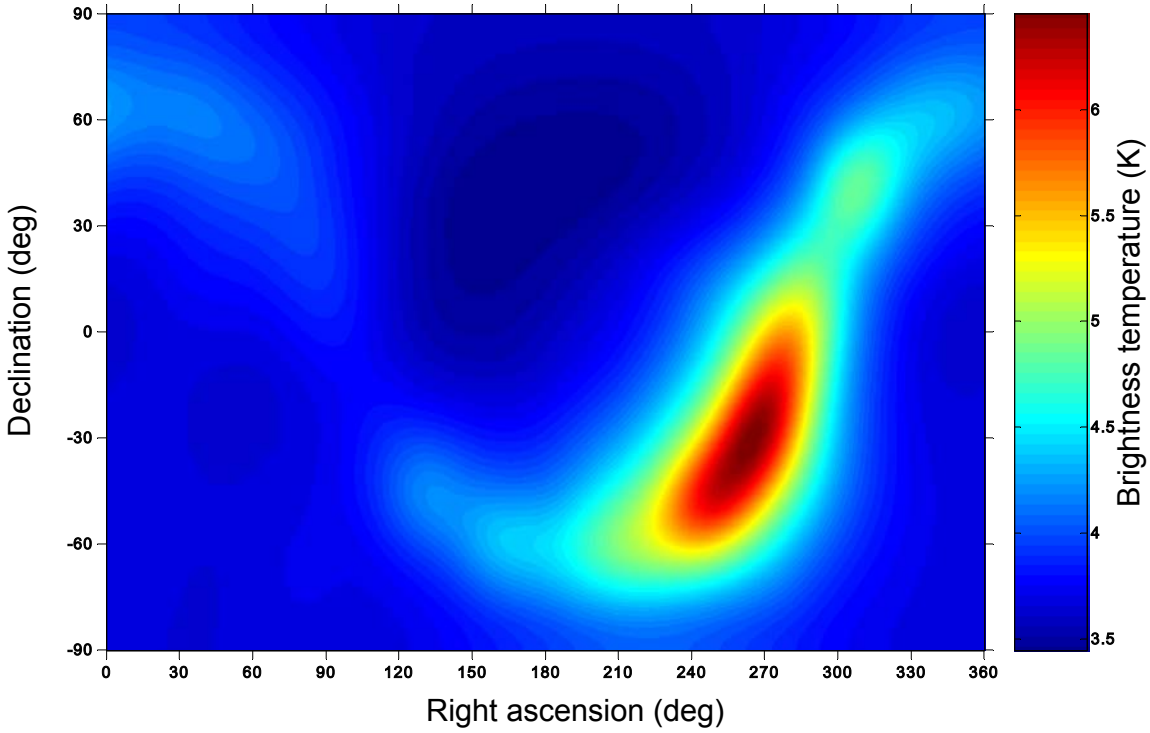

Figure 61 The sky map as seen from L-band antenna

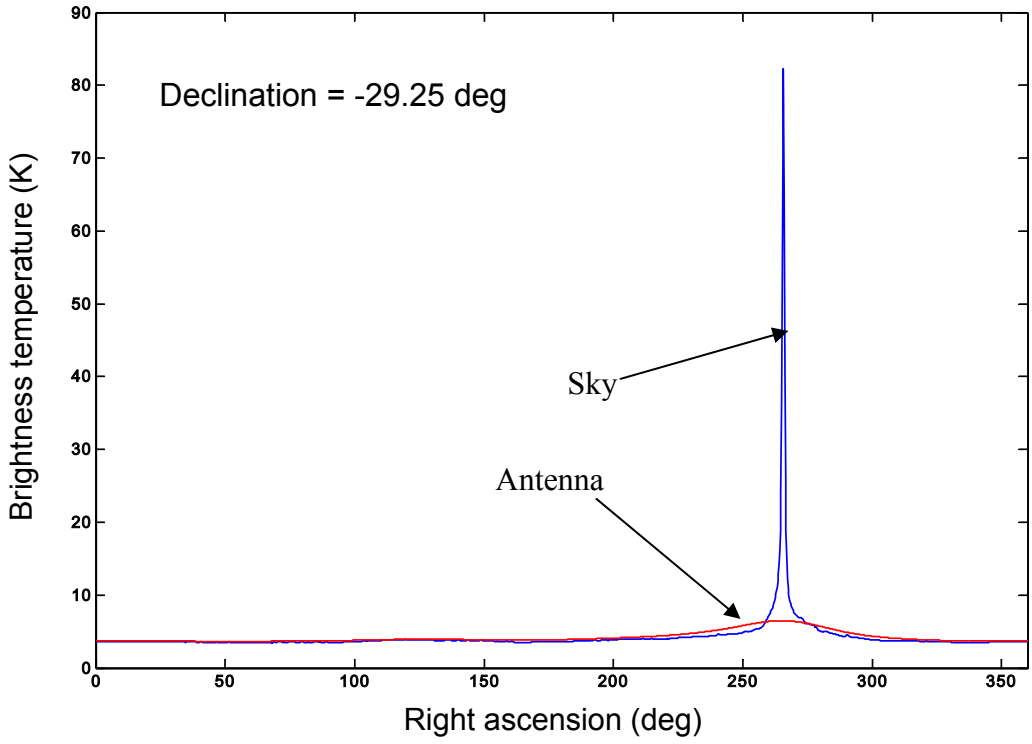

Figure 62 Example of the antenna effect on Tb sky at declination = -29.25 deg

In conclusion, except for a few points of the celestial sphere, the Tb of the sky observed by the L-band antenna was lower than 6 K.

For snow observations the maximum contribution of the galaxy (i.e. the sky emission reflected by the snow) was 0.56 K for a maximum snow emissivity of 0.92. Since this value was negligible with respect to the performances of the L-band radiometer, the sky contribution was not taken into account in the DOMEX data processing.

5.4 *Summary of Domex Results*

As shown in the previous sections, the measured brightness temperature have been corrected for a residual sensitivity of the system to temperature variation, and to the wide beam of L-band antenna. The main results are summarized here as follows.

The brightness temperature versus incidence angle obtained after this correction is represented in Figure 63. This figure shows a composite diagram that includes all data collected during the observation period. As we can see the data are much less scattered compared to those in Figure 38. Due to the different penetration depths of the two frequencies shown in each of the diagrams, we see that the emission from the top layer was more significant at C-band than at L-band, with a well-defined Brewster angle effect evident at C-band.

The brightness temperature, which was measured as a function of time for the entire observation period at an incidence angle θ = 45 degrees at V polarization, is represented in Figure 64, together with the air and IR snow-surface temperatures. It can be noted that, at L band, Tb remained almost constant during the entire period while at C-band, it showed a daily fluctuation with a nearly constant mean daily value. Similar results were obtained at H polarization and at different incidence angles. The air and infrared temperatures showed the same daily trend with a fluctuation of about 15 °C. At this incidence angle (θ = 45°) the mean value of Tb measured at L-band, V polarization during the entire campaign (the average of the mean daily values), was 192.32 K, with a standard deviation of 0.18 K. At θ = 56° the mean value was 190.77 K with a standard deviation of 0.57 K (Figure 65). At H polarization, the standard deviation for both cases was a little higher (about 1 K).

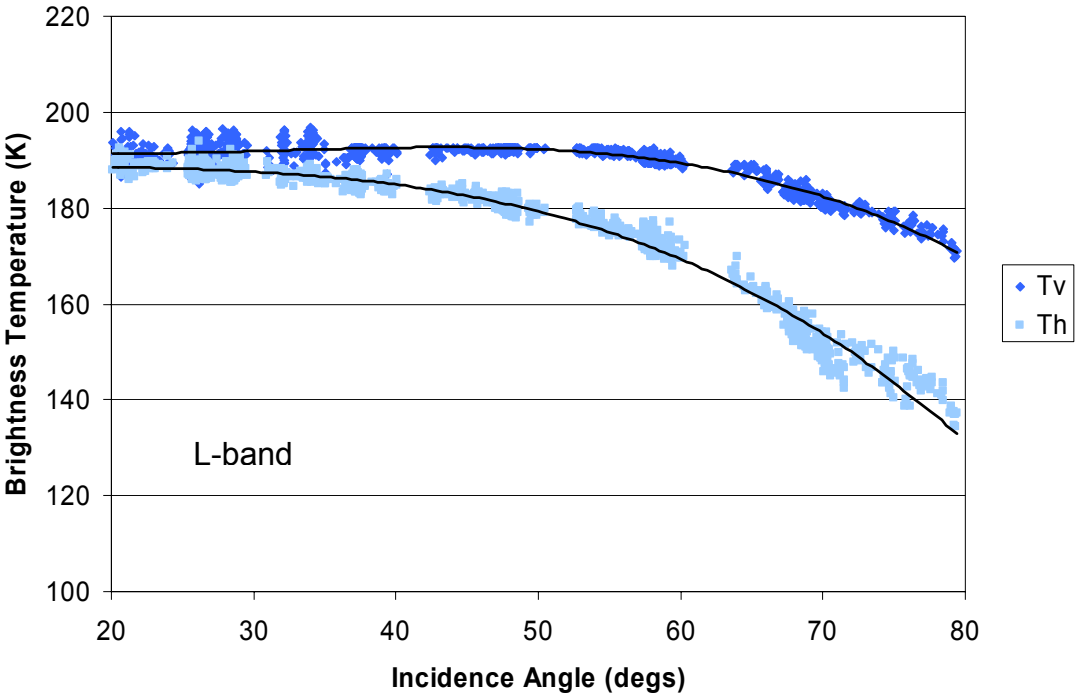

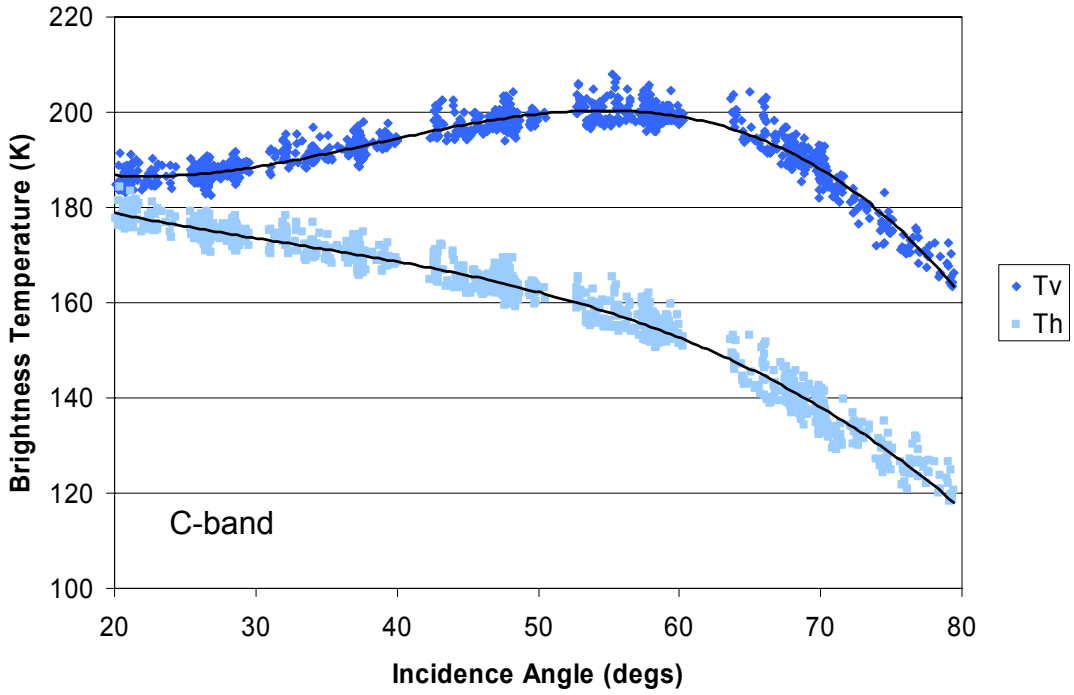

Figure 63 Brightness Temperature at L (top) and C (bottom) bands at horizontal and vertical polarization as a function of incidence angle time. Composite diagram including all data collected during the experiment.

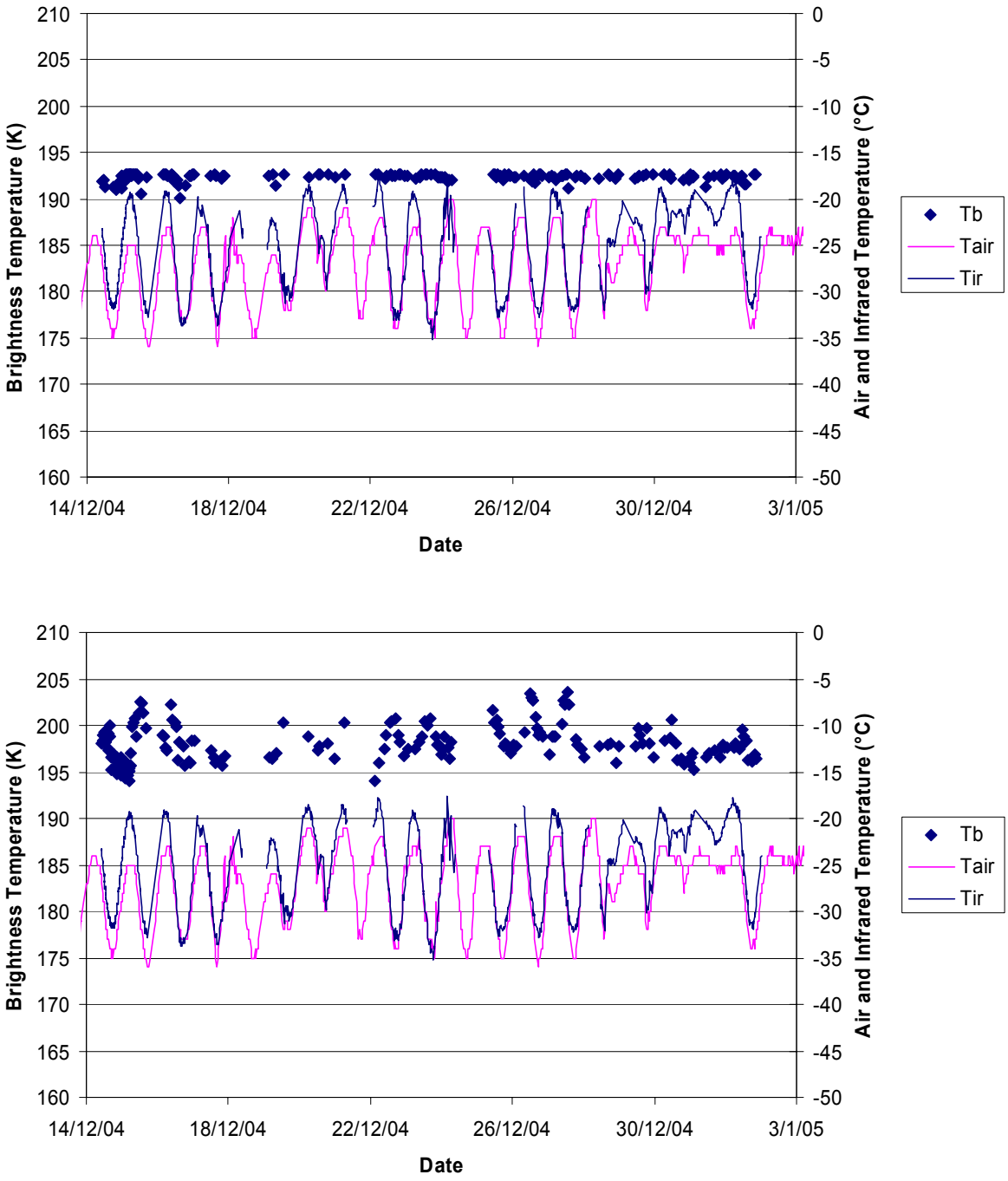

Figure 64 Brightness temperature at L (top) and C (bottom) band, Air and infrared snow surface temperature as a function of time. Incidence angle = 45 degrees. V polarization.

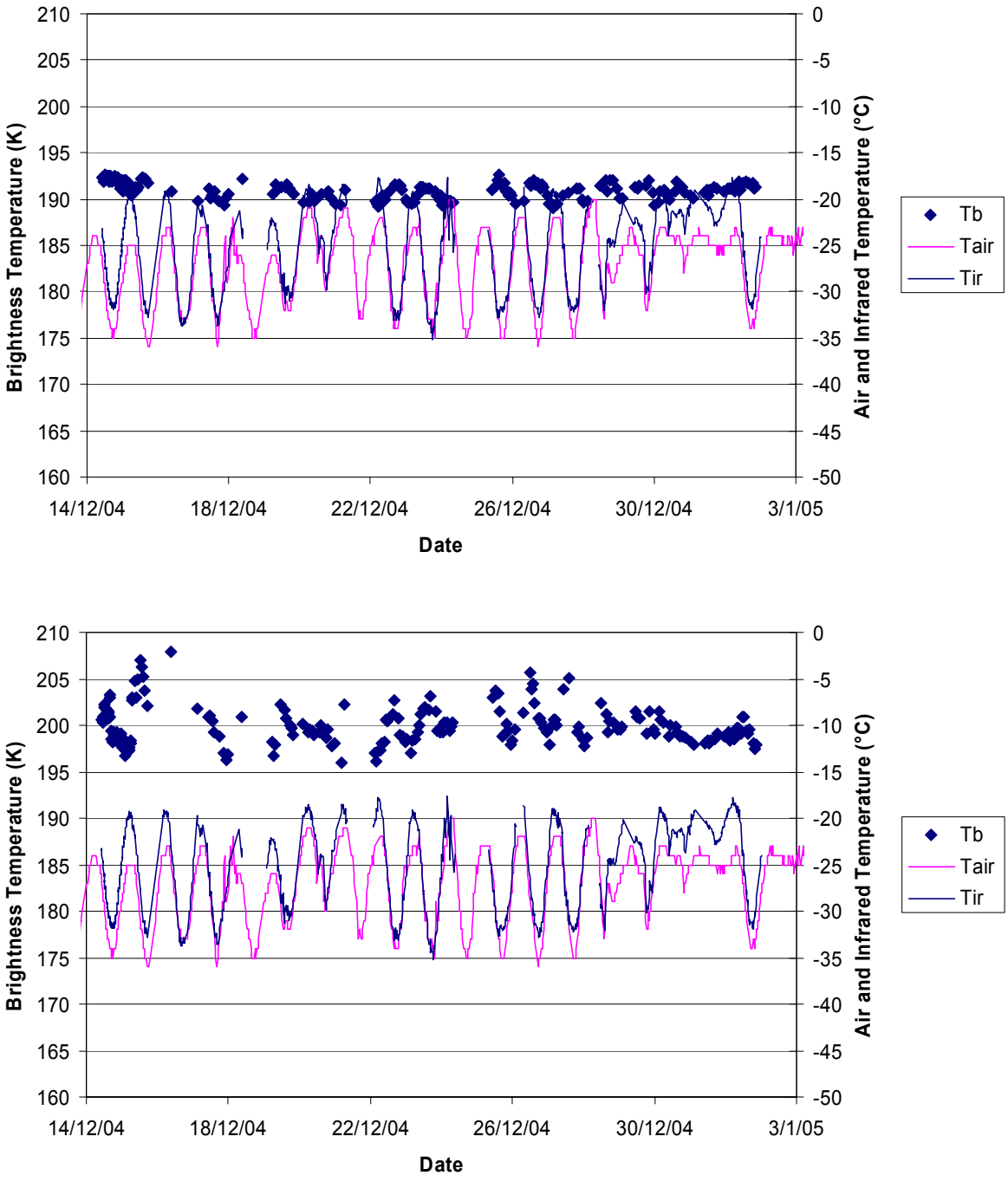

Figure 65 Brightness temperature at L (top) and C (bottom) band, Air and infrared snow surface temperature as a function of time. Incidence angle = 56 degrees. V polarization.

6.0 Comparison with satellite data

AMSR-E satellite data acquired from November 2004 to February 2005, are shown in Figure 66 . The Tb represents the mean value of the data acquired in an area of about 0.05° x 0.05° centered at Dome-C base. Since the data were provided in a 10Km X 10 Km grid this means that, for each satellite orbit there were generally 2 samples contained in the area. Data were available in this area from one to four times per day.

As expected, and as already noted in other studies [8], due to the variation in temperature of the air and top snow layers during this period the Tb first increased up to a maximum value, that corresponded to the maximum air temperature of the year, and then decreased. This effect was more evident at the higher frequencies (Ku and Ka band) which are more sensitive to the changes that occur in the top snow layers.

From the figure it can be noted that, while V polarization exhibited a "regular" trend at all frequencies the H polarization was characterized by anomalous and unexpected increases and decreases in the Tb. Since there was no reason to attribute this behavior to changes in snow emissivity, it appeared evident that they were due to a malfunctioning in the calibration procedure for the AMSR-E data. This fact is not to be disregarded if we take into consideration the fact that these data were obtained from the official data distribution. Furthemore, this case clearly shows that the introduction of an external independent stable target in the satellite data calibration process can bring about evident improvement in the quality of the data.

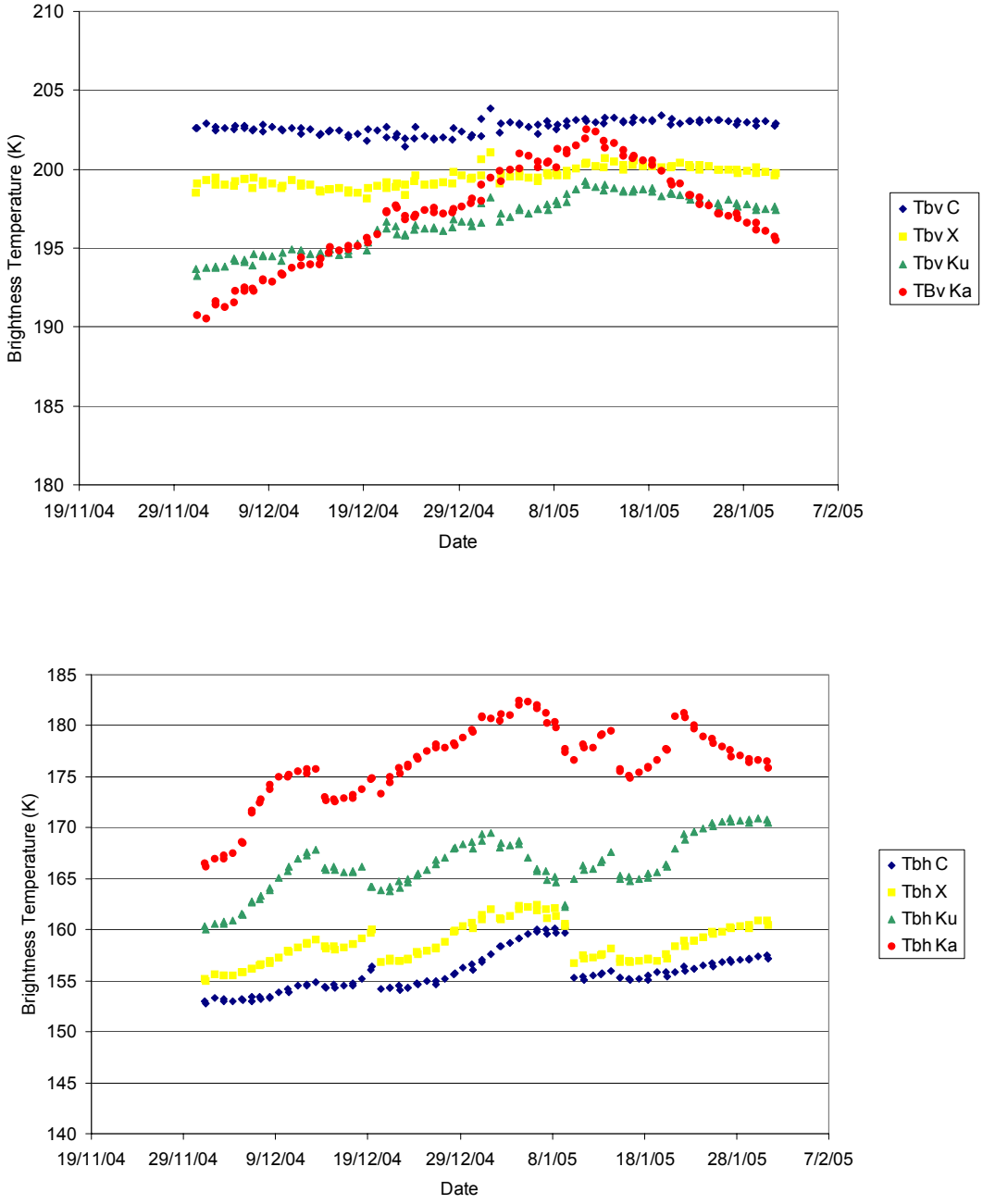

Figure 66 AMSR-E data as a function of time at V (top) and H polarization (bottom).

The Tb at C band measured during DOMEX and by AMSR-E are represented in Figure 67. We see that, whereas H polarized data were generally in good agreement, there was a significant difference of around 4 K between the two measurements at V polarization (203.7 for DOMEX and 199.6 for AMSR-E) which may be interpreted as a V-pol calibration bias over this period of time.

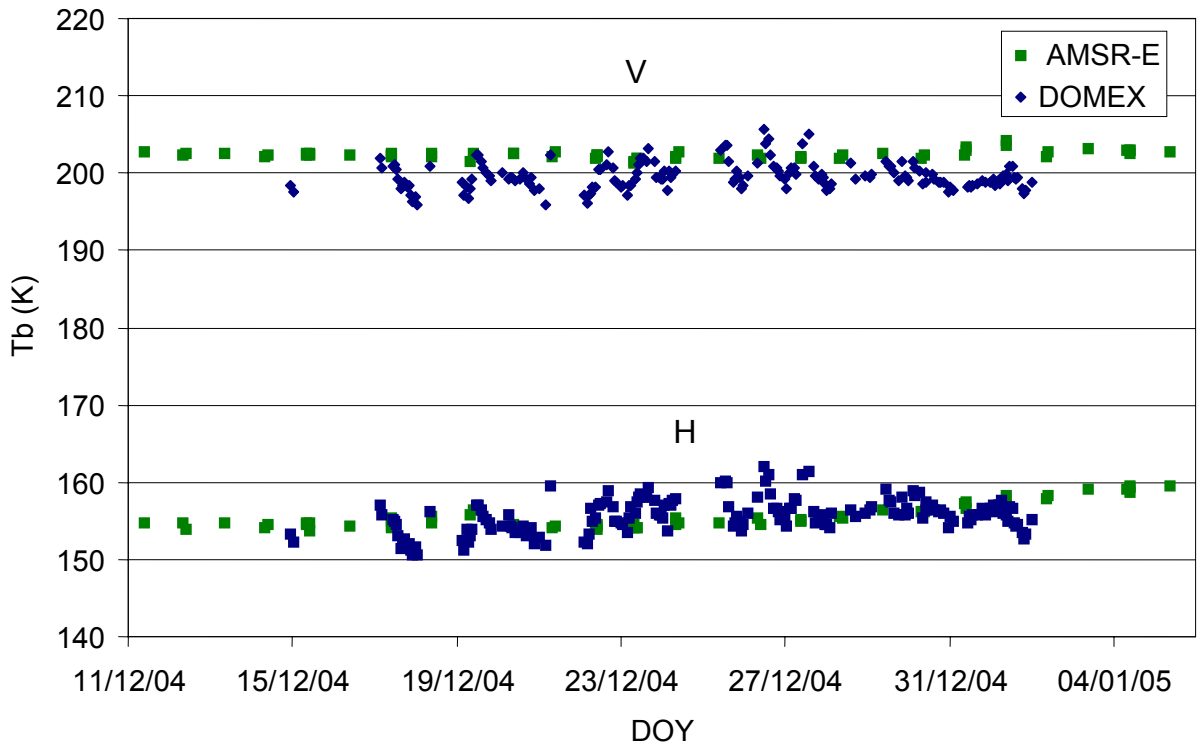

Figure 67 Tb at C band V and H polarization as a function of time from DOMEX (blue) and AMSR-E (green) at 55° incidence angle.

7.0 Conclusions

The calibration and validation of satellite data are an important issue for all space missions. Different strategies and methodologies are defined for each single mission during the preparation phase. The general method used for the calibration of a space-borne microwave radiometer consists of periodic observations of calibration targets during the measurement cycle. In most cases, the antenna of the radiometer alternates the observations of the earth with measurements of deep space and of an artificial target positioned on board the satellite. In the mean time several components are monitored in order to verify their performance.

Nevertheless the possibility of introducing into the calibration procedure the observation of an external independent target , the characteristics of which are not related to the system on board the satellite, represents an attractive opportunity.

This possibility is interesting for all space-borne radiometers but is particularly interesting in the calibration of an instrument that does not use a real antenna but in which the antenna is obtained by using the synthesis method, as in the MIRAS radiometer. The latter is used for the SMOS mission, and the antenna is realized by using a combination of sixty-nine small antennas placed in a three- arm configuration (www.esa.int/livingplanet/smos)

The main problem in defining an external target is that the target has defined characteristics :

- the target dimensions are large enough with respect to the FOV of the satellite;
- the target emission is constant within these dimensions;
- the target is well-positioned with respect to the orbits of the satellite, so that the target is frequently observed;
- the emission of the target is well-known in time.

In the case of microwave radiometers operating at a low frequency (such as SMOS or Aquarius) in which the FOV is of about 50 x 50 km, the Antarctic plateau is probably the only natural target that can come close to satisfying the first 3 requirements. In particular, compared to other areas of the Antarctica, the area near Dome-C is unique in several ways.

The emissivity of the Antarctic plateau above 5 GHz has been measured by satellite sensors during different missions, and it has been well demonstrated that, thanks to its physical characteristics, the emission was extremely stable. The mean value has remained constant over the years, while the annual variability has been found to increase with frequency. From these data, we have estimated that the variation in the emission at L-band is very low (lower than 0.5 K) and is better than the sensitivity of space-borne radiometers. If this fact is confirmed it appears evident that Dome-C reperesents an unique opportunity for the external calibration of low-frequency space-borne radiometers.

The aim of this project, which was carried out within the framework of the SMOS calibration activities, was to realize two low-frequency (L and C band) microwave radiometers, capable of operating in severe weather conditions, and to collect a time series of microwave measurements of the Antarctic plateau at Dome-C.

Before the field campaign, the microwave radiometers were carefully calibrated and tested in order to obtain appropriate sensitivity and accuracy values.

The first experimental campaign in Antarctica was successfully conducted for a continuous period of 20 days. Microwave and snow measurements were carried out continuously during the campaign at several incidence and azimuth angles within the SMOS range.

The results of snow measurements emphasized the spatial uniformity of the physical characteristics of the area near the Dome-C base camp.

Temperature measurements of the snow down to a depth of 10 m, performed over the years had confirmed that the variation in temperature concerned the first 5/6 meters,

while the temperature remained constant down to this depth. This information is very important, since model simulation have shown that the emission at L-band is not influenced by this layer. Therefore, the assumption that the emission at this frequency remains constant in time appears reasonable.

The dielectric constant was also measured during the experiment and the derived snow density was in good agreement with the density measured using conventional methods.

Microwave measurement data confirmed the high stability of the mean value of the brightness temperature measured at L-band on a monthly scale at an incidence angle in the 20° – 60° range.

It should be noted that, due to some problems which were encountered during the experimental campaign, an accurate post-processing of the data was necessary. In particular, the first problem was related to the wide pattern of the L-band antenna, while another problem was caused by an unexpected daily variability in the internal temperature of the box in which the radiometers were contained.

The measurements carried out at C-band were not affected by the antenna problem; but also in this case, the fluctuation in the box temperature produced a fluctuation in the measured brightness temperature that needed to be compensated.
It should be noted that the emission at this frequency was also influenced by the variation in temperature of the uppermost snow layers. Thus, the measured Tb was intrinsically less stable with respect to the one measured at L-band.

Moreover, a comparison of the C-band measurements, taken at an incidence angle of 55°, with satellite data from the AMSR-E, showed very close agreement between the two measured brightness temperatures. The comparison with satellite data also confirmed the importance of an external independent target in the calibration procedure involving satellite radiometers.

In conclusion, the DOMEX experiment was successfully carried out, and the first L-band emission measurements in Antarctica are now available. The objectives of the campaign were reached, and on the basis of this first experiment we can confirm the spatial uniformity and temporal stability of the Dome-C area, at least on a monthly scale. Thus, the possibility of using this area as an extended calibrator for future space-borne radiometer missions is also confirmed.

Nevertheless, this possibility will need to be confirmed by other measurements that will extend the time interval of the measurements and evaluate the spatial uniformity over a larger area. In the following section a proposal for future activities is illustrated.

8.0 Proposal for future activities

As described in the previous section, the necessity for a new experiment is motivated as follows:

1) The need to increase the observation period.

2) The need to monitor a larger area near the Dome-C base. The objective is to verify the spatial stability of the emission of the Antarctic plateau with respect to the size of the area observed by SMOS FOV.

A plan for a new campaign planned for the 2007/2008 Austral summer, was included in the proposal submitted by IFAC-CNR (proposal 32590, PI S. Paloscia) for the SMOS Calibration and Validation activities, which was recently approved by the Agency

In order to comply with the above mentioned objectives, the most important activities of the new experiment will be the following:

- improvement of the short and long term stability of the receiver, the characteristics of the L-band antenna, and the platform pointing system;

- realization of a new fully-automatic, high-stability, two-frequency (L and C-Bands) radiometer, to be installed on the DOME-C tower for at least three months, and the use of the same configuration as that of the first campaign. The said radiometer will operate for a period of one year observing at a single incidence angle;

- development of an additional L-band radiometer, to be installed on a snowmobile available at Dome-C, to monitor a relatively larger area (about 40 x 40 km) near the base, or to be installed on an airplane (e.g. the Twin-Otter, which is used to connect the Dome-C base to the coastal bases).

In all cases, radiometric measurements will be supported by snow measurements and model simulations performed with a coherent multilayer model.

Particular attention will need to be paid in measuring the dielectric constant of snow, especially of imaginary part. Indeed, the methods used so far are not satisfactory in the case of dry snow. The imaginary part is a very important input for the electromagnetic models, and an accurate knowledge of its value, can provide an important improvement in their performance, as well as an important factor in governing the penetration depth within the firn - and thus the depth down to which the emission takes place.

For this campaign support is required to cover the cost of the new instruments, while PNRA will be required to cover the expenses for personnel (travel and maintenance at Dome-c) and logistics.

The schedule of the experiment is subject to several constraints:
1., The experiment must be approved well in advance by the international commission, since the number of experiments to be performed at Dome-C is limited for logistical reasons .

2. The instruments and the materials must be shipped to Antarctica at least 5 months before the beginning of the campaign.

3. Preparation of the new radiometers requires at least 16 months, considering the time needed for supplying the components.
Thus, for a campaign in 2007-2008, approval of the campaign and funds for the instruments should be assured by the end of March 2006 at the latest

9.0 Acknowledgements

This work has been carried out thanks to the financial support of ESA (ESA contact N. 18060/04/NL/CB) and PNRA (PNRA project 2004/3.01).

The authors are grateful to the JRC team for the help provided during calibration tests at JRC –ISPRA, to the Italian-French logistic team at Dome-C for their kind assistance during the experimental campaign and to Roberto Ruisi–IFAC CNR for his contribution to the construction of the instruments.

The authors also thank Richard Brandt and Steven Warren (Washington University) which have allowed the use of the tower at Concordia station.

10.0 References

[1] D. J. Cavalieri, J. P. Crawford, M. R. Drinkwater, D. T. Eppler, L. D. Farmer, R. R. Jentz, and C. C. Wackerman, Aircraft active and passive microwave validation of sea ice concentration from the Defense Meteorological Satellite Program Special Sensor Microwave Imager, *J. Geophys. Res.*, 96, C12, 21989-22008, 1991.

[2] D.G. Long, and M.R. Drinkwater, Azimuth Variation in Microwave Scatterometer and Radiometer Data over Antarctica, *IEEE Trans. Geosci. and Remote Sens.*, Vol. 38, n. 4, 1857-1870, 2000.

[3] K.C. Jezek, C.J. Merry, and D.J. Cavalieri, Comparison of SMMR and SSM/I Passive Microwave Data Collected over Antarctica, *Annals of Glaciology*., 17, 131-136, 1993.

[4] C.J. Van der Veen, and K.C. Jezek, Seasonal variations in brightness temperature for central Antarctica, *Annals of Glaciology*, 17, 300-306,1993.

[5] C.S. Ruf, Detection of Calibration Drifts in Spaceborne Microwave Radiometers Using a Vicarious Cold Reference*, IEEE Transaction on Geoscience and Remote Sensing*, Vol. 44, n. 3, 44-52,2000.

[6] J-Y. Delahaye, P. Golé, and Waldteufel P., Calibration error of L-band sky-looking ground-based radiometers, *Radio Science*, Vol. 37, n. 1 , 1-11, 2002.

[7] EPICA community members, Eight glacial cycles from an Antarctic ice core,*Nature* 429, 623–628, 2004

[8] A. Bingham, M. Drinkwater, Recent Changes in the Microwave Scattering Properties of the Antarctic Ice Sheet, *IEEE Trans. Geosci. Remote Sensing*, Vol. 38, n.4, 1810-1820, 2000

[9] N. Floury, M. Drinkwater, O. Witasse, L-band brightness temperature of ice sheets in Antarctica: Emission modelling, ionospheric contribution and temporal stability, Proc. *IEEE Geosci. Remote Sensing Symp. IGARSS'02*. Toronto, Canada, June 24-28, 2103-2105,2002

[10] M. Drinkwater, N. Floury and M. Tedesco, L-band ice sheet brightness temperatures at Dome C, Antarctica: spectral emission modelling, temporal stability and impact of the ionosphere. *Annals Of Glaciology*, vol. 39, 391-396, 2003

[11] G. Macelloni, G. Nesti, P. Pampaloni, S. Sigismondi, D. Tarchi and S. Lolli, Experimental Validation of Surface Scattering and Emission Models, *IEEE Trans. Geosci. Remote Sensing*, Vol 38, n. 1, 459-469, 2000.

[12] G. Macelloni, S. Paloscia, P. Pampaloni, R. Ruisi, Airborne Multi-frequency L- to Ka - band Radiometric Measurements over Forests, *IEEE Trans. Geosci. Remote Sensing*, vol. 39, n. 11, 2507-2513, 2001

[13] G. Macelloni , S. Paloscia, P. Pampaloni, M. Tedesco, Microwave Emission from Dry Snow: A Comparison of Experimental and Model Result, *IEEE Trans. Geosci. Remote Sensing*, vol. 39, n 12, 2649-2656, 2001.

[14] G. Macelloni, S. Paloscia, P. Pampaloni, R. Ruisi, M. Dechambre, R. Valentin, A. Chanzy, and J. P. Wigneron, Active and passive microwave measurements for the characterization of soils and crops, *Agronomie* 22, 581-586, 2002.

[15] Cagnati A., A.Crepaz, G. Macelloni, P.Pampaloni, R. Ranzi, M. Tedesco, M. Tomirotti and M. Valt, Study of the snow melt-freeze cycle using multi-sensor data and snow modelling, *Journal of Glaciology*, vol. 50, N. 170, 419- 426, 2004.

[16] G. Macelloni; Paloscia, S.; Pampaloni, P.; Brogioni, M.; Ranzi, R.; Crepaz, A.Monitoring of melting refreezing cycles of snow with microwave radiometers: the Microwave Alpine Snow Melting Experiment (MASMEx 2002-2003) *IEEE Trans. Geosci. Remote Sensing* , Vol. 43, n. 11, 2431- 2442, 2005

[17] F. T. Ulaby, R. K. Moore, A. K. Fung, *Microwave Remote Sensing: Active and Passive*, vol. 1, Dedham, MA: Artech House, 1982.

[18] J. Lahtinen, J. Pihlflyckt, I. Mononen, S. J. Tauriainen, M.i Kemppinen and M. T. Hallikainen, Fully, Polarimetric Microwave Radiometer for Remote Sensing, *IEEE Trans. on Geosci. Remote Sensing* , Vol: 41 , n. 8 , 1869 – 1878, 2003.

[19] S.R. Hudson, and R.E. Brandt,: A Look at the Surface-Based Temperature Inversion on the Antarctic Plateau. *J. Climate*, **18**, 1673-96, 2005.

[20] D. Six, M. Fily, S. Alvain, P. Henry, J.P. Benoist, Surface characterization of the Dome Concordia area (Antarctica) as a potential satellite calibration site, using SPOT4/Vegetation instrument, *Remote Sensing of Environment*, 89, 83-94, 2003

[21] S. C. Colbeck, E. Akitaya, R. Armstrong, H. Gubler, J. Lafeuille, K. Lied, D. McClung and E. Morris, “International Classification for Seasonal Snow on the Ground,” *Intern. Commission for Snow and Ice -IAHS*, 1990.

[22] Automatic Weather Stations Project and Antarctic Meteorological Research Center- http://amrc.ssec.wisc.edu/

[23] E. Kärkäs, H.B. Granberg, C. Lavoie, K. Kanto, K. Rasmus and M. Leppäranta. Physical Properties of the Seasonal Snow Cover in Dronning Maud Land,East-Antarctica, *Annals of Glaciology*, 34, 89-94, 2002.

[24] K. Rasmus, H. Granberg, K. Kanto, E. Kärkäs, C. Lavoie and M. Leppäranta. Seasonal snow in Antarctica data report. *Report Series in Geophysics No 47*. University of Helsinki, Division of Geophysics, 2003.

[25] S.H. Yueh; West, R.; Wilson, W.J.; Li, F.K.; Njoku, E.G.; Rahmat-Samii, Y.;Error sources and feasibility for microwave remote sensing of ocean surface salinity, *IEEE Trans. on Geosci. Remote Sensing*, Vol. 39 , n. 5, 1049 – 1060, 2001.

[26] D.M Le Vine; Abraham, S.;Galactic noise and passive microwave remote sensing from space at L-band, *IEEE Trans. on Geosci. Remote Sensing*, Vol. 42 , n. 1 , 119 – 129, 2004.

[27] G. Macelloni.;Pampaloni,P.;Tedesco,M. -Microwave emission from Antarctica and the calibration of low frequency space-borne radiometers, *IEEE Proceedings of IGARSS ,* vol.4, 2462 2464, 2004.

[28] Tedesco M., G. Macelloni, P. Pampaloni, *A study on DOME-C, Antarctic: stratigraphy and electromagnetic modelling.* IFAC internal report, ISSN 1120-2823, RR/OST/10.03,2003

[29] W. Reich, “A radio continuum survey of the northern sky at 1420 MHz—Part 1,” *Astron. Astrophys. Suppl. Series*, vol. 48, 219–297, 1982.

[30] P. Reich and W. Reich, “A radio continuum survey of the northern sky at 1420 MHz—Part II,” *Astron. Astrophys. Suppl. Series*, vol. 63, 205–292, ,1986.

[31] P. Reich, J. C. Testori, and W. Reich, “A radio continuum survey of the southern sky at 1420 MHz, the atlas of contour maps,” *Astron. Astrophys*, vol. 376, 861–877, 2001.

11.0 Publications of the Project

Journals:

Preparation of an experimental campaign in Antarctica for the calibration of low frequency space-borne radiometers,Giovanni Macelloni, Paolo Pampaloni, Marco Brogioni, accepted for publication on Remote Sensing Italian Review (Dec. 2005)

Low-frequency microwave emission of the Antarctic plateau: DOMEX 04 an experimental campaign for the calibration of space-borne radiometers.Macelloni G.,Cagnati A.,Brogioni M.,Pampaloni P.,Drinkwater, submitted to Terra Antarctica (Dec. 2005)

DOMEX 2004: an Experimental Campaign at Dome-C Antarctica for the Calibration of Space-Borne Low-Frequency Microwave Radiometers, G. Macelloni, M. Brogioni, P. Pampaloni, A.Cagnati and M. Drinkwater, submitted to IEEE Transaction on Geoscience and Remote Sensing (Jan. 2006).

Proceedings:

Microwave emission from antarctica and the calibration of low frequency space-borne radiometers; Macelloni ,G.; Pampaloni ,P.; Tedesco, M.; Drinkwater, M.; Geoscience and Remote Sensing Symposium, 2004. IGARSS '04. Proceedings. 2004 IEEE International ,Volume: 4 ,20-24 Sept. 2004 Pages:2462-2464

DOMEX 2004: an experimental campaign at dome-C Antarctica for the calibration of space-borne low-frequency microwave radiometers, Macelloni, G.; Pampaloni, P.; Brogioni, M.; Santi, E.; Cagnati, A.; Drinkwater, M.; Geoscience and Remote Sensing Symposium, 2005. IGARSS '05. Proceedings. 2005 IEEE International Volume 3, 25-29 July 2005 Page(s):1932 – 193

Simulating Microwave Emission in the 1-37 GHz band from Ice Sheet at Dome-C in Antarctica *M. Tedesco, G. Macelloni, P. Pampaloni* PIERS 2004 Progress In Electromagnetic Research Symposium, PISA

DOMEX 2004: an experimental campaign at Dome-C Antarctica for the calibration of space-borne low-frequency microwave radiometers, G. Macelloni, P. Pampaloni, M. Brogioni, A. Cagnati, M. Drinkwater, Proceeding of the URSI commission F Symposium, Barza d'ISPRA 20-21 April 2005, (available on line)

Conferences:
Emissione A Microonde Dell' Antartide E Calibrazione Di Radiometri A Bassa Frequenza Da Satellite; *G. Macelloni, P. Pampaloni, M. Tedesco, M. Drinkwater;* III Workshop AIT- XII Riunione Annuale CeTeM sul Telerilevamento a Microonde- Napoli- 25-26 Novembre 2004

Microwave emission from Antarctica and the calibration of SMOS. Macelloni ,G.; Pampaloni ,P.; Santi E.; Drinkwater 5th SMOS Science Workshop – ESA ESRIN 29 November - 01 December 2004

Snow surface characteristics at Dome C, Antarctica Cagnati A., Macelloni G., Salvietti E., Valt M, 5° CONVEGNO NAZIONALE DI GLACIOLOGIA ANTARTICA- CONGA 5,Milano, Ottobre 2005

Low-frequency microwave emission of the Antarctic plateau: DOMEX 04 an experimental campaign for the calibration of space-borne radiometers.Macelloni G.,Cagnati A.,Brogioni M.,Pampaloni P.,Drinkwater M. 5° CONVEGNO NAZIONALE DI GLACIOLOGIA ANTARTICA- CONGA 5,Milano, Ottobre 2005

On the Contribution of the Surface Layers to Microwave Emission from Dry Snow: The Case of Antarctica Plateau at Dome C. M. Brogioni, G. Macelloni, P. Pampaloni, E. Santi, Geoscience and Remote Sensing Symposium, 2005. IGARSS '05